

NONLINEAR DYNAMICS AND SYSTEMS THEORY

An International Journal of Research and Surveys

Volume 21 Number 2 2021

CONTENTS

Capacity in Anisotropic Sobolev Spaces 115
Y. Akdim, R. Elharch, M. C. Hassib and S. Lalaoui Rhali

About the Restricted Three-Body Problem with the Schwarzschild-de
 Sitter Potential..... 126
John A. Arredondo and Julian Jiménez-Cárdenas

R-Functions and Nonlinear Galerkin Method for Solving the Nonlinear
 Stationary Problem of Flow around Body of Revolution 138
A. V. Artiukh, M. V. Sidorov and S. M. Lamtyugova

Analysis of Dynamic Frictional Contact Problem for Electro-Elastic
 Materials 150
O. Baiz and H. Benaissa

Model-Based Iterative Learning Control for the Trajectory Tracking
 of Disturbed Robot Manipulators 166
*Chems Eddine Boudjedir, Djamel Boukhetala and
 Mohamed Bouri*

Convective Stability of CO₂ Sequestration in a Porous Medium 179
M. H. DarAssi

System Reliability of Ailamujia Model and Additive Failure Rate
 Models..... 193
M. M. Smadi and A. A. Jaradat

Dynamics of Nonlinear Longitudinal Vibrations in a 1D Nano-Scale
 Continuum Described by the Generalized Morse Potential..... 202
S. A. Surulere, M. Y. Shatalov, A. C. Mkolesia and I. Fedotov

Linear Chaos Control of Fractional Generalized Hénon Map 216
*Abdelwahab Zarour, Adel Ouannas, Chahla Latrous and
 Abdelhak Berkane*

NONLINEAR DYNAMICS & SYSTEMS THEORY

Volume 21, No. 2, 2021

Nonlinear Dynamics and Systems Theory

An International Journal of Research and Surveys

EDITOR-IN-CHIEF A.A.MARTYNYUK

*S.P.Timoshenko Institute of Mechanics
National Academy of Sciences of Ukraine, Kiev, Ukraine*

MANAGING EDITOR I.P.STAVROULAKIS

Department of Mathematics, University of Ioannina, Greece

REGIONAL EDITORS

P.BORNE, Lille, France
 M.FABRIZIO, Bologna, Italy
Europe

M.BOHNER, Rolla, USA
 HAO WANG, Edmonton, Canada
USA and Canada

T.A.BURTON, Port Angeles, USA
 C.CRUZ-HERNANDEZ, Ensenada, Mexico
USA and Latin America

M.ALQURAN, Irbid, Jordan
Jordan and Middle East

K.L.TEO, Perth, Australia
Australia and New Zealand

Nonlinear Dynamics and Systems Theory

An International Journal of Research and Surveys

EDITOR-IN-CHIEF A.A.MARTYNYUK

The S.P.Timoshenko Institute of Mechanics, National Academy of Sciences of Ukraine,
Nesterov Str. 3, 03680 MSP, Kiev-57, UKRAINE / e-mail: journalndst@gmail.com

MANAGING EDITOR I.P.STAVROULAKIS

Department of Mathematics, University of Ioannina
451 10 Ioannina, HELLAS (GREECE) / e-mail: ipstav@cc.uoi.gr

ADVISORY EDITOR A.G.MAZKO

Institute of Mathematics of NAS of Ukraine, Kiev (Ukraine)
e-mail: mazko@imath.kiev.ua

REGIONAL EDITORS

M.ALQURAN (Jordan), e-mail: marwan04@just.edu.jo
P.BORNE (France), e-mail: Pierre.Borne@ec-lille.fr
M.BOHNER (USA), e-mail: bohner@mst.edu
T.A.BURTON (USA), e-mail: taburton@olympen.com
C. CRUZ-HERNANDEZ (Mexico), e-mail: ccruz@cicese.mx
M.FABRIZIO (Italy), e-mail: mauro.fabrizio@unibo.it
HAO WANG (Canada), e-mail: hao8@ualberta.ca
K.L.TEO (Australia), e-mail: K.L.Teo@curtin.edu.au

EDITORIAL BOARD

Aleksandrov, A.Yu. (Russia)	Jafari, H. (South African Republic)
Artstein, Z. (Israel)	Khusainov, D.Ya. (Ukraine)
Awrejcewicz, J. (Poland)	Kloedon, P. (Germany)
Benrejeb, M. (Tunisia)	Kokologiannaki, C. (Greece)
Braiek, N.B. (Tunisia)	Krishnan, E.V. (Oman)
Chen Ye-Hwa (USA)	Limarchenko, O.S. (Ukraine)
D'Anna, A. (Italy)	Nguang Sing Kiong (New Zealand)
De Angelis, M. (Italy)	Okninski, A. (Poland)
Denton, Z. (USA)	Peterson, A. (USA)
Vasundhara Devi, J. (India)	Radziszewski, B. (Poland)
Djemai, M. (France)	Shi Yan (Japan)
Dshalalow, J.H. (USA)	Sivasundaram, S. (USA)
Eke, F.O. (USA)	Sree Hari Rao, V. (India)
Gajic Z. (USA)	Staicu V. (Portugal)
Georgiou, G. (Cyprus)	Stavarakakis, N.M. (Greece)
Herlambang T. (Indonesia)	Vatsala, A. (USA)
Honglei Xu (Australia)	Zuyev, A.L. (Germany)
Izobov, N.A. (Belarussia)	

ADVISORY COMPUTER SCIENCE EDITORS

A.N.CHERNIENKO and A.S.KHOROSHUN, Kiev, Ukraine

ADVISORY LINGUISTIC EDITOR

S.N.RASSHYVALOVA, Kiev, Ukraine

INSTRUCTIONS FOR CONTRIBUTORS

(1) General. Nonlinear Dynamics and Systems Theory (ND&ST) is an international journal devoted to publishing peer-refereed, high quality, original papers, brief notes and review articles focusing on nonlinear dynamics and systems theory and their practical applications in engineering, physical and life sciences. Submission of a manuscript is a representation that the submission has been approved by all of the authors and by the institution where the work was carried out. It also represents that the manuscript has not been previously published, has not been copyrighted, is not being submitted for publication elsewhere, and that the authors have agreed that the copyright in the article shall be assigned exclusively to InforMath Publishing Group by signing a transfer of copyright form. Before submission, the authors should visit the website:

<http://www.e-ndst.kiev.ua>

for information on the preparation of accepted manuscripts. Please download the archive Sample_NDST.zip containing example of article file (you can edit only the file Samplefilename.tex).

(2) Manuscript and Correspondence. Manuscripts should be in English and must meet common standards of usage and grammar. To submit a paper, send by e-mail a file in PDF format directly to

Professor A.A. Martynyuk, Institute of Mechanics,
Nesterov str.3, 03057, MSP 680, Kiev-57, Ukraine
e-mail: journalndst@gmail.com

or to one of the Regional Editors or to a member of the Editorial Board. Final version of the manuscript must typeset using LaTeX program which is prepared in accordance with the style file of the Journal. Manuscript texts should contain the title of the article, name(s) of the author(s) and complete affiliations. Each article requires an abstract not exceeding 150 words. Formulas and citations should not be included in the abstract. AMS subject classifications and key words must be included in all accepted papers. Each article requires a running head (abbreviated form of the title) of no more than 30 characters. The sizes for regular papers, survey articles, brief notes, letters to editors and book reviews are: (i) 10-14 pages for regular papers, (ii) up to 24 pages for survey articles, and (iii) 2-3 pages for brief notes, letters to the editor and book reviews.

(3) Tables, Graphs and Illustrations. Each figure must be of a quality suitable for direct reproduction and must include a caption. Drawings should include all relevant details and should be drawn professionally in black ink on plain white drawing paper. In addition to a hard copy of the artwork, it is necessary to attach the electronic file of the artwork (preferably in PCX format).

(4) References. Each entry must be cited in the text by author(s) and number or by number alone. All references should be listed in their alphabetic order. Use please the following style:

Journal: [1] H. Poincare, Title of the article. *Title of the Journal* **volume**
(issue) (year) pages. [Language]

Book: [2] A.M. Lyapunov, *Title of the Book*. Name of the Publishers, Town, year.

Proceeding: [3] R. Bellman, Title of the article. In: *Title of the Book*. (Eds.).
Name of the Publishers, Town, year, pages. [Language]

(5) Proofs and Sample Copy. Proofs sent to authors should be returned to the Editorial Office with corrections within three days after receipt. The corresponding author will receive a sample copy of the issue of the Journal for which his/her paper is published.

(6) Editorial Policy. Every submission will undergo a stringent peer review process. An editor will be assigned to handle the review process of the paper. He/she will secure at least two reviewers' reports. The decision on acceptance, rejection or acceptance subject to revision will be made based on these reviewers' reports and the editor's own reading of the paper.

NONLINEAR DYNAMICS AND SYSTEMS THEORY

An International Journal of Research and Surveys
Published by InforMath Publishing Group since 2001

Volume 21

Number 2

2021

CONTENTS

Capacity in Anisotropic Sobolev Spaces	115
<i>Y. Akdim, R. Elharch, M. C. Hassib and S. Lalaoui Rhali</i>	
About the Restricted Three-Body Problem with the Schwarzschild-de Sitter Potential	126
<i>John A. Arredondo and Julian Jiménez-Cárdenas</i>	
R-Functions and Nonlinear Galerkin Method for Solving the Nonlinear Stationary Problem of Flow around Body of Revolution	138
<i>A. V. Artiukh, M. V. Sidorov and S. M. Lamtyugova</i>	
Analysis of Dynamic Frictional Contact Problem for Electro-Elastic Materials	150
<i>O. Baiz and H. Benaissa</i>	
Model-Based Iterative Learning Control for the Trajectory Tracking of Disturbed Robot Manipulators	166
<i>Chems Eddine Boudjedir, Djamel Boukhetala and Mohamed Bouri</i>	
Convective Stability of CO_2 Sequestration in a Porous Medium	179
<i>M. H. DarAssi</i>	
System Reliability of Ailamujia Model and Additive Failure Rate Models	193
<i>M. M. Smadi and A. A. Jaradat</i>	
Dynamics of Nonlinear Longitudinal Vibrations in a 1D Nano-Scale Continuum Described by the Generalized Morse Potential	202
<i>S. A. Surulere, M. Y. Shatalov, A. C. Mkolesia and I. Fedotov</i>	
Linear Chaos Control of Fractional Generalized Hénon Map	216
<i>Abdelwahab Zarour, Adel Ouannas, Chahla Latrous and Abdelhak Berkane</i>	

Founded by A.A. Martynyuk in 2001.

Registered in Ukraine Number: KB No 5267 / 04.07.2001.

NONLINEAR DYNAMICS AND SYSTEMS THEORY

An International Journal of Research and Surveys

Impact Factor from SCOPUS for 2019: SJR – 0.328, SNIP – 0.591 and CiteScore – 1.4

Nonlinear Dynamics and Systems Theory (ISSN 1562–8353 (Print), ISSN 1813–7385 (Online)) is an international journal published under the auspices of the S.P. Timoshenko Institute of Mechanics of National Academy of Sciences of Ukraine and Curtin University of Technology (Perth, Australia). It aims to publish high quality original scientific papers and surveys in areas of nonlinear dynamics and systems theory and their real world applications.

AIMS AND SCOPE

Nonlinear Dynamics and Systems Theory is a multidisciplinary journal. It publishes papers focusing on proofs of important theorems as well as papers presenting new ideas and new theory, conjectures, numerical algorithms and physical experiments in areas related to nonlinear dynamics and systems theory. Papers that deal with theoretical aspects of nonlinear dynamics and/or systems theory should contain significant mathematical results with an indication of their possible applications. Papers that emphasize applications should contain new mathematical models of real world phenomena and/or description of engineering problems. They should include rigorous analysis of data used and results obtained. Papers that integrate and interrelate ideas and methods of nonlinear dynamics and systems theory will be particularly welcomed. This journal and the individual contributions published therein are protected under the copyright by International InforMath Publishing Group.

PUBLICATION AND SUBSCRIPTION INFORMATION

Nonlinear Dynamics and Systems Theory will have 4 issues in 2021, printed in hard copy (ISSN 1562–8353) and available online (ISSN 1813–7385), by InforMath Publishing Group, Nesterov str., 3, Institute of Mechanics, Kiev, MSP 680, Ukraine, 03057. Subscription prices are available upon request from the Publisher, EBSCO Information Services (<mailto:journals@ebSCO.com>), or website of the Journal: <http://e-ndst.kiev.ua>. Subscriptions are accepted on a calendar year basis. Issues are sent by airmail to all countries of the world. Claims for missing issues should be made within six months of the date of dispatch.

ABSTRACTING AND INDEXING SERVICES

Papers published in this journal are indexed or abstracted in: Mathematical Reviews / MathSciNet, Zentralblatt MATH / Mathematics Abstracts, PASCAL database (INIST–CNRS) and SCOPUS.



Capacity in Anisotropic Sobolev Spaces

Y. Akdim¹, R. Elharch^{2*}, M. C. Hassib² and S. Lalaoui Rhali²

¹ *LAMA Laboratory, Department of Mathematics, Faculty of Sciences Dhar El Mahraz, Sidi Mohamed Ben Abdellah University, P.O. Box 1796 Atlas Fez, Morocco.*

² *Laboratory of Engineering Sciences (LSI), Polydisciplinary Faculty of Taza, Sidi Mohamed Ben Abdellah University, P.O. Box 1223 Taza, Morocco.*

Received: November 28, 2019; Revised: March 16, 2021

Abstract: This paper is devoted to the study of the theory of capacity in an anisotropic Sobolev space $W^{1,\vec{p}}(\Omega)$, where Ω is a bounded set of \mathbb{R}^N ($N \geq 2$), $\vec{p} = (p_0, p_1, \dots, p_N)$ with $1 < p_0, p_1, \dots, p_N < \infty$. We will define the $C_{k,\vec{p}}$ capacity and prove its main properties, especially, it will be shown that $C_{k,\vec{p}}$ defines a Choquet capacity. To illustrate our results, we will present an application of this capacity.

Keywords: *anisotropic Sobolev spaces; capacity; potential.*

Mathematics Subject Classification (2010): 31C15.

1 Introduction

The theory of capacity and non-linear potential in the classical Lebesgue space $L^p(\Omega)$ ($1 < p < \infty$) was studied by Maz'ya and Khavin in [16] and Meyers in [18]. These authors introduced the concept of capacity and non-linear potential in these spaces and provided very rich applications in functional analysis, harmonic analysis, theory of partial differential equations and theory of probabilities.

It has been developed specially by Adams [1], by Hedberg in [13], by Hedberg and Wolff in [14] and others. The Sobolev capacity for constant exponent spaces has found a great number of applications (see [12, 15]) and, for example, Boccardo et al. [8] studied the existence and non existence of solutions of the following problem:

$$(\mathcal{P}) \begin{cases} -\Delta u + u |\nabla u|^2 = \mu & \text{in } \Omega, \\ u = 0 & \text{on } \partial\Omega, \end{cases}$$

* Corresponding author: <mailto:rachid.elharch@usmba.ac.ma>

where Ω is a bounded open set in \mathbb{R}^N , $N \geq 2$ and μ is a radon measure on Ω .

More precisely, the authors proved the existence of a solution u in $H_0^1(\Omega)$ for the problem (\mathcal{P}) if and only if the measure μ does not charge the sets of capacity zero in Ω . Also, Kilpeläinen [17] introduced the weighted Sobolev capacity and discussed the role of capacity in the pointwise definition of functions in Sobolev spaces involving weights of Muckenhoupt's A_p -class. The previous concept was generalized by N. Aissaoui and A. Benkirane in [2], by replacing L^p with an Orlicz space. Later, this theory was studied by M. C Hassib, Y. Akdim, A. Benkirane and N. Aissaoui in Musielak-Orlicz spaces (see [3] and [4]).

The notion of capacity offers a standard way to characterize exceptional sets in various function spaces. Depending on the starting point of the study, the capacity of a set can be defined in many appropriate ways. A common property of capacities is that they measure small sets more precisely than the usual Lebesgue measure. The Choquet theory [10] provides a standard approach to capacities. Capacity is a necessary tool in both classical and non-linear potential theory.

The main purpose of this paper is to study the theory of capacity in an anisotropic Sobolev space $W^{1,\vec{p}}(\Omega)$. Our results generalize those in [18] obtained in Lebesgue spaces, in order to apply them to some problems of partial differential equations and harmonic analysis.

The present paper is organized as follows. In Section 2, we present some necessary preliminary knowledge on the anisotropic Sobolev space and we recall main properties of capacities. In Section 3, we define the $C_{k,\vec{p}}$ -capacity in the anisotropic Sobolev space and we show some of its properties. As an application of our results, we consider a variational problem, where X is a subset of \mathbb{R}^N . We give a sufficient condition on the $C_{k,\vec{p}}$ capacity of X to ensure the existence and uniqueness of a $C_{k,\vec{p}}$ -capacitary distribution of X such that the $C_{k,\vec{p}}$ -capacitary potential of X is greater than or equal to one.

2 Preliminaries

2.1 Anisotropic Sobolev spaces

Let Ω be an open bounded domain in \mathbb{R}^N ($N \geq 2$) with boundary $\partial\Omega$.

Let $1 < p_0, p_1, \dots, p_N < \infty$, we denote

$$\vec{p} = (p_0, p_1, \dots, p_N), \quad D^0 u = u \quad \text{and} \quad D^i u = \frac{\partial u}{\partial x_i} \quad \text{for } i = 1, \dots, N.$$

The anisotropic Sobolev space $W^{1,\vec{p}}(\Omega)$ is defined as follows:

$$W^{1,\vec{p}}(\Omega) = \{u \in L^{p_0}(\Omega) \text{ and } D^i u \in L^{p_i}(\Omega), i = 1, \dots, N\}.$$

We recall that the $W^{1,\vec{p}}(\Omega)$ is a separable and reflexive Banach space (see [19]) with respect to the norm

$$\|u\|_{W^{1,\vec{p}}(\Omega)} = \sum_{i=0}^N \|D^i u\|_{L^{p_i}(\Omega)}.$$

We denoted

$$W_+^{1,\vec{p}}(\Omega) = \{u \in W^{1,\vec{p}}(\Omega) \setminus u \geq 0\}.$$

The space $W_0^{1,\vec{p}}(\Omega)$ is the closure of $C_0^\infty(\Omega)$ with respect to this norm. The theory of such anisotropic spaces was developed in [20–23]. It was proved that $C_0^\infty(\Omega)$ is dense in $W_0^{1,\vec{p}}(\Omega)$, and $W_0^{1,\vec{p}}(\Omega)$ is a reflexive Banach space.

For any $\vec{p} = (p_0, p_1, \dots, p_N)$, with $1 < p_i < \infty$, $i = 0, 1, \dots, N$, the dual space of the anisotropic Sobolev space $W_0^{1, \vec{p}}(\Omega)$ is equivalent to $W^{-1, \vec{p}'}(\Omega)$, where $\vec{p}' = (p'_0, p'_1, \dots, p'_N)$ and $p'_i = \frac{p_i}{p_i - 1}$ for all $i = 0, 1, \dots, N$.

Proposition 2.1 *Let $p \in [1, +\infty[$ and $(f_n)_n$ be a sequence in $(L^p(\mu), \|\cdot\|_p)$ whose series of norms $\sum_n \|f_n\|_p$ converges. Then the series of functions $\sum_n f_n$ converges for the norm $\|\cdot\|_p$ and we have $\|\sum_n f_n\|_p \leq \sum_n \|f_n\|_p$.*

Proof. For $n \in \mathbb{N}^*$ fixed, according to the inequality of Minkowski, we have

$$\left\| \sum_{k=0}^n |f_k| \right\|_p \leq \sum_{k=0}^n \|f_k\|_p \leq \sum_{k=0}^{+\infty} \|f_k\|_p.$$

It follows from the monotone convergence theorem that

$$\left(\int_{\Omega} \left(\sum_{k=0}^{+\infty} |f_k| \right)^p d\mu \right)^{\frac{1}{p}} \leq \sum_{k=0}^{+\infty} \|f_k\|_p.$$

Thus,

$$\left\| \sum_{k=0}^{+\infty} f_k \right\|_p \leq \sum_{k=0}^{+\infty} \|f_k\|_p.$$

Lemma 2.1 [see [9]] *Let E be a Banach space. If $(f_n)_n$ converges weakly to f in E , then the sequence $\|f_n\|$ is bounded and $\|f\| \leq \liminf \|f_n\|$.*

2.2 Capacity

Definition 2.1 Let E be a topological space and T be the class of Borel sets in E , and a function $C : T \rightarrow [0, +\infty]$.

- 1) The function C is called a capacity if the following axioms are satisfied:
 - i) $C(\emptyset) = 0$.
 - ii) $X \subset Y \Rightarrow C(X) \leq C(Y)$ for all X and Y in T .
 - iii) For all sequences $(X_n) \subset T$,

$$C\left(\bigcup_n X_n\right) \leq \sum_n C(X_n).$$

- 2) The function C is called an outer capacity if, for all $X \in T$,

$$C(X) = \inf\{C(O) : O \supset X, O \text{ is open}\}.$$

- 3) The function C is called an interior capacity if, for all $X \in T$,

$$C(X) = \sup\{C(K) : K \subset X, K \text{ is compact}\}.$$

- 4) A property, that holds true except perhaps on a set of capacity zero, is said to be true C -quasi everywhere (abbreviated C - q.e.).

5) Let f and (f_n) be real-valued finite functions C -q.e. We say that (f_n) converges to f in C -capacity if

$$\forall \varepsilon > 0, \lim_{n \rightarrow +\infty} C(\{x : |f_n(x) - f(x)| > \varepsilon\}) = 0.$$

6) Let f and (f_n) be real-valued finite functions C -q.e. We say that (f_n) converges to f C -quasi-uniformly (abbreviated C -q.u) if $(\forall \varepsilon > 0), (\exists X \in T) : C(X) < \varepsilon$ and (f_n) converges to f uniformly on X^c .

3 Capacity in Anisotropic Sobolev Spaces

3.1 $C_{k, \vec{p}}$ -capacity

Let k be a positive integrable function on \mathbb{R}^N and $X \subset \mathbb{R}^N$ ($N \geq 2$). We denote

$$S_{\vec{p}}(X) = \{f \in W^{1, \vec{p}}(\Omega) : k * f \geq 1 \text{ on } X\},$$

where $k * f$ is the convolution of k and f .

The anisotropic Sobolev \vec{p} -capacity of X is defined by

$$C_{k, \vec{p}}(X) = \inf_{f \in S_{\vec{p}}(X)} \{\|f\|_{W^{1, \vec{p}}(\Omega)}\}.$$

In the case where $S_{\vec{p}}(X) = \emptyset$, we set $C_{k, \vec{p}}(X) = \infty$.

Functions $f \in S_{\vec{p}}(X)$ are said to be \vec{p} -admissible for the X .

The anisotropic \vec{p} -capacity enjoys all relevant properties of general capacities, specifically, it will be shown that $C_{k, \vec{p}}(X)$ defines a Choquet capacity.

Theorem 3.1 *The anisotropic Sobolev \vec{p} -capacity $C_{k, \vec{p}}$ is an outer capacity.*

Remark 3.1 Let $B_{k, \vec{p}}(X) = \inf\{\|f\|_{W^{1, \vec{p}}(\Omega)} : f \in W_+^{1, \vec{p}}(\Omega) \text{ and } k * f \geq 1 \text{ on } X\}$, then $C_{k, \vec{p}}(X) = B_{k, \vec{p}}(X)$.

Indeed, it is obvious that $C_{k, \vec{p}}(X) \leq B_{k, \vec{p}}(X)$.

On the other hand, let $f \in W_+^{1, \vec{p}}(\Omega)$, then $|f| \in W_+^{1, \vec{p}}(\Omega)$, and if $k * f \geq 1$ on X , then $k * |f| \geq 1$ on X , thus

$$B_{k, \vec{p}}(X) \leq \|f\|_{W^{1, \vec{p}}(\Omega)}.$$

Therefore,

$$B_{k, \vec{p}}(X) \leq C_{k, \vec{p}}(X).$$

A direct application of Proposition 2.1 is the following result.

Lemma 3.1 *Let $(f_n)_n$ be a sequence in $W^{1, \vec{p}}(\Omega)$ whose series of norms $\sum_n \|f_n\|_{W^{1, \vec{p}}(\Omega)}$ converges. Then we have*

$$\left\| \sum_n f_n \right\|_{W^{1, \vec{p}}(\Omega)} \leq \sum_n \|f_n\|_{W^{1, \vec{p}}(\Omega)}.$$

Proof. (**Theorem 3.1**) It is obvious that $C_{k, \vec{p}}(\emptyset) = 0$ and $C_{k, \vec{p}}(X) \leq C_{k, \vec{p}}(Y)$ if $X \subset Y$. Let (X_i) be a subset of \mathbb{R}^N . If $\sum_{i=0}^{\infty} C_{k, \vec{p}}(X_i) = +\infty$, there is nothing to show.

We may assume that

$$\sum_{i=0}^{\infty} C_{k,\bar{p}}(X_i) < +\infty, \text{ then } (\forall i \in \mathbb{N}) C_{k,\bar{p}}(X_i) < +\infty,$$

thus,

$$(\forall i \in \mathbb{N}) (\forall \varepsilon > 0) (\exists f_i \in W_+^{1,\bar{p}}(\Omega)) \text{ so that } k * f_i \geq 1 \text{ on } X_i,$$

and we have

$$\|f_i\|_{W^{1,\bar{p}}(\Omega)} \leq C_{k,\bar{p}}(X_i) + \frac{\varepsilon}{2^{i+1}}.$$

Let $f = \sup f_i$, we show that $f \in W_+^{1,\bar{p}}(\Omega)$. For all $i \geq 0$, we have by Lemma 3.1

$$\|\sup f_i\|_{W^{1,\bar{p}}(\Omega)} \leq \left\| \sum_{i=0}^{\infty} f_i \right\|_{W^{1,\bar{p}}(\Omega)} \leq \sum_{i=0}^{\infty} \|f_i\|_{W^{1,\bar{p}}(\Omega)}.$$

Thus,

$$\|f\|_{W^{1,\bar{p}}(\Omega)} \leq \sum_{i=0}^{\infty} \|f_i\|_{W^{1,\bar{p}}(\Omega)} \leq \sum_{i=0}^{\infty} C_{k,\bar{p}}(X_i) + \varepsilon.$$

This implies that $f \in W_+^{1,\bar{p}}(\Omega)$. Since $k * f \geq 1$ on $\bigcup_{i \geq 0} X_i$, we deduce that

$$C_{k,\bar{p}}\left(\bigcup_{i=0}^{\infty} X_i\right) \leq \|f\|_{W^{1,\bar{p}}(\Omega)} \leq \sum_{i=0}^{\infty} C_{k,\bar{p}}(X_i) + \varepsilon, \text{ for all } \varepsilon > 0.$$

The claim follows by letting $\varepsilon \rightarrow 0$.

Now, it remains only to verify that $C_{k,\bar{p}}(X)$ is an outer capacity. Let $X \subset \mathbb{R}^N$, we have

$$C_{k,\bar{p}}(X) \leq \inf\{C_{k,\bar{p}}(O), O \supset X, O \text{ is open}\}.$$

For the reverse inequality, if $C_{k,\bar{p}}(X) = +\infty$, there is nothing to show.

Assume that $C_{k,\bar{p}}(X) < +\infty$ and $0 < \varepsilon < 1$, then there exists $g \in W_+^{1,\bar{p}}(\Omega)$ so that $k * g \geq 1$ on X and

$$\|g\|_{W^{1,\bar{p}}(\Omega)} \leq C_{k,\bar{p}}(X) + \varepsilon.$$

We put $g_\varepsilon = \frac{g}{1-\varepsilon}$ and let the set $O_\varepsilon = \{x : (k * g_\varepsilon)(x) > 1\}$.

Thus O_ε is open, and

$$\forall x \in X; \quad (k * g_\varepsilon)(x) \geq \frac{1}{1-\varepsilon} > 1.$$

Hence $X \subset O_\varepsilon$. On the other hand, we have $C_{k,\bar{p}}(O_\varepsilon) \leq \|g_\varepsilon\|_{W^{1,\bar{p}}(\Omega)}$, and we deduce that

$$C_{k,\bar{p}}(O_\varepsilon) \leq \frac{1}{1-\varepsilon} \|g\|_{W^{1,\bar{p}}(\Omega)} \leq \frac{1}{1-\varepsilon} (C_{k,\bar{p}}(X) + \varepsilon), \forall \varepsilon > 0.$$

Thus,

$$\inf\{C_{k,\bar{p}}(O), O \supset X, O \text{ open}\} \leq C_{k,\bar{p}}(X).$$

Proposition 3.1 *The anisotropic Sobolev \vec{p} -capacity $C_{k,\vec{p}}$ verifies the following properties:*

- 1) *If there exists $f \in W^{1,\vec{p}}(\Omega)$ such that $|k * f| = +\infty$ on X , then $C_{k,\vec{p}}(X) = 0$.*
- 2) *If $C_{k,\vec{p}}(X) = 0$, then there exists $f \in W_+^{1,\vec{p}}(\Omega)$ such that $k * f = +\infty$.*

Proof.

- 1) Let $f \in W^{1,\vec{p}}(\Omega)$ be such that $|k * f| = +\infty$ on X , then for all $\alpha > 0$, $|k * f| > \alpha$ on X , thus,

$$C_{k,\vec{p}}(X) \leq \frac{\|f\|_{W^{1,\vec{p}}(\Omega)}}{\alpha}, \quad \forall \alpha > 0.$$

This means that

$$C_{k,\vec{p}}(X) = 0.$$

- 2) If $C_{k,\vec{p}}(X) = 0$, then $(\forall i \in \mathbb{N}) (\exists f_i \in W_+^{1,\vec{p}}(\Omega))$ with $k * f_i \geq 1$ on X and

$$\|f_i\|_{W^{1,\vec{p}}(\Omega)} \leq 2^{-i}.$$

Let $f = \sum_i f_i$. By Lemma 3.1 we have

$$\|f\|_{W^{1,\vec{p}}(\Omega)} \leq \sum_i \|f_i\|_{W^{1,\vec{p}}(\Omega)} \leq \sum_i 2^{-i}.$$

Then

$$\|f\|_{W^{1,\vec{p}}(\Omega)} < +\infty.$$

We conclude that $f \in W_+^{1,\vec{p}}(\Omega)$ such that $k * f = +\infty$ on X .

Theorem 3.2 *Let f and $(f_n)_n$ be in $W^{1,\vec{p}}(\Omega)$ and consider the following propositions:*

- i) $f_n \rightarrow f$ strongly in $W^{1,\vec{p}}(\Omega)$.
- ii) $k * f_n \rightarrow k * f$ $C_{k,\vec{p}}$ -capacity.
- iii) *There is a subsequence (f_{n_j}) such that $k * f_{n_j} \rightarrow k * f$ $C_{k,\vec{p}}$ -q.u.*
- iv) $k * (f_{n_j}) \rightarrow k * f$ in $C_{k,\vec{p}}$ -q.e.

Then we have

$$i) \Rightarrow ii) \Rightarrow iii) \Rightarrow iv).$$

Proof.

- We show $i) \Rightarrow ii)$.

By Proposition 3.1, we have $k * f$ and $k * f_n$ are finite $C_{k,\vec{p}}$ -q.e, for all n . Let $\varepsilon > 0$, then

$$C_{k,\vec{p}}(\{x : |k * f_n - k * f|(x) > \varepsilon\}) \leq \frac{\|f_n - f\|_{W^{1,\vec{p}}(\Omega)}}{\varepsilon}.$$

- We show $ii) \Rightarrow iii)$.

Let $\varepsilon > 0$, there exists f_{n_j} such that

$$C_{k,\bar{p}}(\{x : |k * f_{n_j} - k * f|(x) > 2^{-j}\}) \leq \varepsilon \cdot 2^{-j}.$$

We put

$$E_j = \{x : |k * f_{n_j} - k * f|(x) > 2^{-j}\} \text{ and } G_m = \bigcup_{j \geq m} E_j.$$

Then we have

$$C_{k,\bar{p}}(G_m) \leq \sum_{j \geq m} \varepsilon \cdot 2^{-j} < \varepsilon.$$

On the other hand,

$\forall x \in (G_m)^c, \forall j \geq m \quad |k * f_{n_j} - k * f|(x) \leq 2^{-j}$, thus $k * f_{n_j} \rightarrow k * f$ $C_{k,\bar{p}}$ -q.u.

- We show *iii*) \Rightarrow *iv*).

We have $\forall j \in \mathbb{N}, \exists X_j : C_{k,\bar{p}}(X_j) \leq \frac{1}{j}$ and $k * f_{n_j} \rightarrow k * f$ converges uniformly on $(X_j)^c$. We put $X = \bigcap_j X_j$, then $C_{k,\bar{p}}(X) = 0$ and $k * f_{n_j} \rightarrow k * f$ on X^c .

Theorem 3.3 *Let $(K_n)_n$ be a decreasing sequence of compacts and $K = \bigcap_n K_n$. Then*

$$\lim_{n \rightarrow +\infty} C_{k,\bar{p}}(K_n) = C_{k,\bar{p}}(K).$$

Proof. First, we observe that $C_{k,\bar{p}}(K) \leq \lim_{n \rightarrow +\infty} C_{k,\bar{p}}(K_n)$.

On the other hand, let O be an open set that satisfies $K \subset O$; then

$$K \cap O^c = \emptyset.$$

The sequence defined, for all $n, K'_n = K_n \cap O^c$ is a decreasing sequence of compacts and satisfies $\bigcap_n K'_n = \emptyset$. Then there exists n_0 such that $K'_{n_0} = \emptyset$.

Hence $\forall n \geq n_0, K'_n = \emptyset$, then $\forall n \geq n_0, K_n \subset O$. Therefore,

$$\lim_{n \rightarrow +\infty} C_{k,\bar{p}}(K_n) \leq C_{k,\bar{p}}(O).$$

Since $C_{k,\bar{p}}$ is an outer capacity, we have

$$\lim_{n \rightarrow +\infty} C_{k,\bar{p}}(K_n) \leq C_{k,\bar{p}}(K).$$

Proposition 3.2 *Let $(f_n)_n, f \in W^{1,\bar{p}}(\Omega)$ be such that $f_n \rightarrow f$ weakly in $W^{1,\bar{p}}(\Omega)$, then $\liminf(k * f_n) \leq k * f \leq \limsup(k * f_n)$ $C_{k,\bar{p}}$ -q.e.*

Proof. Since $W^{1,\bar{p}}(\Omega)$ is a reflexive space, $f_n \rightarrow f$ weakly in $W^{1,\bar{p}}(\Omega)$, then by the Banach-Saks theorem, there is a subsequence denoted again by (f_n) such that the sequence $g_n = \frac{1}{n} \sum_{i=1}^n f_i$ converges to f strongly in $W^{1,\bar{p}}(\Omega)$.

By Theorem 3.2, there is a subsequence of (g_n) , denoted again (g_n) , such that

$$\lim_{n \rightarrow +\infty} (k * g_n) = (k * f) \quad C_{k,\bar{p}} - q.e.$$

On the other hand,

$$\liminf(k * f_n) \leq \lim_{n \rightarrow +\infty} (k * g_n).$$

Therefore,

$$\liminf(k * f_n) \leq (k * f) \quad C_{k,\bar{p}} - q.e.$$

For the second inequality, it suffices to replace f_n by $(-f_n)$ in the first inequality.

Theorem 3.4 *If $(X_n)_n$ is an increasing sequence of sets and $X = \bigcup_n X_n$, then*

$$\lim_{n \rightarrow +\infty} C_{k,\bar{p}}(X_n) = C_{k,\bar{p}}(X).$$

Proof. First, we have $\lim_{n \rightarrow +\infty} C_{k,\bar{p}}(X_n) \leq C_{k,\bar{p}}(X)$.

For the reverse inequality, if $\lim_{n \rightarrow +\infty} C_{k,\bar{p}}(X_n) = +\infty$, there is nothing to show.

We assume that the sequence $C_{k,\bar{p}}(X_n)$ converges to the finite ℓ . Let f_n be \bar{p} -admissible for (X_n) such that

$$\|f_n\|_{W^{1,\bar{p}}(\Omega)} \leq C_{k,\bar{p}}(X_n) + \frac{1}{n}. \quad (1)$$

Since (f_n) forms a bounded sequence in $W_+^{1,\bar{p}}(\Omega)$, there exists a subsequence denoted again (f_n) which converges weakly to a function $f \in W_+^{1,\bar{p}}(\Omega)$.

We have by Proposition 3.2

$$\forall i \in \mathbb{N}, \quad k * f \geq 1 \text{ on } X_n, \quad C_{k,\bar{p}} - q.e.$$

Therefore,

$$k * f \geq 1 \text{ on } X, \quad C_{k,\bar{p}} - q.e. \quad (2)$$

Let B be a subset of X where $k * f \geq 1$, then from (1) and by Lemma 2.1 we have

$$C_{k,\bar{p}}(X) = C_{k,\bar{p}}(B) \leq \|f\|_{1,\bar{p}} \leq \ell, \quad (3)$$

the desired result is now a simple consequence of (3).

Corollary 3.1 *Let $(E_n)_n$ be a sequence of subsets of \mathbb{R}^N , then*

$$C_{k,\bar{p}}(\liminf E_n) \leq \liminf C_{k,\bar{p}}(E_n).$$

Proof. Let $E = \liminf E_n$, we have $E = \bigcup_n \left(\bigcap_{i \geq n} E_i \right)$.

We put $G_n = \bigcap_{i \geq n} E_i$, thus a sequence is increasing and by Theorem 3.4, we have

$$C_{k,\bar{p}}(E) = \lim_{n \rightarrow +\infty} C_{k,\bar{p}}(G_n).$$

Hence,

$$C_{k,\bar{p}}(G_n) \leq C_{k,\bar{p}}(E_n).$$

Therefore,

$$C_{k,\bar{p}}(E) \leq \liminf C_{k,\bar{p}}(E_n).$$

Definition 3.1 In the terminology of Choquet, C is called a capacity if it satisfies the following four properties:

- i) $C(\emptyset) = 0$,
- ii) C is increasing,
- iii) If (E_n) is an increasing sequence of sets, then $\sup_n C(X_n) = C(\bigcup_n X_n)$,
- iv) If (K_n) is a decreasing sequence of compacts, then $\inf_n C(K_n) = C(\bigcap_n K_n)$.

Remark 3.2 By Theorems 3.1, 3.3 and 3.4, $C_{k,\bar{p}}$ is a capacity in the sense of Choquet.

Definition 3.2 Let C be a capacity in the sense of Choquet. A subset $X \subset \mathbb{R}^N$ is called capacitable if

$$C(X) = \sup\{C(K) : K \subset X, K \text{ compact}\}.$$

Theorem 3.5 All analytic sets are $C_{k,\bar{p}}$ -capacitable.

Proof. It is an immediate consequence of the Choquet theorem in [11].

3.2 Application of a $C_{k,\bar{p}}$ - capacity

In this subsection, we propose to study an application of $C_{k,\bar{p}}$ capacities, more precisely, we treat the following variational problem.

Let X be a subset of \mathbb{R}^N such that $C_{k,\bar{p}}(X) < \infty$. There exists $f_0 \in W_+^{1,\bar{p}}(\Omega)$ such that $k * f_0 \geq 1$ $C_{k,\bar{p}}$ -q.e on X , and

$$\|f_0\|_{W^{1,\bar{p}}(\Omega)} = \inf\{\|f\|_{W^{1,\bar{p}}(\Omega)} : f \in W_+^{1,\bar{p}}(\Omega) \text{ and } k * f \geq 1 \text{ on } X\}. \tag{4}$$

Definition 3.3 We call a solution, f_0 , of problem (4) a $C_{k,\bar{p}}$ -capacitary distribution of X and we call $k * f_0$ a $C_{k,\bar{p}}$ -capacitary potential of X .

Theorem 3.6 Let X be a subset of \mathbb{R}^N such that $C_{k,\bar{p}}(X) < \infty$ and denote by Ω_X the set $\Omega_X = \{f \in W_+^{1,\bar{p}}(\Omega) : k * f \geq 1 \text{ } C_{k,\bar{p}}(X) \text{ -q.e on } X\}$. Then there exists a unique $f_0 \in W_+^{1,\bar{p}}(\Omega)$ such that:

- i) $\|f_0\|_{W^{1,\bar{p}}(\Omega)} = \inf\{\|f\|_{W^{1,\bar{p}}(\Omega)} : f \in \Omega_X\}$.
- ii) $k * f_0 \geq 1$ on X and $\|f_0\|_{W^{1,\bar{p}}(\Omega)} = C_{k,\bar{p}}(X)$.

Proof. i) Let the function $\theta : W^{1,\bar{p}}(\Omega) \rightarrow \mathbb{R}^+$ be defined by $\theta(f) = \|f\|_{W^{1,\bar{p}}(\Omega)}$; $\forall f \in W^{1,\bar{p}}(\Omega)$. θ is lower semi-continuous on $W^{1,\bar{p}}(\Omega)$ and coercive. By Theorem 3.2, Ω_X is strongly closed in $W^{1,\bar{p}}(\Omega)$. On the other hand, Ω_X is convex. Since $W^{1,\bar{p}}(\Omega)$ is reflexive, there exists a unique $f_0 \in W_+^{1,\bar{p}}(\Omega)$ such that

$$\|f_0\|_{W^{1,\bar{p}}(\Omega)} = \inf\{\|f\|_{W^{1,\bar{p}}(\Omega)} : f \in \Omega_X\}.$$

ii) Let Y be a subset of X where $k * f_0 < 1$, then $C_{k,\bar{p}}(X) = C_{k,\bar{p}}(X - Y)$.

Since $k * f_0 \geq 1$ on $X - Y$, $C_{k, \vec{p}}(X - Y) \leq \|f_0\|_{W^{1, \vec{p}}(\Omega)}$, on the other hand, we have

$$\{f \in W_+^{1, \vec{p}}(\Omega) : k * f \geq 1 \text{ on } X\} \subset \Omega_X.$$

Then

$$\|f_0\|_{W^{1, \vec{p}}(\Omega)} \leq C_{k, \vec{p}}(X).$$

4 Concluding Remarks

In this paper we defined the notion of $C_{k, \vec{p}}$ -capacity in the anisotropic Sobolev space $W^{1, \vec{p}}(\Omega)$ for $\vec{p} = (p_0, p_1, \dots, p_N)$, with $1 < p_0, p_1, \dots, p_N < \infty$. We showed that this capacity is an outer capacity and proved some convergence properties related to it. Moreover, we proved that $C_{k, \vec{p}}$ is a Choquet capacity. Finally, we gave an application of this capacity in anisotropic Sobolev spaces.

Note that the results obtained previously, especially, the properties of the anisotropic Sobolev \vec{p} -capacity $C_{k, \vec{p}}$ will be useful in the study of some differential equations problems. Namely, for problems, studied previously in [5–7], we can treat solutions in anisotropic Sobolev spaces and we can assume that the right hand side is a measure data.

A perspective of this work will focus on the application of our results to a unilateral problem that was addressed in a previous study [4] in Musielak–Orlicz–Sobolev spaces.

References

- [1] D. R. Adams. Sets and functions of finite L^p -capacity. *Indiana Univ. Math. J.* **27** (4) (1978) 611–627.
- [2] N. Aissaoui and A. Benkirane. Capacites dans les espaces d’Orlicz. *Ann. Sci. Math. Québec.* **18** (1) (1994) 1–23.
- [3] N. Aissaoui, Y. Akdim, A. Benkirane, M. C. Hassib. Capacity and Non-linear Potential in Musielak–Orlicz Spaces. *Nonlinear Dynamics and Systems Theory.* **16** (3) (2016) 276–293.
- [4] N. Aissaoui, Y. Akdim, A. Benkirane M. C. Hassib. Capacity, Theorem of H. Brezis and F.E. Browder Type in Musielak–Orlicz–Sobolev Spaces and Application. *Nonlinear Dynamics and Systems Theory.* **17** (2) (2017) 175–192.
- [5] Y. Akdim, A. Chakir, M. Mekour, et al. Entropy solutions of nonlinear $p(x)$ -Parabolic inequalities. *Nonlinear Dynamics and Systems Theory.* **18** (2) (2018) 107–129.
- [6] Y. Akdim, M. Rhoudaf and A. Salmani. Existence of Solution for Nonlinear Anisotropic Degenerated Elliptic Unilateral Problems. *Nonlinear Dynamics and Systems Theory* **18** (3) (2018) 213–224.
- [7] A. Benkirane, M. S. B. Elemine Vall and A. Talha. Existence of Renormalized Solutions for Some Strongly Parabolic Problems in Musielak–Orlicz–Sobolev Spaces. *Nonlinear Dynamics and Systems Theory.* **19** (1) (2019) 97–110.
- [8] L. Boccardo, T. Gallouët and L. Orsina. Existence and nonexistence of solutions for some nonlinear elliptic equations. *Journal d’Analyse Mathématique.* **73** (1) (1997) 203–223.
- [9] H. Brezis. *Analyse Fonctionnelle: Théorie et Applications.* Masson, Paris, 1983.
- [10] G. Choquet. Theory of capacities. *Ann. Inst. Fourier.* **5** (1954) 131–295.

- [11] G. Choquet. Forme abstraite du théorème de capacitabilité. *Ann. Inst. Fourier*. **9** (1959) 83–89.
- [12] L. C. Evans and R. F. Gariepy. *Measure Theory and Fine Properties of functions*. Studies in Advanced Mathematics, CRC Press, Boca Raton, Fla, USA, 1992.
- [13] L. I. Hedberg. Nonlinear potentials and approximation in the mean by analytic functions. *Math. Z.* **129** (1972) 299–319.
- [14] L. I. Hedberg and T. H. Wolff. Thin sets in nonlinear potential theory. *Ann. Inst. Fourier*. **33** (1983) 161–187.
- [15] J. Heinonen, T. Kilpeläinen and O. Martio, *Nonlinear Potential Theory of Degenerate Elliptic Equations*. Oxford Mathematical Monographs, Oxford University Press, 1993.
- [16] V. P. Khavin and V. G. Maz'ya. Nonlinear potential theory. *Uspekhi Math. Nauk.* **27** (1972) 71–148.
- [17] T. Kilpeläinen. Weighted Sobolev spaces and capacity. *Annales Academi Scientiarum Fennic. Mathematica*. **19** (1) 1994 95–113.
- [18] N. G. Meyers. A theory of capacities for potentials of functions in Lebesgue classes. *Math. Scand.* **26** (2) (1970) 255–292.
- [19] Mihailescu, Mihai, Patrizia Pucci and Vicentiu Radulescu. Eigenvalue problems for anisotropic quasilinear elliptic equations with variable exponent. *Journal of Mathematical Analysis and Applications*. **340** (1) (2008) 687–698.
- [20] S. M. Nikolski. On imbedding, continuation and approximation theorems for differentiable functions of several variables. *Russian Math. Surveys* **16** (5) (1961) 55–104.
- [21] J. Rakosnik. Some remarks to anisotropic Sobolev spaces I. *Beiträge zur Analysis*. **13** (1979) 55–68.
- [22] J. Rakosnik. Some remarks to anisotropic Sobolev spaces II. *Beiträge zur Analysis*. **15** (1981) 127–140.
- [23] M. Troisi. Teoremi di inclusione per spazi di Sobolev non isotropi. *Ricerche Mat.* **18** (1969) 3–24.



About the Restricted Three-Body Problem with the Schwarzschild-de Sitter Potential

John A. Arredondo and Julian Jiménez-Cárdenas

*Department of Mathematics, Fundación Universitaria Konrad Lorenz,
Carrera 9 Bis No. 62 - 43. Bogotá - Colombia.*

Received: June 18, 2020; Revised: March 8, 2021

Abstract: In this paper the restricted three body problem in the context of Schwarzschild-de Sitter's space-time is studied. The equations of motion that govern the bodies are derived using the Schwarzschild-de Sitter metric, by introducing a set known as the parameter domain, the existence of equilibrium points for any element of this set is shown. The stability conditions for the orbital motion of the system are established by the analysis of the eigenvalues of the linearized system.

Keywords: *restricted three body problem; Schwarzschild-de Sitter potential; relative equilibria; linear stability.*

Mathematics Subject Classification (2010): 70F15, 70F07.

1 Introduction

A de Sitter universe is an exact solution to the Einstein field equations of general relativity, named after Willem de Sitter. Setting the foundations of a particular cosmological universe, which is characterized as spatially flat and neglects ordinary matter, thus, the dynamics of the universe is dominated by a positive cosmological constant [7], or equivalent, de Sitter solution corresponds to a metric of a space-time of constant curvature. When the curvature is negative, the cosmological constant is too, and the corresponding universe is called anti-de Sitter space. In both cases, the metric corresponds to a general symmetry of Einstein's field equations, see Brinkmann's theorem [6]. The current observations indicate that the universe is expanding in an accelerated rate, and may approach de Sitter space asymptotically, that is, the concordance models of physical cosmology are converging on a consistent model that is best described as a de Sitter universe. See

* Corresponding author: <mailto:alexander.arredondo@konradlorenz.edu.co>

Carroll [3] and Zwicky [14] for a preliminary introduction, and [8] for a more detailed description and a consistent mathematical deduction.

Under the assumptions of this universe, we present a study of the Lagrangian triangular equilibria in the planar restricted three body problem, where the primaries are homogeneous spheroids rotating around their axis of symmetry and whose equatorial planes coincide throughout their motion. We follow closely the work of Arredondo *et al.* [1] for the Schwarzschild potential and the reference found there [9], but with the new ingredient of a potential associated to a more general metric, that is, in terms of relativistic effects, a new physical universe endowed with other qualities [4]. On the other hand, we introduce a new algebraic idea to give an analytical proof of the existence and uniqueness of a Lagrangian equilibrium, while as usual, linear stability of this equilibria is studied numerically.

2 Schwarzschild-de Sitter Potential

The Schwarzschild metric is the simplest solution of Einstein's equation with zero cosmological constant, while a de Sitter space is the simplest solution when a positive cosmological constant is considered [2], but both are obtained from considering a spherical symmetry [8]. As described in [10], a de Sitter-Schwarzschild space-time is just a combination of the two, and we can imagine it as the horizon of a black hole that is centered in a universe with de Sitter properties, which from the mathematical point of view, is properly described as a Riemannian space with one independent component of its curvature tensor. All the discussion behind this object and its beautiful developments can be found in Theorems 8.10 to 8.15 of [12]. For the purpose of this paper we just have to establish that the Schwarzschild-de Sitter metric is given by

$$ds^2 = c^2 \left(1 - \frac{2GM}{c^2 r} - \frac{\Lambda}{3} r^2 \right) dt^2 - \left(1 - \frac{2GM}{c^2 r} - \frac{\Lambda}{3} r^2 \right)^{-1} dr^2 - r^2 (d\theta^2 + \sin^2 \theta d\phi^2), \quad (1)$$

where G is the universal gravitational constant, M is the mass of the filed source, c is the speed of light and Λ is the cosmological constant. It is known that the associated potential to this metric is given by the time-time component of the metric

$$U(r) = \frac{-(c^2 + g_{00})}{2} = \frac{k}{r} + \frac{B}{r^3} + Cr^2, \quad (2)$$

where $k = GM$, $C = \frac{\Lambda c^2}{6}$ and $B = \frac{GML^2}{c^2}$ (see [3] and [10] for details).

3 Approach to the Restricted Problem

Let us consider two bodies, m_1 and m_2 , that interact mutually under the Schwarzschild-de Sitter potential, describing a circular orbit, and m_3 be the mass of a body with spherical symmetry such that $m_1, m_2 \gg m_3$. Also, we assume that the center of mass of m_1, m_2 is fixed at the origin. As we consider m_1 and m_2 source of the potential of type (2), that we rewrite as

$$U(r) = G \frac{m_1 m_2}{r} \left(1 + \frac{B_1 + B_2}{r^2} + (C_1 + C_2) r^3 \right), \quad (3)$$

the interaction among masses m_1 and m_2 is given by the equation

$$\left(\frac{m_1 m_2}{m_1 + m_2}\right) \ddot{R} = -\frac{dU(R)}{dR} = -\frac{d}{dR} \left(\frac{Gm_1 m_2}{R} \left(1 + \frac{B_1 + B_2}{R^2} + (C_1 + C_2)R^3 \right) \right),$$

i.e.,

$$\left(\frac{m_1 m_2}{m_1 + m_2}\right) \ddot{R} = -\frac{Gm_1 m_2}{R} \left(1 + \frac{3(B_1 + B_2)}{R^3} - 2R^2(C_1 + C_2) \right).$$

As it is supposed that m_1, m_2 are in an orbit with uniform circular movement, we have (R_0, ω) . This is equivalent to finding the equilibrium points of the increased potential or effective potential [5]. Doing a rescaling, we consider $Gm_1 m_2 = 1$; then the increased potential will be defined by

$$U_{aug}(R) = -\frac{1}{r} \left(1 + \frac{B_1 + B_2}{r^2} + (C_1 + C_2)r^3 \right) + \frac{r^2 \omega^2}{2} \quad (4)$$

and the effective potential as

$$U_{eff}(r) = -\frac{1}{r} \left(1 + \frac{B_1 + B_2}{r} + (C_1 + C_2)r^3 \right) + \frac{L^2}{2r^2}. \quad (5)$$

Remember that equilibrium points are critical ones in the effective potential. So, operating and making $R = 1$, we have

$$\omega = \sqrt{1 + 3(B_1 + B_2) - 2(C_1 + C_2)}. \quad (6)$$

Now, to guarantee orbit's stability, we use the fact that a critical point is further a minimal potential, namely, $U''_{eff}(R)|_{R=1} > 0$.

$$U''_{eff}(R)|_{R=1} = \left[-\frac{2}{R^3} - 12\frac{B_1 + B_2}{R^4} - 2(C_1 + C_2) + \frac{3L^2}{R^4} \right]_{R=1} > 0, \quad (7)$$

and replacing (6) in (7) we get

$$\begin{aligned} -2 - 12(B_1 + B_2) - 2(C_1 + C_2) + 3(1 + 3(B_1 + B_2) - 2(C_1 + C_2)) &> 0. \\ 1 &> 3(B_1 + B_2) + 8(C_1 + C_2). \end{aligned} \quad (8)$$

In the other way, the expression inside the root of (6) must be positive. So, another constraint for the coefficients is

$$1 + 3(B_1 + B_2) \geq 2(C_1 + C_2). \quad (9)$$

With (8) and (9), it is possible to uncouple one pair of the coefficients:

$$\frac{1}{5} > C_1 + C_2. \quad (10)$$

Also, in (8), since C_1 and C_2 are always non-negative, the other pair of coefficients is uncoupled:

$$\frac{1}{3} > B_1 + B_2. \quad (11)$$

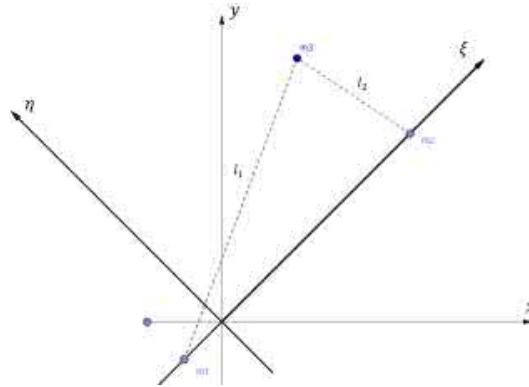


Figure 1: Representation of the restricted three body problem in the non-inertial system.

A particle’s Hamiltonian in a central field is given by $H(r, \dot{r}) = \frac{1}{2}m\dot{r}^2 - U(r)$, then the Hamiltonian of m_3 in the inertial reference system is

$$H(r, \dot{r}) = \frac{1}{2}m\dot{r}^2 - \frac{(1 - \mu)}{l_1} \left(1 + \frac{B_1}{l_1^2} + C_1 l_1^3 \right) - \frac{\mu}{l_2} \left(1 + \frac{B_2}{l_2^2} + C_2 l_2^3 \right), \quad (12)$$

where

$$l_1 = \sqrt{(\xi + \mu)^2 + \eta^2} \quad (13)$$

and

$$l_2 = \sqrt{(\xi + \mu - 1)^2 + \eta^2} \quad (14)$$

are the distances from the masses m_1, m_2 to the mass m_3 , respectively.

Now, we name $m_1 = \mu$, located on ξ_1 ; and $m_2 = 1 - \mu$, located on ξ_2 . In this order, $\mu \leq \frac{1}{2}$, $\xi_1 - \xi_2 = 1$ and $\mu\xi_2 + (1 - \mu)\xi_1 = 0$. So, $\xi_1 = -\mu$ and $\xi_2 = 1 - \mu$. Also,

$$m_1 = \begin{cases} x = -\mu \cos(\omega t), \\ y = -\mu \sin(\omega t), \end{cases} \quad (15)$$

and

$$m_2 = \begin{cases} x = (1 - \mu) \cos(\omega t), \\ y = (1 - \mu) \sin(\omega t), \end{cases} \quad (16)$$

as in Figure 1.

Consider (ξ, η) as the coordinates of m_3 in the non-inertial system; therefore, the interaction between the masses m_1 and m_2 with m_3 is given by the following potential:

$$U_{m_3}(\xi, \eta) = \frac{(1 - \mu)}{l_1} \left(1 + \frac{B_1}{l_1^2} + C_1 l_1^3 \right) + \frac{\mu}{l_2} \left(1 + \frac{B_2}{l_2^2} + C_2 l_2^3 \right), \quad (17)$$

and the Hamiltonian for m_3 in the non-inertial system is

$$H(\xi, \eta, P_\xi, P_\eta) = \frac{1}{2}(P_\xi^2 + P_\eta^2) + \omega(P_\xi \eta - P_\eta \xi) - U_{m_3}(\xi, \eta). \quad (18)$$

Apply Hamilton’s motion equations

$$\frac{\partial H}{\partial P_\xi} = P_\xi + \omega \eta = \dot{\xi}, \quad (19)$$

$$\frac{\partial H}{\partial P_\eta} = P_\eta - \omega\xi = \omega\dot{\eta}. \quad (20)$$

Multiply the equation (19) by ω and derive it with respect to time, knowing that $\dot{\omega} = 0$, since the circular movement is uniform:

$$\omega\dot{P}_\xi = \omega^2(\ddot{\xi} - \dot{\eta}),$$

$$\boxed{\dot{P}_\xi = \omega(\ddot{\xi} - \dot{\eta})}. \quad (21)$$

In an analogous way, multiply the equation (20) by ω and derive it with respect to time:

$$\boxed{\dot{P}_\eta = \omega(\dot{\eta} + \dot{\xi})}. \quad (22)$$

Before continuing, the partial derivatives of U_{m_3} are going to be calculated, in order to facilitate the calculus of the other two Hamilton's motion equations:

$$\begin{aligned} \frac{\partial U_{m_3}(\xi, \eta)}{\partial \xi} &= (1 - \mu) \frac{\partial l_1}{\partial \xi} \left(-\frac{1}{l_1^2} - \frac{3B_1}{l_1^4} + 2C_1 l_1 \right) + \mu \frac{\partial l_2}{\partial \xi} \left(-\frac{1}{l_2^2} - \frac{3B_2}{l_2^4} + 2C_2 l_2 \right), \\ &= -\frac{(1 - \mu)(\xi + \mu)}{l_1^3} \left(1 + \frac{3B_1}{l_1^2} - 2C_1 l_1^3 \right) - \frac{\mu(\xi + \mu - 1)}{l_2^3} \left(1 + \frac{3B_2}{l_2^2} - 2C_2 l_2^3 \right), \end{aligned} \quad (23)$$

on the other hand,

$$\frac{\partial U_{m_3}(\xi, \eta)}{\partial \eta} = -\eta \left[\frac{(1 - \mu)}{l_1^3} \left(1 + \frac{3B_1}{l_1^2} - 2C_1 l_1^3 \right) + \frac{\mu}{l_2^3} \left(1 + \frac{3B_2}{l_2^2} - 2C_2 l_2^3 \right) \right]. \quad (24)$$

By the last two Hamilton's motion equations we have

$$\frac{\partial H}{\partial \xi} = -\omega\dot{P}_\xi, \quad (25)$$

$$\frac{\partial H}{\partial \eta} = -\omega\dot{P}_\eta. \quad (26)$$

Replacing (18) in these equations we get

$$-\omega P_\eta - \frac{\partial U_{m_3}}{\partial \xi} = -\omega\dot{P}_\xi \cdot \omega P_\xi - \frac{\partial U_{m_3}}{\partial \eta} = -\omega\dot{P}_\eta. \quad (27)$$

Therefore, using (21) and (22) in the last couple of equations, it is obtained that

$$\omega^2(\ddot{\xi} - \dot{\eta}) = \omega P_\eta + \frac{\partial U_{m_3}}{\partial \xi}, \quad (28)$$

$$\omega^2(\dot{\eta} + \dot{\xi}) = -\omega P_\xi + \frac{\partial U_{m_3}}{\partial \eta}. \quad (29)$$

Now, with the centrifuge potential

$$\boxed{\Omega(\xi, \eta) = \frac{\omega^2}{2}(\xi^2 + \eta^2) + U_{m_3}(\xi, \eta)}, \quad (30)$$

one can find the critical points of m_3 by deriving it with respect to ξ and μ and making it equal to zero. Before doing that, one should consider the following equations:

$$\frac{\partial \Omega}{\partial \xi} = \omega^2(\ddot{\xi} - 2\dot{\eta}), \tag{31}$$

$$\frac{\partial \Omega}{\partial \eta} = \omega^2(\ddot{\eta} + 2\dot{\xi}). \tag{32}$$

Obtain summing (28)– $\omega \cdot$ (20) and $\omega \cdot$ (19)+(29), respectively. With this pair of equations, it is possible to deduce that the components (ξ, η) are orthogonal between them, but this is already known because of the nature of the problem and the coordinate axis. Consequently, the relation that is going to be used to find the critical points is

$$\frac{\partial \Omega}{\partial \xi} = \frac{\partial \Omega}{\partial \eta} = 0.$$

3.1 Collinear stability points

In order to obtain the collinear stability points, the partial derivative of Ω with respect to ξ is done, and all the η are replaced by zero. This gives the stability points that are in the ξ axis. After some algebra, one obtains that

$$-\mu x^4[3B_2 + (x - 1)^2] - (x - 1)^4[3B_1(\mu - 1) + 2C_1x^5(\mu - 1) - 2C_2\mu x^4(x - 1) + \omega^2x^4(\mu - x) - x^2(\mu - 1)] = 0, \tag{33}$$

where $x = \xi + \mu$. Since (33) is a ninth grade polynomial, it has at least a real solution.

3.2 Non-collinear stability points ($\eta \neq 0$)

In this case, both partial derivatives of Ω are zero, but $\eta \neq 0$, so one has two equations, the derivative with respect to ξ and η of (30). These two equations can be written as

$$0 = \frac{(1 - \mu)(\xi + \mu)}{l_1^3} \left(1 + \frac{3B_1}{l_1^2} - 2C_1l_1^3 - \omega^2l_1^3\right) + \frac{\mu(\xi + \mu - 1)}{l_2^3} \left(1 + \frac{3B_2}{l_2^2} - 2C_2l_2^3 - \omega^2l_2^3\right) \tag{34}$$

and

$$0 = \eta \left[\frac{(1 - \mu)}{l_1^3} \left(1 + \frac{3B_1}{l_1^2} - 2C_1l_1^3 - \omega^2l_1^3\right) + \frac{\mu}{l_2^3} \left(1 + \frac{3B_2}{l_2^2} - 2C_2l_2^3 - \omega^2l_2^3\right) \right], \tag{35}$$

respectively, due to the fact that $(1 - \mu)(\xi + \mu) + \mu(\xi + \mu - 1) = \xi$. Consider l_1, l_2 as an independent system of variables, last two equations hold if and only if

$$(\omega^2 + 2C_i)l_i^5 - l_i^2 - 3B_i = 0, \tag{36}$$

for $i = 1, 2$. Since (36) has a single change of sign, by Descartes’s rule of signs, each equation has exactly one positive root. The next proposition shows that these roots satisfy the triangle inequalities.

Definition 3.1 [Parameter domain] The set of all possible combinations of the non-negative parameters (B_1, B_2, C_1, C_2) that satisfy the constraints (8) – (11) will be called D .

Theorem 3.1 *For every combination in D , there exists a unique non-collinear rotating equilibrium.*

Proof. It will be shown that every possible combination of D gives positive solutions in (36) that satisfy the triangle inequalities. It can be seen that l_1 and l_2 depend on the values of the constants in D , and moreover,

$$l_1 = l_1(B_1, B_2, C_1, C_2) = l_2(B_2, B_1, C_2, C_1) = l_2 \quad (37)$$

taking advantage of the symmetry in (36). Define \bar{D} as the set D with its frontier, *i.e.*,

$$\bar{D} = D \cup \delta D.$$

It is known that a differentiable real-valued function whose domain is closed and bounded attains its extreme values either at a critical point or on the boundary. In this context, the functions

$$l_i : \begin{array}{ccc} \bar{D} & \rightarrow & \mathbb{R}, \\ (B_1, B_2, C_1, C_2) & \rightarrow & l_i = l_i(B_1, B_2, C_1, C_2), \end{array}$$

despite of being implicitly defined, are differentiable. A direct calculation proves that l_i does not accept critical points inside \bar{D} , so the extreme values of it must be in the frontier. All cases are shown below [11].

1. For $B_1 = 0$,

$$l_1 = \frac{1}{\sqrt[3]{1 + 3B_2 - 2C_2}}.$$

Given the constraints for the sum of two constants, it follows that $l_1^{\min} = \sqrt[3]{\frac{1}{2}} \approx 0.79$.

2. For $B_2 = 0$, the equation (36) becomes

$$l_1^5 - \frac{1}{(1 + 3B_1 - 2C_2)} l_1^2 - \frac{3B_1}{(1 + 3B_1 - 2C_2)} = 0.$$

To find a minimum bound, notice that the last polynomial can be rearranged as

$$l_1^2 \left(l_1^3 - \frac{1}{1 + 3B_1 - 2C_2} \right) = \frac{3B_1}{1 + 3B_1 - 2C_2},$$

from where it is deduced that

$$l_1 \geq \frac{1}{\sqrt[3]{1 + 3B_1 - 2C_2}} \geq \sqrt[3]{\frac{1}{2}} = l_1^{\min}.$$

3. For $C_1 = 0$, the minimum value for l_1 is given by the same arguments shown in the last case, so

$$l_1^{\min} = \sqrt[3]{\frac{1}{2}}.$$

4. For $C_2 = 0$, by similar reasons as in the previous cases, it follows that

$$l_1^{\min} = \sqrt[3]{\frac{1}{2}}.$$

5. For $C_1 + C_2 = \frac{1}{5}$, equation (36) can be written as

$$\begin{aligned} 0 &= (1 + 3(B_1 + B_2) - 2(C_1 + C_2) + 2C_1)l_1^5 - l_1^2 - 3B_1 \\ &= \left(\frac{3}{5} + 3(B_1 + B_2) + 2C_1\right)l_1^5 - l_1^2 - 3B_1. \end{aligned}$$

Calculating the derivative of the last polynomial expression with respect to C_1 and clearing dl_1/dC_1 yield to

$$\frac{dl_1}{dC_1} = \frac{-6l_1^5}{5(3/5 + 3(B_1 + B_2) + 2C_1)l_1^4 - 2l_1} = \frac{-6l_1^6}{3l_1^2 + 15B_1} < 0,$$

since $5(3/5 + 3(B_1 + B_2) + 2C_1)l_1^5 = 5l_1^2 + 15B_1$. This implies that the function $l_1(C_1)$ with its other variables fixed is decreasing on $C_1 + C_2 = 1/5$. Then its minimum is reached when C_1 is maximum. Therefore, if $C_1 = 1/5$, notice that the polynomial equation can be rearranged as

$$l_1^2 \left(l_1^3 - \frac{1}{1 + 3(B_1 + B_2)} \right) = \frac{3B_1}{1 + 3(B_1 + B_2)},$$

from where it is deduced that

$$l_1 \geq \frac{1}{\sqrt[3]{1 + 3(B_1 + B_2)}} \geq \frac{1}{\sqrt[3]{2}} = l_1^{\min}.$$

6. For $B_1 + B_2 = \frac{1}{3}$, equation (36) becomes

$$(2 - 2C_2)l_1^5 - l_1^2 - 3B_1 = 0.$$

Differentiating it with respect to B_1 and clearing dl_1/dB_1 lead to

$$\frac{dl_1}{dB_1} = \frac{3}{5(2 - 2C_2)l_1^4 - 2l_1} = \frac{3l_1}{5(2 - 2C_2)l_1^5 - 2l_1^2} = \frac{3l_1}{3l_1^2 + 15B_1} > 0$$

since $5(2 - 2C_2)l_1^5 = 5l_1^2 + 15B_1$. This implies that the function $l_1(B_1)$ with its other variables fixed is increasing on $B_1 + B_2 = 1/3$. Then its minimum value is reached when B_1 is minimum. Therefore, when $B_1 = 0$,

$$l_1^{\min} = \sqrt[3]{\frac{1}{2}}.$$

7. For $1 = 3(B_1 + B_2) + 8(C_1 + C_2)$, one writes equation (36) as

$$l_1^3 \left(l_1^3 - \frac{1}{2 - 8C_1 - 10C_2} \right) = \frac{3B_1}{2 - 8C_1 - 10C_2},$$

replacing $3(B_1 + B_2)$ with $1 - 8(C_1 + C_2)$. Using the same argument as in the previous cases,

$$l_1 > \sqrt[3]{\frac{1}{2 - 8C_1 - 10C_2}} \geq \sqrt[3]{\frac{1}{2}} = l_1^{\min}.$$

Testing the triangular inequalities with $l_1^{\min} = \sqrt[3]{\frac{1}{2}}$, one gets that if l_1^{\max} is in the vicinity

$$1 - \sqrt[3]{\frac{1}{2}} \leq l_1^{\max} \leq 1 + \sqrt[3]{\frac{1}{2}},$$

l_1^{\max} and l_1^{\min} satisfy the triangular inequalities. Therefore, a candidate to be an upper bound is $l_1^{\max} = 1 + \sqrt[3]{\frac{1}{2}}$. To show that it is, in fact, a valid bound, notice that replacing $l_1 = l_1^{\max}$ in (36) yields

$$(\omega^2 + 2C_1)(l_1^{\max})^5 - (l_1^{\max})^2 - 3B_1 \geq \frac{3}{5} \left(1 + \sqrt[3]{\frac{1}{2}}\right)^5 - \left(1 + \sqrt[3]{\frac{1}{2}}\right)^2 - 1 > 0.$$

Since the result is positive, independently of the constant value, l_1^{\max} is effectively an upper bound for the real root of (36), because the polynomial is positive only after the root.

By (37), l_1 and l_2 share the same minimum and maximum values, so every combination of constants

$$(B_1, B_2, C_1, C_2) \in D$$

raises solutions of (36) for l_1 and l_2 that satisfy the triangular inequalities since their bounds satisfy them.

3.2.1 Isosceles cases

The distances between the primaries were normalized to be one. Thus, a possible isosceles solution is when $l_i = 1$, and for that (36) raises the following condition:

$$3B_i = 2C_i, \tag{38}$$

and with this, equation (36) for $j \neq i$ becomes

$$(\omega^2 + 2C_j)l_j^5 - l_j^2 - 2C_j = 0.$$

Therefore, if (38) holds, $l_i = 1$ and l_j is given by the last polynomial equation that can be numerically solved in terms of ω^2 and C_j (see Figure 2). Another possible case is when $l_1 = l_2$, and a sufficient condition for this to happen is the trivial case when the bodies m_1 and m_2 have the same constants and the same mass.

4 Stability

To study the movement near the equilibrium points in this problem, the Hamiltonian (18) is expanded through the Taylor series around these points, the linear terms in this are omitted because the equilibrium points are zeroes in the potential and the constant term does not affect the form of the motion equation, so it is not taken into account. The Hamiltonian function rises the Hamiltonian matrix

$$\begin{pmatrix} 0 & \omega & 1 & 0 \\ -\omega & 0 & 0 & 1 \\ \frac{\partial^2 U_{m3}}{\partial \xi^2} & \frac{\partial^2 U_{m3}}{\partial \xi \partial \eta} & 0 & \omega \\ \frac{\partial^2 U_{m3}}{\partial \xi \partial \eta} & \frac{\partial^2 U_{m3}}{\partial \eta^2} & -\omega & 0 \end{pmatrix}, \tag{39}$$

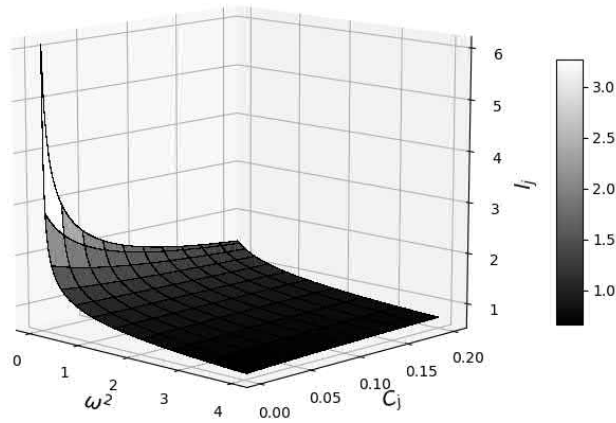


Figure 2: l_j in function as C_j and ω^2 when $l_i = 1$.

whose eigenvalues determine the behavior of the linearized system. The characteristic equation reads

$$\lambda^4 + \left(2\omega^2 - \frac{\partial^2 U_{m3}}{\partial \xi^2} - \frac{\partial^2 U_{m3}}{\partial \eta^2}\right)\lambda^2 + \left(\frac{\partial^2 U_{m3}}{\partial \xi^2} + \frac{\partial^2 U_{m3}}{\partial \eta^2}\right)\omega^2 + \omega^4 - \left(\frac{\partial^2 U_{m3}}{\partial \xi \eta}\right)^2 + \frac{\partial^2 U_{m3}}{\partial \xi^2} \frac{\partial^2 U_{m3}}{\partial \eta^2} = 0. \tag{40}$$

The conditions that insure linear stability are given by the root of the quadratic formula

$$G_1(B_1, B_2, C_1, C_2, \mu) \equiv \left(2\omega^2 - \frac{\partial^2 U_{m3}}{\partial \xi^2} - \frac{\partial^2 U_{m3}}{\partial \eta^2}\right)^2 - 4\left(\left(\frac{\partial^2 U_{m3}}{\partial \xi^2} + \frac{\partial^2 U_{m3}}{\partial \eta^2}\right)\omega^2 + \omega^4 - \left(\frac{\partial^2 U_{m3}}{\partial \xi \eta}\right)^2 + \frac{\partial^2 U_{m3}}{\partial \xi^2} \frac{\partial^2 U_{m3}}{\partial \eta^2}\right) > 0 \tag{41}$$

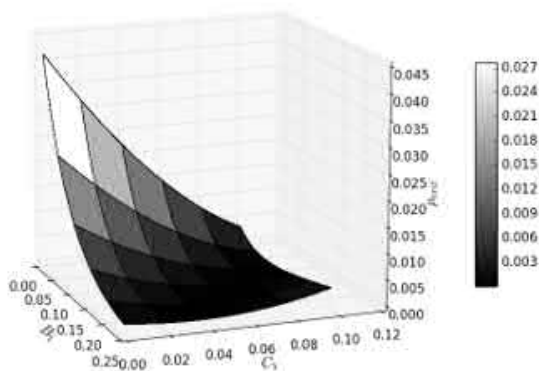


Figure 3: μ_{crit} as a function of B_1 and C_1 when $B_2 = C_2 = 0.1$.

and by the sign of the part outside the root

$$G_1(B_1, B_2, C_1, C_2, \mu) \equiv 2\omega^2 - \frac{\partial^2 U_{m3}}{\partial \xi^2} - \frac{\partial^2 U_{m3}}{\partial \eta^2} > 0. \quad (42)$$

Both conditions must be fulfilled in order to have spectral stability. Five dimensions are needed to visualize the regions of the parameter domain and the values of μ for which the spectral stability exists. One way to display the data in three dimensions is to make projections: fix B_1 and B_2 and graph μ_{crit} (the maximum value of μ that satisfies both conditions) as a function of B_2 and C_2 (see Figures 3 and 4).

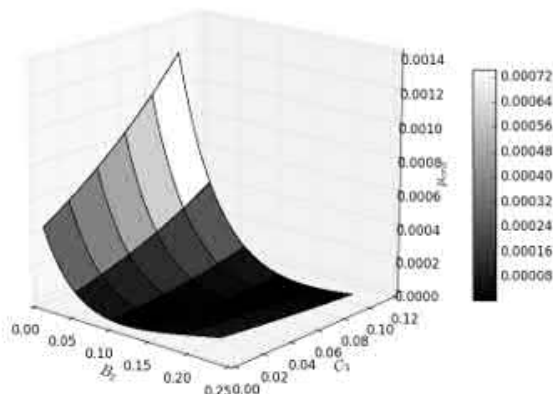


Figure 4: μ_{crit} as a function of B_2 and C_2 when $B_1 = C_1 = 0.1$.

5 Conclusion

We have shown that always the primaries are in a rotational equilibrium (a.k.a, when the coefficients belong to the parameter domain), there is a collinear and a non-collinear relative equilibrium in the restricted three body problem induced by this configuration. Knowing the exact numerical value of these coefficients allows a direct calculation of the position of these equilibrium points.

Also, we discussed the particular case when the non-collinear relative equilibrium is in an isosceles configuration with the primaries, plotting its value given ω^2 , C_j and $l_i = 1$. Finally, we provided two conditions necessary to have spectral stability for a given non-collinear equilibrium point. With these conditions, we plotted μ_{crit} for some values of the parameter domain.

6 References

- [1] J.A. Arredondo, J. Guo, C. Stoica and C. Tamayo. On the restricted three body problem with oblate primaries. *Astrophysics and space science* **341** (2012) 315–322.
- [2] R. Bousso. *Workshop on Conference on the Future of Theoretical Physics and Cosmology in Honor of Steven Hawking's 60th Birthday*, pages 539–569, 2002.
- [3] S. Carroll. *Lecture Notes on General Relativity*. Institute of Theoretical Physics, University of California, 1997.
- [4] D.H. Clark and J.L. Caswell. A Study of Galactic Supernova Remnants. *Monthly Notices of the Royal Astronomical Society* **174** (2) (1976) 267–305.
- [5] A. Celletti. *Stability and Chaos in Celestial Mechanics*. Springer, 2010.
- [6] V. Daftardar-Gejji. A generalization of Brinkmann's theorem. *General Relativity and Gravitation* **30** (5) (1998) 695–700.
- [7] W de Sitter. On Einsteins Theory of Gravitation and its Astronomical Consequences. *Monthly Notices of the Royal Astronomical Society* **76** (9) (1916) 699–728.
- [8] H. Mohajan. A Brief Analysis of de Sitter Universe in Relativistic Cosmology. *Journal of Scientific Achievements* **2** (11) (2017) 1–17.
- [9] V. Mioc and M. Stavinschi. The Schwarzschild de Sitter problem I. *Rom. Astron. J.* **8** (2) (1998) 125–138.
- [10] H. Nariai. On Some Static Solutions of Einstein's Gravitational Field Equations in a Spherically Symmetric Case. *General Relativity and Gravitation* **31** (1999) 951–961.
- [11] V. Prasolov. *Polynomials. Algorithms and Computation in Mathematics*. Springer, 2010.
- [12] H. Stephani, D. Kramer, M. MacCallum, C. Hoenselaers and E. Herlt. *Exact Solutions of Einstein's Field Equations*. Cambridge University Press, 2003.
- [13] J. Van Loon. Ophiuchi and the Recurrent Nova Phenomenon. *ASP Conference Series* **401** (2006) 90–101.
- [14] F. Zwicky. *Adventures in de Sitter Space*. Springer-Verlag, Berlin, 1957.



R-Functions and Nonlinear Galerkin Method for Solving the Nonlinear Stationary Problem of Flow around Body of Revolution

A. V. Artiukh¹, M. V. Sidorov¹ and S. M. Lamtyugova^{2*}

¹ *Department of Applied Mathematics, Kharkiv National University of Radioelectronics, Kharkiv, Ukraine*

² *Department of Advanced Mathematics, O. M. Beketov National University of Urban Economy in Kharkiv, Kharkiv, Ukraine*

Received: May 28, 2018; Revised: March 7, 2021

Abstract: In the paper the steady flow of viscous incompressible fluid around a body of revolution is considered. The mathematical model of the process under consideration is the external boundary value problem for the stream function. For solving this problem a numerical method is proposed. The method is based on the joint use of the R-functions by V.L. Rvachev and the nonlinear Galerkin method. With the help of the R-functions, the problem solution structure is constructed. The structure exactly satisfies all the boundary conditions of the problem and has the necessary behavior at infinity. To approximate the uncertain components of the structure, the nonlinear Galerkin method is used. A computational experiment was carried out for the problem of the flow around a sphere, two touching, and two jointed spheres at different Reynolds numbers.

Keywords: *steady flow; viscous incompressible fluid; external boundary value problem; stream function; R-functions method; nonlinear Galerkin method.*

Mathematics Subject Classification (2010): 65N30, 76D05, 76D17.

* Corresponding author: <mailto:maliatko@gmail.com>

1 Introduction

Let us consider the nonlinear steady-state problem of the viscous incompressible fluid flow past a body of revolution in a spherical coordinate system [11, 16]:

$$\nu E^2\psi = \frac{1}{r^2 \sin \theta} \left(\frac{\partial \psi}{\partial \theta} \frac{\partial E\psi}{\partial r} - \frac{\partial \psi}{\partial r} \frac{\partial E\psi}{\partial \theta} \right) + \frac{1}{r^2 \sin \theta} \left(2\text{ctg}\theta \frac{\partial \psi}{\partial r} - \frac{2}{r} \frac{\partial \psi}{\partial \theta} \right) E\psi \text{ in } \Omega, \quad (1)$$

$$\psi|_{\partial\Omega} = 0, \quad \frac{\partial \psi}{\partial \mathbf{n}} \Big|_{\partial\Omega} = 0, \quad (2)$$

$$\lim_{r \rightarrow +\infty} \psi \cdot r^{-2} = \frac{1}{2} U_\infty \sin^2 \theta, \quad (3)$$

where $\nu = \text{Re}^{-1}$ is the coefficient of viscosity, Re is the Reynolds number, $\psi = \psi(r, \theta)$ is the stream function, $E\psi = \frac{\partial^2 \psi}{\partial r^2} + \frac{\sin \theta}{r^2} \frac{\partial}{\partial \theta} \left(\frac{1}{\sin \theta} \frac{\partial \psi}{\partial \theta} \right)$, $E^2\psi = E(E\psi)$, \mathbf{n} is the outer normal to $\partial\Omega$, U_∞ is the unperturbed fluid velocity at infinity.

The methods of solving problem (1) – (3) have not been sufficiently developed. This is due to the fourth order and nonlinearity of equation (1), as well as the unboundedness of the region in which equation (1) is considered.

Mathematical modeling is becoming an increasingly effective tool for researchers in the study of viscous fluid dynamics. The need to model such flows arises, for example, in hydrodynamics, thermal energy, chemical kinetics, biomedicine, radio electronics, etc. [2,11,14–16]. Due to using a computer, one can obtain an overall picture of the entire fluid flow and graphically visualize the velocity, pressure, or temperature fields throughout the flow region.

The purpose of the paper is to develop a new method of mathematical modeling for the nonlinear stationary problem of the flow of viscous incompressible fluid around a body of revolution on the basis of the R-functions method and nonlinear Galerkin method.

The use of the R-functions method [17, 18] to construct the boundary value problem solution structure will allow us to accurately take into account the geometric and analytical information included into the statement of the problem. Using further the nonlinear Galerkin method [6, 13] to approximate the uncertain components of the structure will allow us to obtain an approximate solution in an analytical form.

2 R-Functions Method

The R-functions method applied to hydrodynamics problems of viscous fluid (steady and unsteady flows) in bounded domains or in the presence of helical symmetry was used in [1, 3, 12]. The problems of the steady flow of viscous fluid past bodies of revolution were solved using the R-functions method in [4, 5, 7–10], but there the authors considered the slow flow of viscous incompressible fluid past bodies (the Stokes linearization) or the application of the R-functions method, successive approximations and Galerkin-Petrov method for calculating the axisymmetric steady flows of viscous incompressible fluid.

To apply the R-functions method to the problems of hydrodynamics it is necessary:

- 1) To construct such a function that is equal to zero at the boundary points, positive inside the region and whose normal derivative (in the direction of the outer normal)

on the boundary is equal to -1 . It will allow to accurately describe analytically the geometry of the computational domain and to continue the functions and operators, defined on the boundary, at the interior points of the area.

- 2) To construct the general structure of the solution, i.e., such a formula that depends on some indeterminate functions and exactly satisfies all the boundary conditions of the problem for any choice of these functions.
- 3) To construct an approximate solution by approximating the undefined functions included in the structure by the chosen numerical method.

Let us consider the general principles of the R-functions method theory [9, 17, 18].

Definition 2.1 A function whose sign is completely determined by the signs of its arguments is called an R-function (V.L. Rvachev's function) corresponding to the partition of the numerical axis into intervals $(-\infty, 0)$ and $[0, +\infty)$, i.e., a function $z = f(x, y)$ is called the R-function if there exists a Boolean function F such that $S[z(x, y)] = F[S(x), S(y)]$, where $S(x) = \begin{cases} 0, & x < 0, \\ 1, & x \geq 0 \end{cases}$ is a two-valued predicate. In this case, the Boolean function F is called a companion function.

Each R-function is associated with a Boolean function. It allows us to use logic algebra methods to describe complex geometric objects.

The following system \mathfrak{R}_α is the most commonly used system of the R-functions:

$$\bar{x} \equiv -x,$$

$$x \wedge_\alpha y \equiv \frac{1}{1+\alpha} \left(x + y - \sqrt{x^2 + y^2 - 2\alpha xy} \right),$$

$$x \vee_\alpha y \equiv \frac{1}{1+\alpha} \left(x + y + \sqrt{x^2 + y^2 - 2\alpha xy} \right),$$

where $-1 < \alpha(x, y) \leq 1$, $\alpha(x, y) \equiv \alpha(y, x) \equiv \alpha(-x, y) \equiv \alpha(x, -y)$. Their companion Boolean functions are, respectively, negation, conjunction and disjunction.

Suppose that a geometric object Ω with a piecewise-smooth boundary $\partial\Omega$ is given in \mathbb{R}^2 . Let us assume that Ω can be constructed from auxiliary (supporting) loci $\Sigma_1 = \{\omega_1(x, y) \geq 0\}$, ..., $\Sigma_m = \{\omega_m(x, y) \geq 0\}$ according to the logical rules defined by the Boolean function F , by means of the operations of union, intersection, and complement:

$$\Omega = F(\Sigma_1, \Sigma_2, \dots, \Sigma_m),$$

and all functions $\omega_i(x, y)$ ($i = 1, 2, \dots, m$) are elementary. Replacing Ω by $\omega(x, y)$, Σ_i by $\omega_i(x, y)$ ($i = 1, 2, \dots, m$), and the symbols $\{\cap, \cup, \neg\}$ by the R-operations symbols $\{\wedge_\alpha, \vee_\alpha, \bar{}\}$, we obtain an analytic expression that defines in the elementary functions the equation of the boundary $\omega(x, y) = 0$. In this case, $\omega(x, y) > 0$ for the interior points of the region, and $\omega(x, y) < 0$ for the external points.

Thus, the equation $\omega(x, y) = 0$ in an implicit form determines the locus of points representing the boundary $\partial\Omega$ of the domain Ω , and the function $\omega(x, y) = 0$ has the form of a single analytic expression.

Definition 2.2 The equation $\omega(x, y) = 0$ is called normalized to the n -th order if

$$\omega|_{\partial\Omega} = 0, \quad \frac{\partial\omega}{\partial\mathbf{n}}\Big|_{\partial\Omega} = -1, \quad \frac{\partial^l\omega}{\partial\mathbf{n}^l}\Big|_{\partial\Omega} = 0 \quad (l = 2, 3, \dots, n),$$

where \mathbf{n} is a vector of the outer normal to $\partial\Omega$.

The equation $\omega(x, y) = 0$, normalized to the first order, can be obtained from the equation $\omega_1(x, y) = 0$ as follows.

Theorem 2.1 *If $\omega_1(x, y) \in C^m(\mathbb{R}^2)$ satisfies the conditions $\omega_1|_{\partial\Omega} = 0$ and $\frac{\partial\omega_1}{\partial\mathbf{n}}\Big|_{\partial\Omega} > 0$, then the function $\omega \equiv \frac{\omega_1}{\sqrt{\omega_1^2 + |\nabla\omega_1|^2}} \in C^{m-1}(\mathbb{R}^2)$ satisfies the conditions*

$$\omega|_{\partial\Omega} = 0, \quad \frac{\partial\omega}{\partial\mathbf{n}}\Big|_{\partial\Omega} = -1 \text{ at all regular points of the boundary } \partial\Omega.$$

To construct the equation normalized to the first order, one can also use the formula

$$\omega \equiv \frac{\omega_1}{|\nabla\omega_1|}$$

if $|\nabla\omega_1| \neq 0$ in $\bar{\Omega} = \Omega \cup \partial\Omega$.

Let us construct the normalized equation $\omega(x, y) = 0$ of the boundary of the closed area $\bar{\Omega} = \left\{0 \leq x \leq 3, \quad 3 - \sqrt{9 - x^2} \leq y \leq 3\right\}$ with the help of the system \mathfrak{R}_0 (Figure 1).

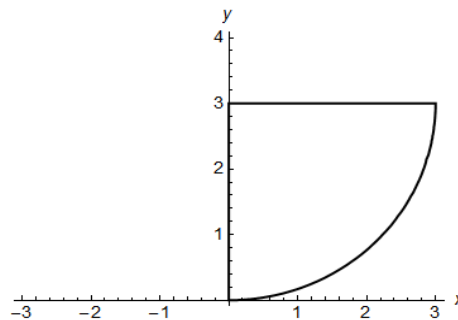


Figure 1: The area $\bar{\Omega}$.

The area $\bar{\Omega}$ can be constructed from the following primitive regions:

- the interior of a circle of radius 3 centered at the point $(0, 3)$:
 $\Sigma_1 = \left(\frac{1}{6} \left(9 - x^2 - (y - 3)^2\right) \geq 0\right),$
- the half-plane below the line $y = 3$: $\Sigma_2 = (3 - y \geq 0),$
- the half-plane to the right of the line $x = 0$: $\Sigma_3 = (x \geq 0).$

Then $\bar{\Omega} = \Sigma_1 \wedge \Sigma_2 \wedge \Sigma_3$ and the equation of the boundary of the area Ω is determined by the equation $\omega(x, y) = 0$, where

$$\begin{aligned} \omega(x, y) &= \left[\frac{1}{6} (9 - x^2 - (y - 3)^2) \right] \wedge_0 [3 - y] \wedge_0 x = \\ &= \left[\frac{1}{6} (9 - x^2 - (y - 3)^2) \right] \wedge_0 \left[3 - y + x - \sqrt{(3 - y)^2 + x^2} \right] = \\ &= \frac{1}{6} (9 - x^2 - (y - 3)^2) + 3 - y + x - \sqrt{(3 - y)^2 + x^2} - \\ &-\sqrt{\left[\frac{1}{6} (9 - x^2 - (y - 3)^2) \right]^2 + \left[3 - y + x - \sqrt{(3 - y)^2 + x^2} \right]^2}. \end{aligned} \quad (4)$$

The contour lines of the obtained normalized boundary equation (4) are shown in Figure 2.

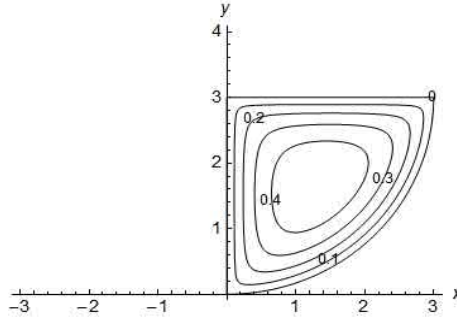


Figure 2: The area $\bar{\Omega}$.

The constructed function (4) is positive inside the area Ω and negative outside Ω . If it is necessary to obtain a function that is positive in the exterior of the finite area Ω , then it is required to use the function $-\omega(x, y)$.

Let us consider the problem

$$Au = f, \quad (5)$$

$$L_i u|_{\partial\Omega_i} = \varphi_i, \quad i = \overline{1, m}, \quad (6)$$

where A and L_i are some differential operators; f and φ_i are functions defined inside the region Ω and on its boundary regions $\partial\Omega_i$.

Definition 2.3 The expression $u = B(\Phi, \omega, \{\omega_i\}_{i=1}^m, \{\varphi_j\}_{j=1}^m)$ is called the general structure of the solution of the boundary value problem (5) – (6) if it exactly satisfies the boundary conditions (6) for any choice of the indeterminate component Φ . Here, B is an operator that depends on the geometry of the area Ω and parts $\partial\Omega_i$ of its border, as well as the operators of the boundary conditions, but does not depend on the type of the operator A and the function f .

The solution structure extends the boundary conditions inside the region.

The undefined component Φ of the solution structure in the R-functions method is represented as a sum

$$\Phi(x, y) \approx \Phi_n(x, y) = \sum_{k=1}^n c_k \varphi_k(x, y),$$

where $\varphi_k(x, y)$ are known elements of the complete functional sequence, and c_k ($k = 1, 2, \dots, n$) are unknown coefficients of the expansion. To determine unknown coefficients one can use, for example, variational methods (Ritz, least squares, etc.), projection methods (Galerkin, collocations, etc.), grid methods and others.

3 The Method for Solving Problem (1) – (3)

For an exact analytical description of the geometry of computational domain, let us introduce a function $\omega(r, \theta)$ satisfying the conditions:

$$\text{a) } \omega(r, \theta) > 0 \text{ in } \Omega, \quad \text{b) } \omega(r, \theta)|_{\partial\Omega} = 0, \quad \text{c) } \left. \frac{\partial\omega}{\partial\mathbf{n}} \right|_{\partial\Omega} = -1,$$

where \mathbf{n} is the outer normal to $\partial\Omega$.

Let us introduce the function [3]

$$\omega_M = f_M(\omega) = \begin{cases} 1 - \exp \frac{M\omega}{\omega - M}, & 0 \leq \omega < M; \\ 1, & \omega \geq M \quad (M = \text{const} > 0), \end{cases} \quad (7)$$

that satisfies the conditions:

$$1) \omega_M > 0 \text{ in } \Omega, \quad 2) \omega_M|_{\partial\Omega} = 0, \quad 3) \left. \frac{\partial\omega_M}{\partial\mathbf{n}} \right|_{\partial\Omega} = -1, \quad 4) \omega_M \equiv 1 \text{ if } \omega_M \geq M.$$

The introduction of the function (7) allows us to carry out calculations in the finite region since function (7) differs from unity only in some finite ring-shaped region $\{0 \leq \omega(r, \theta) < M\}$ adjacent to the contour $\partial\Omega$.

Let us construct the general structure of the solution. In [7, 9, 10] it was proved that for any choice of sufficiently smooth functions Φ_1 and Φ_2 ($\Phi_1 \cdot r^{-2} \rightarrow 0$ as $r \rightarrow +\infty$) the boundary conditions (2) and the condition at infinity (3) are exactly satisfied by a function of the form

$$\psi = \omega_M^2(\psi_0 + \Phi_1) + \omega_M^2(1 - \omega_M)\Phi_2, \quad (8)$$

where $\psi_0 = \frac{1}{4}U_\infty(r - R)^2 \left(2 + \frac{R}{r}\right) \sin^2 \theta$ is the Stokes solution for the problem of the flow past a sphere of radius R (the sphere of radius R lies entirely inside the streamlined body). Thus, the function (8) is the structure of the solution of the boundary value problem (1) – (3).

Let us construct an approximate solution by approximating the undefined components Φ_1 and Φ_2 of structure (8) by the nonlinear Galerkin method [6, 13]. The functions Φ_1 and Φ_2 will be presented in the form

$$\Phi_1 \approx \Phi_1^{m_1} = \sum_{k=1}^{m_1} \alpha_k \cdot \varphi_k, \quad \Phi_2 \approx \Phi_2^{m_2} = \sum_{j=1}^{m_2} \beta_j \cdot \tau_j,$$

where

$$\{\varphi_k(r, \theta)\} = \{r^{1-k} J_k(\cos \theta), k = 2, 3, \dots; r^{3-k} J_k(\cos \theta), k = 4, 5, \dots\}$$

is a complete system of particular solutions of the equation $E^2\psi = 0$ with respect to the exterior of a sphere of finite radius;

$$\{\tau_j(r, \theta)\} = \{rJ_2(\cos \theta), J_3(\cos \theta), r^j J_j(\cos \theta), r^{j+2} J_j(\cos \theta), j = 2, 3, \dots\}$$

is a complete system of particular solutions of the equation $E^2\psi = 0$ relative to the domain $\{\omega(r, \theta) < M\}$, $J_k(\cos \theta)$ are the Gegenbauer functions of the first kind.

Thus, the approximate solution of the problem (1) – (3) is sought in the form

$$\psi_N = \omega_M^2 \left(\frac{1}{4} U_\infty (r - R)^2 \left(2 + \frac{R}{r} \right) \sin^2 \theta + \sum_{k=1}^{m_1} \alpha_k \cdot \varphi_k \right) + \omega_M^2 (1 - \omega_M) \cdot \sum_{j=1}^{m_2} \beta_j \cdot \tau_j.$$

The complete with respect to the whole plane sequence of functions has the form

$$\{\phi_i(r, \theta)\} = \{\omega_M^2(r, \theta) \varphi_k(r, \theta), \omega_M^2(r, \theta) (1 - \omega_M(r, \theta)) \tau_j(r, \theta)\}. \quad (9)$$

The values of the coefficients α_k ($k = 1, 2, \dots, m_1$) and β_j ($j = 1, 2, \dots, m_2$) in accordance with the nonlinear Galerkin method [6, 13] will be found from the condition of the residual orthogonality to the first N ($N = m_1 + m_2$) elements of the sequence (9):

$$\left(\nu E^2 \psi_N - \frac{1}{r^2 \sin \theta} \left(\frac{\partial \psi_N}{\partial \theta} \frac{\partial E \psi_N}{\partial r} - \frac{\partial \psi_N}{\partial r} \frac{\partial E \psi_N}{\partial \theta} \right) - \frac{1}{r^2 \sin \theta} \left(2 \operatorname{ctg} \theta \frac{\partial \psi_N}{\partial r} - \frac{2}{r} \frac{\partial \psi_N}{\partial \theta} \right) E \psi_N, \phi_i \right) = 0, \quad i = \overline{1, N}.$$

As a result, a system of nonlinear equations is obtained, where each equation is a quadratic function with respect to α_k and β_j . This system can be solved by the Newton method. As an initial approximation, a set of α_k and β_j is chosen corresponding to the solution of the Stokes problem, or, for large Reynolds numbers, to the solution obtained for smaller Reynolds numbers.

4 Computational Experiment

A computational experiment was carried out for the problems of the flow around a sphere, two touching, and two jointed spheres. The double integrals in the systems for determining α_k and β_j were taken approximately by the Gauss formula with 50 nodes for each variable.

4.1 First problem

The problem of the flow past a sphere $x^2 + y^2 + z^2 = 1$ at $U_\infty = 1$, $M = 10$, $m_1 = 10$, $m_2 = 14$, $\operatorname{Re} = 10; 20; 25$, is solved.

The normalized equation of the boundary (in the plane $\varphi = 0$) has the form

$$\omega(x, z) = \frac{1}{2}(1 - x^2 - z^2) = 0.$$

The streamlined contours of the obtained approximate solution are shown in Figure 3. Figure 4 shows detailed pictures of the streamlined contours and vector fields of velocities behind the sphere. For small Reynolds numbers, the flow around a sphere is symmetrical, without the formation of a detachment zone in the aft region of the body. With an increase in the Reynolds number to approximately 20–25, the secondary vortices appear behind the body and then their size and intensity increase.

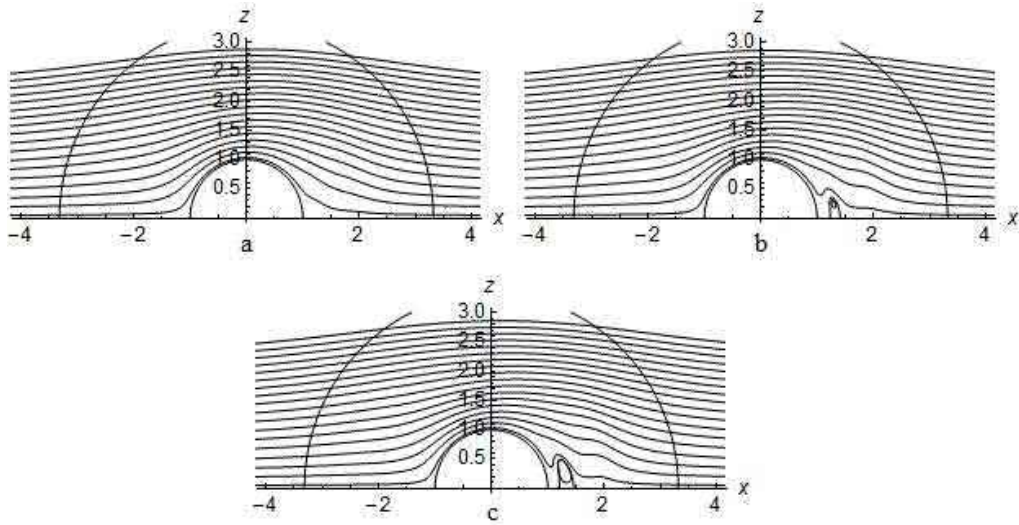


Figure 3: The streamlined contours for the problem of the flow past a sphere: (a) $Re = 10$, (b) $Re = 20$, (c) $Re = 25$.

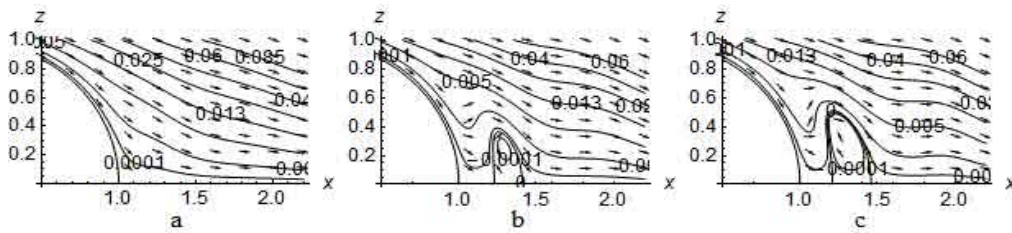


Figure 4: Detailed pictures of streamlined contours and vector fields of velocities behind the sphere: (a) $Re = 10$, (b) $Re = 20$, (c) $Re = 25$.

The results obtained are in good agreement with the results obtained by the method of successive approximations [8] (for $Re \leq 10$), known results of physical experiments [20] and results obtained by other authors [2, 19], which indicates the effectiveness of the developed numerical method.

4.2 Second problem

The problem of the flow past two touching spheres, bounded by surfaces $(x-1)^2 + y^2 + z^2 = 1$, $(x+1)^2 + y^2 + z^2 = 1$, at $U_\infty = 1$, $M = 10$, $m_1 = 10$, $m_2 = 14$, $\text{Re} = 30; 60; 70$, is solved.

The normalized equation of the boundary (in the plane $\varphi = 0$) has the form

$$\omega(x, z) = \left[\frac{1}{2} \left(1 - (x-1)^2 - z^2 \right) \right] \wedge_0 \left[\frac{1}{2} \left(1 - (x+1)^2 - z^2 \right) \right] = 0.$$

The streamlined contours of the obtained approximate solution are shown in Figure 5. Figure 6 shows detailed pictures of the streamlined contours and vector fields of velocities behind the spheres and in the hollow between them. The computational experiment showed that as the Reynolds number increases to approximately 60, vortices appear behind the body.

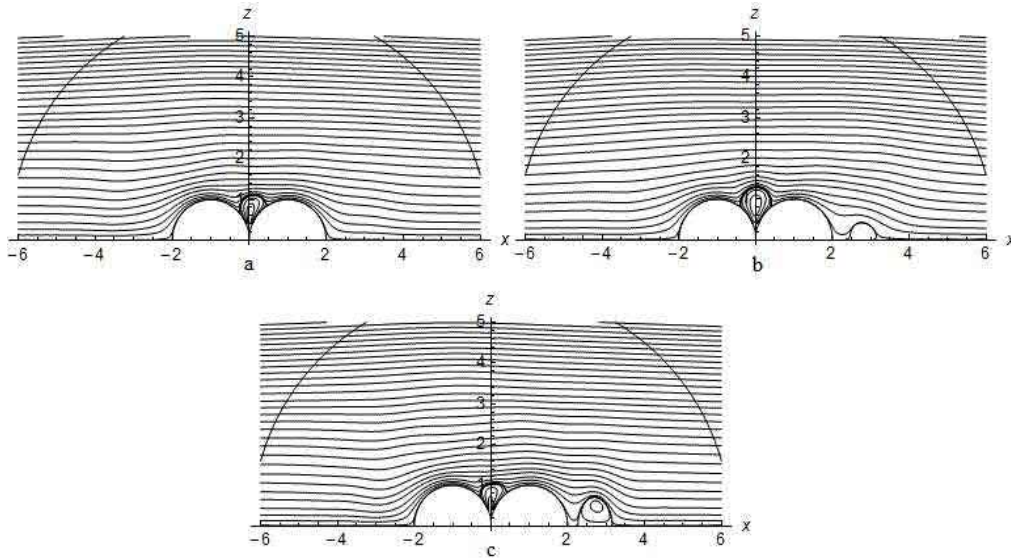


Figure 5: The streamlined contours for the problem of the flow past two touching spheres: (a) $\text{Re} = 30$, (b) $\text{Re} = 60$, (c) $\text{Re} = 70$.

4.3 Third problem

The problem of the flow past two jointed spheres, bounded by surfaces $\left(x - \frac{1}{2}\right)^2 + y^2 + z^2 = 1$, $\left(x + \frac{1}{2}\right)^2 + y^2 + z^2 = 1$, at $U_\infty = 1$, $M = 10$, $m_1 = 10$, $m_2 = 14$, $\text{Re} = 5; 10; 30$, is solved.

The normalized equation of the boundary (in the plane $\varphi = 0$) has the form

$$\omega(x, z) = \left[\frac{1}{2} \left(1 - \left(x - \frac{1}{2}\right)^2 - z^2 \right) \right] \wedge_0 \left[\frac{1}{2} \left(1 - \left(x + \frac{1}{2}\right)^2 - z^2 \right) \right] = 0.$$

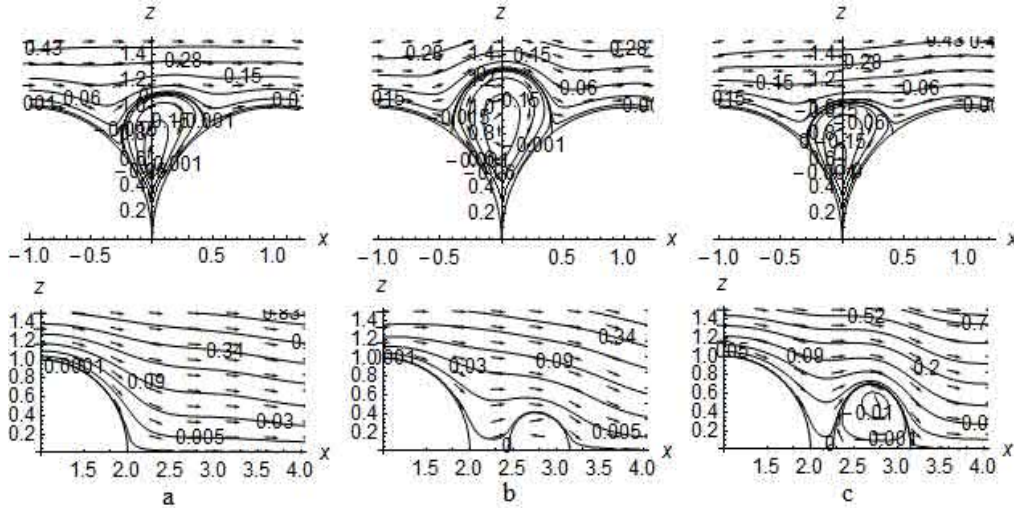


Figure 6: Detailed pictures of streamlined contours and vector fields of velocities behind the spheres in the hollow between them: (a) $Re = 30$, (b) $Re = 60$, (c) $Re = 70$.

The streamlined contours of the obtained approximate solution are shown in Figure 7. Figure 8 shows detailed pictures of the streamlined contours and vector fields of velocities behind the spheres. The computational experiment showed that as the Reynolds number increases to approximately 10, vortices appear behind the body.

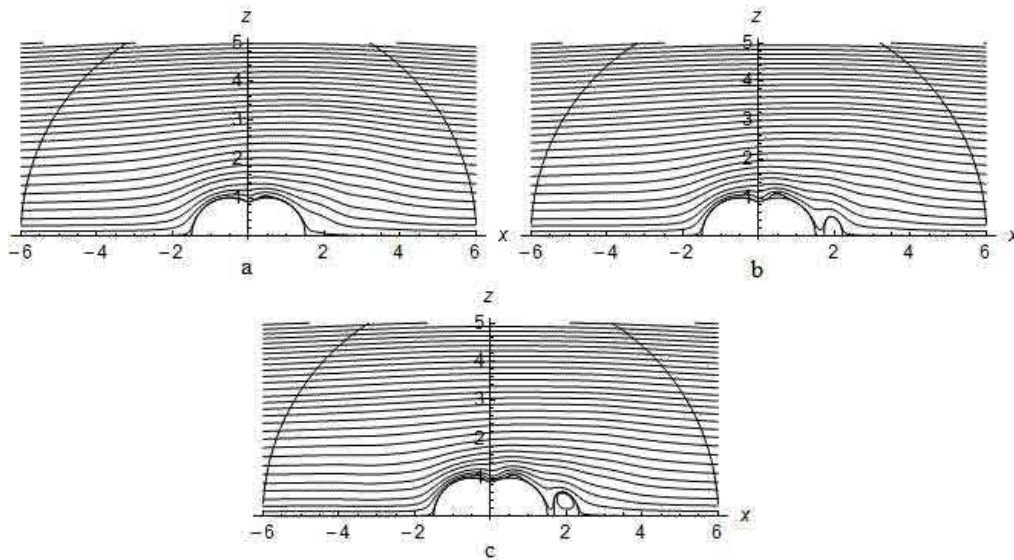


Figure 7: The streamlined contours for the problem of the flow past two jointed sphere: (a) $Re = 5$, (b) $Re = 10$, (c) $Re = 30$.

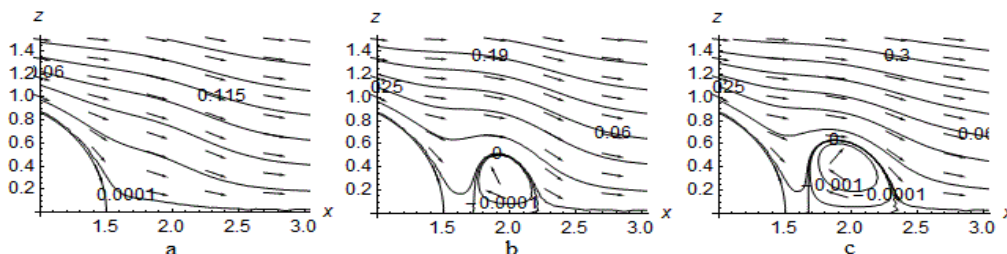


Figure 8: Detailed pictures of streamlined contours and vector fields of velocities behind the spheres: (a) $Re = 5$, (b) $Re = 10$, (c) $Re = 30$.

5 Conclusions

A new numerical method for solving the problem of the flow of viscous incompressible fluid past a body of revolution is proposed based on the joint application of the R-function method and the nonlinear Galerkin method. The advantage of the proposed method is that the method algorithm does not change when the domain geometry is changed, and the solution structure accurately takes into account both the boundary conditions on the boundary of the streamlined body and the condition at infinity. For various Reynolds numbers, the stationary problem of the flow past a body of revolution in a spherical coordinate system for a sphere, two touching, and two jointed spheres is solved numerically. The Reynolds numbers, at which secondary vortices appear behind the body, are experimentally determined for each body.

References

- [1] A. Artyukh and M. Sidorov. Mathematical modeling and numerical analysis of nonstationary plane-parallel flows of viscous incompressible fluid by R-functions and Galerkin method. *Econtechmod* **3** (3) (2014) 3–11.
- [2] G. K. Batchelor. *An Introduction to Fluid Dynamics*. Cambridge University Press, 1967.
- [3] S. V. Kolosova. *The use of projection methods and R-functions method to the solution of boundary value problems in infinite domains*. PhD thesis. Kharkiv: Kharkiv National University of Radioelectronics, 1972. [Russian]
- [4] S. V. Kolosova, S. N. Lamtyugova and M. V. Sidorov. On one method of numerical analysis of viscous flows, complicated with the mass transfer (flow problem). *Radioelectron. Inform.* **1** (64) (2014) 25–30. [Russian]
- [5] S. V. Kolosova, S. N. Lamtyugova and M. V. Sidorov. The iterative methods application to solving the external tasks of hydrodynamics. *Radioelectron. Inform.* **3** (2012) 13–17. [Russian]
- [6] M. A. Krasnoselskiy, G. M. Vainikko, P. P. Zabreiko, Va. B. Rutitskii and V. Va. Stecenko. *Approximate Solution of Operator Equations*. Wolters-noordhoff publishing, Groningen, 1972. DOI: 10.1007/978-94-010-2715-1.
- [7] S. N. Lamtyugova. Mathematical modelling of flow linearized problems in the spherical and cylindrical coordinate systems. *Visn ZNU. Ser. Fiz. Math. Nauky.* **1** (2012) 112–122. [Russian]

- [8] S. N. Lamtyugova. The iterative methods application for calculating the flow over body by stationary current of viscous fluid. *Radioelectron. Inform.* **2** (2015) 49–56. [Russian]
- [9] S. N. Lamtyugova and M. V. Sidorov. Numerical analysis of the external slow flows of a viscous fluid using the R-function method. *J. Eng. Math.* **91** (1) (2015) 59–79. DOI: 10.1007/s10665-014-9746-x.
- [10] S. N. Lamtyugova and M. V. Sidorov. The R-functions method application to calculation of external slow flows of viscous fluid. *Information Extraction and Process* **36** (112) (2012) 56–62. [Ukrainian]
- [11] L. G. Loitsyansky. *Mechanics of Liquids and Gases*. Begell House, New York, 2003.
- [12] K. V. Maksimenko-Shejko. Mathematical modeling of heat transfer at motion of fluid through the channels with the screw type symmetry of the R-functions method. *Dop. NAN Ukr.* **9** (2005) 41–46. [Russian]
- [13] S. G. Mikhlin. *Variational Methods in Mathematical Physics*. Pergamon Press, Oxford, 1964.
- [14] A. Najafi and B. Raeisy. Boundary Stabilization of a Plate in Contact with a Fluid. *Nonlinear Dynamics and Systems Theory* **12** (2) (2012) 193–205.
- [15] W. Parandyk, D. Lewandowski and J. Awrejcewicz. Mathematical Modeling of the Hydro-Mechanical Fluid Flow System on the Basis of the Human Circulatory System. *Nonlinear Dynamics and Systems Theory* **15** (1) (2015) 50–62.
- [16] A. D. Polyinin, A. M. Kutepov, D. A. Kazenin and A. V. Vyazmin. *Hydrodynamics, Mass and Heat Transfer in Chemical Engineering*. CRC Press, Taylor & Francis Group, 2002.
- [17] V. L. Rvachev. *Theory of R-functions and its Some Applications*. Kiev: Nauk. Dumka, 1982. [Russian]
- [18] V. Shapiro. Semi-analytic geometry with R-functions. *Acta Numer.* **16** (2007) 239–303. DOI: 10.1017/S096249290631001X.
- [19] Y. Taamneh. CFD Simulations of Drag and Separation Flow Around Ellipsoids. *Jordan Journal of Mechanical and Industrial Engineering* **5** (2) (2011) 129–132.
- [20] M. Van-Dajk. *Album of Fluid and Gas Flows*. Moscow: Mir, 1986. [Russian]



Analysis of Dynamic Frictional Contact Problem for Electro-Elastic Materials

O. Baiz^{1*} and H. Benaissa²

¹ *Ibn Zohr University, FP of Ouarzazate, Morocco.*

² *Sultan Moulay Slimane University, FP of Khouribga, Morocco.*

Received: August 24, 2020; Revised: March 19, 2021

Abstract: In this paper, we study a dynamic frictional contact problem for a piezoelectric body and an electrically conductive foundation. The frictional contact is modeled by a normal compliance condition that depends on both the interpenetrations and the electrical potential difference between the body and the foundation on the contact interface, coupled with a version of Coulomb's law of dry friction with a slip dependent friction coefficient and regularized normal stress, and with an electrical contact condition in which the electrical conductivity coefficient depends on the normal velocity. First, we consider our frictional electro-elastic model and after introducing a convenient functional framework, we derive its weak formulation. Next, we establish the existence and uniqueness result for the weak solution to the problem. Finally, we study the continuous dependence of the weak solution on the data and prove a first convergence result.

Keywords: *piezoelectric material; dynamic frictional contact; variational inequality; history dependent variational inequality; fixed point arguments; existence and uniqueness result; dependence and convergence results.*

Mathematics Subject Classification (2010): 35J87, 47J20, 49J40, 74F15, 74G30, 74M10, 74M15, 74S05.

* Corresponding author: <mailto:othman.baiz@gmail.com>,

1 Introduction

Due to their intrinsic coupling between mechanical and electrical properties, the piezoelectric materials remain an active area of research and engineering applications. In fact, these materials can serve as sensors, actuators or transducers, and their ability is used in various industrial devices such as medical equipment, fuel injection pistons or piezoelectric composites. Motivated by their importance in various engineering devices, the study of frictional contact phenomena involving piezoelectric materials is still relevant, both in modeling and in analysis, and the literature on this topic is still growing. General models using materials with piezoelectric effects can be found, for example, in [7, 21, 23] and the references therein. The static frictional contact problem for electro-elastic materials was considered in [12, 16–18] under the assumption that the foundation is insulated, and in [19, 20] under the assumption that the foundation is electrically conductive. For quasi-static and dynamic models dealing with electro-elastic or electro-viscoelastic materials, we can see [3, 4, 24] and the references therein.

The present paper is devoted to the variational analysis of a dynamic frictional piezoelectric contact problem under small deformations hypothesis. The material's behavior is described by a nonlinear visco-electro-elastic constitutive law and the contact is modeled with a normal compliance condition that depends on both the interpenetrations and the electrical potential difference between the body and the foundation, coupled with an electrical contact condition in which the electrical conductivity coefficient depends on the normal velocity. The friction is described by a version of Coulomb's law of dry friction in which the slip is supposed to depend on the friction coefficient and the non-local regularized normal contact stress. To the best of our knowledge, such piezoelectric model, coupling the electrical potential dependent compliance contact condition and the velocity dependent electrical contact condition, has not been studied so far. The variational formulation of this problem is different from that studied previously, particularly in [1, 13, 14], and hence it leads to a new mathematical model, which is a system coupling a nonlinear variational inequality for the displacement field and a nonlinear variational equation for the electric potential. Our goal is to prove the unique solvability of this model and to establish some related dependence and convergence results.

The rest of this paper is structured as follows. In Section 2, we introduce some notations and we present our frictional contact model for an electro-elastic body and an electrically conductive foundation. In Section 3, we list assumptions on the data, we derive the weak formulation of the model and we provide a result on its unique weak solvability, stated in Theorem 3.1. The proof of this theorem is given in Section 4 and it is based on the arguments of variational inequalities and the Banach fixed point theorem. Finally, in Section 5, we state and prove our convergence result which states the continuous dependence of the solution on the data.

2 Problem Statement

We consider a piezoelectric body occupying a bounded domain $\Omega \subset \mathbb{R}^d$ ($d = 2, 3$) with a sufficiently regular boundary Γ , partitioned into three disjoint measurable parts Γ_1 , Γ_2 and Γ_3 such that Γ_1 is of non-zero measure. The body is clamped on Γ_1 , a volume force f_0 and volume electric charges q_0 act in Ω and a surface traction f_2 acts on Γ_2 . To describe the electric constraints, we consider a partition of $\Gamma_1 \cup \Gamma_2$ into two disjoint parts Γ_a and Γ_b such that Γ_a is of non-zero measure. We assume the electrical potential vanishes on

Γ_a and a surface electrical charge q_2 is prescribed on Γ_b . In the initial configuration, the body may come in contact over Γ_3 with an electrically conductive foundation. Finally, we suppose that the process is dynamic, and it is studied in a time interval $[0, T]$, where T is a positive finite constant.

To simplify the notation, we do not indicate explicitly the dependence of various functions on the spatial variable $x \in \bar{\Omega}$. The indices i, j, k, l run between 1 and d , the summation convention over repeated indices is used, the index that follows the comma indicates the partial derivative with respect to the corresponding component of the independent variable, e.g., $u_{i,j} = \frac{\partial u_i}{\partial x_j}$, and the dot above the variable represents the derivative with respect to time, e.g., $\dot{u} = \frac{du}{dt}$. Moreover, we denote by \mathbb{S}^d the linear space of second order symmetric tensors on \mathbb{R}^d . We recall that the inner products on \mathbb{R}^d and \mathbb{S}^d are given by $u \cdot v = u_i v_i$ and $\sigma \cdot \tau = \sigma_{ij} \tau_{ij}$, respectively. Throughout the paper, we adopt the notation: $u = (u_i) : \Omega \times (0, T) \rightarrow \mathbb{R}^d$ for the displacement field, $\sigma = (\sigma_{ij}) : \Omega \times (0, T) \rightarrow \mathbb{S}^d$ for the stress tensor, $D = (D_i) : \Omega \times (0, T) \rightarrow \mathbb{R}^d$ for the electric displacement field and $E(\varphi) = (E_i(\varphi)) = -\nabla \varphi$ for the electric vector field, where $\varphi : \Omega \times (0, T) \rightarrow \mathbb{R}$ is the electric potential field. In addition, let ν be the unit outward normal vector on Γ , then the normal and tangential components for a vector field v and stress tensor σ on Γ are given by $v_\nu = v \cdot \nu$, $v_\tau = v - v_\nu \nu$, $\sigma_\nu = (\sigma \nu) \cdot \nu$ and $\sigma_\tau = \sigma \nu - \sigma_\nu \nu$.

Then the classical formulation of our frictional contact problem is as follows.

Problem (P). *Find a displacement field $u : \Omega \times (0, T) \rightarrow \mathbb{R}^d$ and an electric potential field $\varphi : \Omega \times (0, T) \rightarrow \mathbb{R}$ such that*

$$\sigma = \mathcal{A}\varepsilon(\dot{u}) + \mathfrak{F}\varepsilon(u) - \mathcal{E}^* E(\varphi) \quad \text{in } \Omega \times (0, T), \quad (1)$$

$$D = \mathcal{E}\varepsilon(u) + \beta E(\varphi) \quad \text{in } \Omega \times (0, T), \quad (2)$$

$$\rho \ddot{u} = \text{Div } \sigma + f_0 \quad \text{in } \Omega \times (0, T), \quad (3)$$

$$\text{div } D = q_0 \quad \text{in } \Omega \times (0, T), \quad (4)$$

$$u = 0 \quad \text{on } \Gamma_1 \times (0, T), \quad (5)$$

$$\sigma \nu = f_2 \quad \text{on } \Gamma_2 \times (0, T), \quad (6)$$

$$\varphi = 0 \quad \text{on } \Gamma_a \times (0, T), \quad (7)$$

$$D \cdot \nu = q_2 \quad \text{on } \Gamma_b \times (0, T), \quad (8)$$

$$\sigma_\nu = -h_\nu(\varphi - \varphi_F) p_\nu(u_\nu - g) \quad \text{on } \Gamma_3 \times (0, T), \quad (9)$$

$$\left. \begin{aligned} \|\sigma_\tau\| &\leq \mu |R\sigma_\nu(u, \varphi)| \\ \|\sigma_\tau\| &< \mu |R\sigma_\nu(u, \varphi)| \Rightarrow \dot{u}_\tau = 0 \\ \|\sigma_\tau\| &= \mu |R\sigma_\nu(u, \varphi)| \Rightarrow \exists \lambda \in \mathbb{R}_+, \sigma_\tau = -\lambda \dot{u}_\tau \end{aligned} \right\} \quad \text{on } \Gamma_3 \times (0, T), \quad (10)$$

$$D \cdot \nu = p_e(\dot{u}_\nu) h_e(\varphi - \varphi_F) \quad \text{on } \Gamma_3 \times [0, T], \quad (11)$$

$$u(0) = 0, \quad \dot{u}(0) = 0 \quad \text{in } \Omega. \quad (12)$$

Equations (1)–(2) represent the electro-visco-elastic constitutive law of the material. Here, $\varepsilon(u) = (\nabla u + (\nabla u)^\top)/2$ stands for the linearized strain tensor, $\mathcal{A} : \Omega \times \mathbb{S}^d \rightarrow \mathbb{S}^d$ is a nonlinear viscosity tensor, $\mathfrak{F} : \Omega \times \mathbb{S}^d \rightarrow \mathbb{S}^d$ is a nonlinear elasticity tensor, $\mathcal{E} = (e_{ijk}) : \Omega \times \mathbb{S}^d \rightarrow \mathbb{R}^d$ is a linear piezoelectric tensor, $\beta = (\beta_{ij}) : \Omega \times \mathbb{R}^d \rightarrow \mathbb{R}^d$ is a nonlinear electric permittivity tensor and \mathcal{E}^* denotes the transpose tensor of \mathcal{E} defined as follows:

$$\mathcal{E}\sigma \cdot v = \sigma \cdot \mathcal{E}^* v, \quad \forall \sigma \in \mathbb{S}^d, \forall v \in \mathbb{R}^d. \quad (13)$$

Equations (3)–(4) are the equilibrium equations where the mass density ρ is chosen to be normalized $\rho = 1$. Relations (5)–(8) represent the displacement, the traction and the electric boundary conditions. Condition (9) represents the normal compliance contact condition in which p_ν is a prescribed nonnegative function which vanishes when its argument is negative, h_ν is a given positive function, g represents the maximum interpenetration of body's and foundation's asperities and φ_F denotes the electric potential of the foundation. Relations (10) represent Coulomb's friction law written in terms of the tangential components of the velocity \dot{u}_τ and the stress σ_τ , the coefficient of friction μ and the regularized normal stress $R\sigma_\nu$. The normal regularization operator R is introduced in (10) for mathematical considerations since σ_ν is only square-integrable on Ω and hence its trace on a contact surface Γ_3 is not a well-defined function, see [9, 22]. For some examples of such operator, we refer to [7, 9, 22]. Equation (11) is a regularized electrical contact condition where p_e represents the electrical conductivity coefficient which vanishes when its argument is nonnegative and h_e is a given function, see [15]. Finally, conditions (12) represents the initial displacement and the initial velocity.

The variational analysis of Problem (P) will be presented in the next sections, where we give our main existence and uniqueness result for the weak solution of Problem (P).

3 Variational Formulation and Main Result

In this section, we state hypotheses and derive a weak formulation of Problem (P). First, we introduce the following real Hilbert spaces:

$$H = L^2(\Omega)^d, \quad \mathcal{H} = \{\sigma = (\sigma_{ij}); \sigma_{ij} = \sigma_{ji} \in L^2(\Omega)\},$$

$$H_1 = H^1(\Omega)^d, \quad \mathcal{H}_1 = \{\sigma \in \mathcal{H}; \text{Div } \sigma \in H\},$$

endowed with the norms $\|\cdot\|_H$, $\|\cdot\|_{\mathcal{H}}$, $\|\cdot\|_{H_1}$ and $\|\cdot\|_{\mathcal{H}_1}$ induced by the inner products

$$(u, v)_H = \int_{\Omega} u_i v_i \, dx, \quad (\sigma, \tau)_{\mathcal{H}} = \int_{\Omega} \sigma_{ij} \tau_{ij} \, dx,$$

$$(u, v)_{H_1} = (u, v)_H + (\varepsilon(u), \varepsilon(v))_{\mathcal{H}}, \quad (\sigma, \tau)_{\mathcal{H}_1} = (\sigma, \tau)_{\mathcal{H}} + (\text{Div } \sigma, \text{Div } \tau)_H.$$

Let $\gamma : H_1 \rightarrow H_\Gamma = H^{\frac{1}{2}}(\Gamma)^d$ be the trace operator. For every element $v \in H_1$, we also use the notation v to denote the trace γv of v on Γ . Recalling the boundary condition (5), we introduce the following closed subspace of H_1 given by

$$V = \{v \in H_1; v = 0 \text{ on } \Gamma_1\}.$$

Since Γ_1 is of non-zero measure, it follows from Korn's inequality that there exists $c_k > 0$ depending only on Ω and Γ_1 such that

$$\|v\|_{H_1} \leq c_k \|\varepsilon(v)\|_{\mathcal{H}} \quad \text{for all } v \in V. \tag{14}$$

We consider over the space V , the following inner product and associated norm:

$$(u, v)_V = (\varepsilon(u), \varepsilon(v))_{\mathcal{H}}, \quad \|u\|_V = \|\varepsilon(v)\|_{\mathcal{H}} = (u, u)_V^{\frac{1}{2}}. \tag{15}$$

It follows from inequality (14) that the norms $\|\cdot\|_{H_1}$ and $\|\cdot\|_V$ are equivalent on V . Therefore, $(V, \|\cdot\|_V)$ is a Hilbert space. Moreover, by the Sobolev trace theorem, (14) and (15), there exists a constant $c_0 > 0$ depending only on Ω , Γ_3 and Γ_1 such that

$$\|v\|_{L^2(\Gamma_3)^d} \leq c_0 \|v\|_V \quad \text{for all } v \in V. \tag{16}$$

For the real Hilbert space V previously defined, we recall the dense continuous and compact embeddings $V \subset H \subset V'$, where V' denotes the dual space of V , see [5, 25]. For the electric unknowns, we introduce the following spaces:

$$W = \{\xi \in H^1(\Omega) ; \xi = 0 \text{ on } \Gamma_a\}, \quad \mathcal{W} = \{D \in H^1(\Omega) ; \operatorname{div} D \in L^2(\Omega)\},$$

which are real Hilbert spaces for the norms $\|\cdot\|_W$ and $\|\cdot\|_{\mathcal{W}}$ induced by the inner products

$$(\varphi, \xi)_W = (\nabla\varphi, \nabla\xi)_H, \quad (D, E)_{\mathcal{W}} = (D, E)_{L^2(\Omega)^d} + (\operatorname{div} D, \operatorname{div} E)_{L^2(\Omega)}.$$

Since $\operatorname{meas}(\Gamma_a) > 0$, the following Friedrichs-Poincaré inequality holds:

$$\|\xi\|_W \leq c_F \|\nabla\xi\|_{\mathcal{W}} \quad \text{for all } \xi \in W, \quad (17)$$

for a constant $c_F > 0$ which depends only on Ω and Γ_a . Moreover, by the Sobolev trace theorem, there exists a constant $c_1 > 0$, depending only on Ω , Γ_a and Γ_3 , such that

$$\|\xi\|_{L^2(\Gamma_3)} \leq c_1 \|\xi\|_W \quad \text{for all } \xi \in W. \quad (18)$$

Since $\Omega \subset \mathbb{R}^d$ is bounded, it follows from the Korn and Friedrichs-Poincaré inequalities that

$$\|v\|_{L^2(\Omega)^d} \leq c_p \|v\|_V \quad \text{for all } v \in V, \quad (19)$$

$$\|\xi\|_{L^2(\Omega)} \leq c'_p \|\xi\|_W \quad \text{for all } \xi \in W, \quad (20)$$

for some nonnegative constants c_p and c'_p . Finally, for any Hilbert space X , let X' denote the dual space of X , $\langle \cdot, \cdot \rangle_{X' \times X}$ denote the duality pairing between X' and X and the notations $C(0, T; X)$ and $C^1(0, T; X)$ stand for the space of continuous and continuously differentiable functions from $[0, T]$ to X , respectively, equipped with the following norms:

$$\|f\|_{C(0, T; X)} = \max_{t \in [0, T]} \|f(t)\|_X, \quad \|f\|_{C^1(0, T; X)} = \max_{t \in [0, T]} \|f(t)\|_X + \max_{t \in [0, T]} \|\dot{f}(t)\|_X.$$

In the study of Problem (P), we need the following assumptions on the data of the problem.

(h_1) The viscosity and elasticity tensors $\mathcal{A}, \mathfrak{F} : \Omega \times \mathbb{S}^d \rightarrow \mathbb{S}^d$ and the electric permittivity tensor $\beta : \Omega \times \mathbb{R}^d \rightarrow \mathbb{R}^d$ satisfy, for a.e. $x \in \Omega$, the following usual properties:

$$\left\{ \begin{array}{l} (a) : \exists M_{\mathcal{A}} > 0, \forall \varepsilon_1, \varepsilon_2 \in \mathbb{S}^d; \|\mathcal{A}(x, \varepsilon_1) - \mathcal{A}(x, \varepsilon_2)\| \leq M_{\mathcal{A}} \|\varepsilon_1 - \varepsilon_2\|, \\ (b) : \exists m_{\mathcal{A}} > 0, \forall \varepsilon_1, \varepsilon_2 \in \mathbb{S}^d; (\mathcal{A}(x, \varepsilon_1) - \mathcal{A}(x, \varepsilon_2)) \cdot (\varepsilon_1 - \varepsilon_2) \geq m_{\mathcal{A}} \|\varepsilon_1 - \varepsilon_2\|^2, \\ (c) : \text{the mapping } x \mapsto \mathcal{A}(x, \varepsilon) \text{ is Lebesgue-measurable on } \Omega \text{ for all } \varepsilon \in \mathbb{S}^d, \\ (e) : \text{the mapping } x \mapsto \mathcal{A}(x, \varepsilon) \text{ belongs to } \mathcal{H}, \text{ for all } \varepsilon \in \mathbb{S}^d, \end{array} \right. \quad (21)$$

$$\left\{ \begin{array}{l} (a) : \exists M_{\mathfrak{F}} > 0, \forall \varepsilon_1, \varepsilon_2 \in \mathbb{S}^d; \|\mathfrak{F}(x, \varepsilon_1) - \mathfrak{F}(x, \varepsilon_2)\| \leq M_{\mathfrak{F}} \|\varepsilon_1 - \varepsilon_2\|, \\ (b) : \exists m_{\mathfrak{F}} > 0, \forall \varepsilon_1, \varepsilon_2 \in \mathbb{S}^d; (\mathfrak{F}(x, \varepsilon_1) - \mathfrak{F}(x, \varepsilon_2)) \cdot (\varepsilon_1 - \varepsilon_2) \geq m_{\mathfrak{F}} \|\varepsilon_1 - \varepsilon_2\|^2, \\ (c) : \text{the mapping } x \mapsto \mathfrak{F}(x, \varepsilon) \text{ is Lebesgue-measurable on } \Omega \text{ for all } \varepsilon \in \mathbb{S}^d, \\ (e) : \text{the mapping } x \mapsto \mathfrak{F}(x, \varepsilon) \text{ belongs to } \mathcal{H}, \text{ for all } \varepsilon \in \mathbb{S}^d, \end{array} \right. \quad (22)$$

$$\left\{ \begin{array}{l} (a) : \exists M_{\beta} > 0, \forall \xi_1, \xi_2 \in \mathbb{R}^d; \|\beta(x, \xi_1) - \beta(x, \xi_2)\| \leq M_{\beta} \|\xi_1 - \xi_2\|, \\ (b) : \exists m_{\beta} > 0, \forall \xi_1, \xi_2 \in \mathbb{R}^d; (\beta(x, \xi_1) - \beta(x, \xi_2)) \cdot (\xi_1 - \xi_2) \geq m_{\beta} \|\xi_1 - \xi_2\|^2, \\ (c) : \text{the mapping } x \mapsto \beta(x, \xi) \text{ is Lebesgue-measurable on } \Omega \text{ for all } \xi \in \mathbb{R}^d, \\ (e) : \text{the mapping } x \mapsto \beta(x, \xi) \text{ belongs to } \mathcal{W}, \text{ for all } \xi \in \mathbb{R}^d. \end{array} \right. \quad (23)$$

(h_2) The piezoelectric tensor $\mathcal{E} = (e_{ijk}) : \Omega \times \mathbb{S}^d \rightarrow \mathbb{R}^d$ satisfies $e_{ijk} = e_{ikj} \in L^\infty(\Omega)$.

We note here that under hypotheses (h_2), $M_{\mathcal{E}} = \sup_{i,j,k} \|e_{ijk}\|_{L^\infty(\Omega)}$ is well-defined.

(h_3) The function $p_r : \Gamma_3 \times \mathbb{R} \rightarrow \mathbb{R}_+$ with $r = e, \nu$ satisfies the following conditions:

(a) : $\exists M_{p_r} > 0, \forall s \in \mathbb{R}; 0 < p_r(x, s) \leq M_{p_r}$ a.e. $x \in \Gamma_3$,

(b) : $x \mapsto p_r(x, s)$ is measurable on Γ_3 for any $s \in \mathbb{R}$ and is zero for $s \leq 0$.

(h_4) The function $h_r : \Gamma_3 \times \mathbb{R} \rightarrow \mathbb{R}$ with $r = e, \nu$ satisfies the following conditions:

(a) : $\exists M_{h_e} > 0, \forall \varphi \in \mathbb{R}; |h_e(x, \varphi)| \leq M_{h_e}$ a.e. $x \in \Gamma_3$,

(b) : $\exists M_{h_\nu} > 0, \forall \varphi \in \mathbb{R}; 0 \leq h_\nu(x, \varphi) \leq M_{h_\nu}$ a.e. $x \in \Gamma_3$,

(c) : $\forall \varphi_1, \varphi_2 \in \mathbb{R}; (h_e(x, \varphi_1) - h_e(x, \varphi_2))(\varphi_1 - \varphi_2) \geq 0$, a.e. $x \in \Gamma_3$,

(d) : $x \mapsto h_r(x, \varphi)$ is measurable on Γ_3 for all $\varphi \in \mathbb{R}$.

(h_6) The mappings $s \mapsto p_r(x, s)$ and $\varphi \mapsto h_r(x, \varphi)$ are Lipschitz continuous, i.e.,

(a) : $\exists L_{p_r} > 0, \forall s_1, s_2 \in \mathbb{R}; |p_r(x, s_1) - p_r(x, s_2)| \leq L_{p_r}|s_1 - s_2|$ a.e. $x \in \Gamma_3$,

(b) : $\exists L_{h_r} > 0, \forall \varphi_1, \varphi_2 \in \mathbb{R}; |h_r(x, \varphi_1) - h_r(x, \varphi_2)| \leq L_{h_r}|\varphi_1 - \varphi_2|$ a.e. $x \in \Gamma_3$.

(h_7) The mapping $R : H^{-\frac{1}{2}}(\Gamma_3) \rightarrow L^\infty(\Gamma_3)$ is linear continuous. We denote $\|R\| = M_R$.

(h_8) The forces, the traction, the volume and surface charge densities satisfy

$$f_0 \in C(0, T; L^2(\Omega)^d), f_2 \in C(0, T; L^2(\Gamma_2)^d),$$

$$q_0 \in C(0, T; L^2(\Omega)), q_2 \in C(0, T; L^2(\Gamma_b)).$$

(h_9) The friction coefficient, the contact surface potential and the gap function satisfy

$$\mu \in L^\infty(\Gamma_3), \mu \geq 0 \text{ a.e. on } \Gamma_3; \varphi_F \in L^2(\Gamma_3); g \in L^2(\Gamma_3), g \geq 0 \text{ a.e. on } \Gamma_3.$$

Let $t \in (0, T)$, we use Riesz's representation to define $f(t) \in V$ and $q_e(t) \in W$ by

$$(f(t), v)_V = \int_{\Omega} f_0(t) \cdot v \, dx + \int_{\Gamma_2} f_2(t) \cdot v \, da \text{ for all } v \in V, \tag{24}$$

$$(q_e(t), \xi)_W = \int_{\Omega} q_0(t)\xi \, dx - \int_{\Gamma_b} q_2(t)\xi \, da \text{ for all } \xi \in W. \tag{25}$$

We consider the functionals j_1, j_2 and j_3 defined, respectively, as follows:

$$j_1(u, \varphi, v) = \int_{\Gamma_3} h_\nu(\varphi - \varphi_F)p_\nu(u_\nu - g) v_\nu \, da, \text{ for all } (u, \varphi, v) \in V \times W \times V, \tag{26}$$

$$j_2(\sigma, v) = \int_{\Gamma_3} \mu |R\sigma_\nu| \|v_\tau\| \, da, \text{ for all } (\sigma, v) \in \mathcal{H} \times V, \tag{27}$$

$$j_3(u, \varphi, \xi) = \int_{\Gamma_3} p_e(u_\nu)h_e(\varphi - \varphi_F)\xi \, da, \text{ for all } (u, \varphi, \xi) \in V \times W \times W. \tag{28}$$

Recalling (h_3)-(h_5) and (h_8)-(h_9), we find that the integrals in (24)-(28) are well-defined. Under these notations, the Green formula implies that if (u, σ, ϕ, D) are regular functions

satisfying (3)-(11), we obtain the following weak formulation of Problem (P).

Problem (PV). Find a displacement $u : (0, T) \rightarrow V$, an electric potential $\varphi : (0, T) \rightarrow W$ such that

$$\begin{aligned} & \langle \ddot{u}(t), v - \dot{u}(t) \rangle_{V' \times V} + (\mathcal{A}\varepsilon(\dot{u})(t), \varepsilon(v) - \varepsilon(\dot{u}(t)))_{\mathcal{H}} + (\mathfrak{F}\varepsilon(u)(t), \varepsilon(v) - \varepsilon(\dot{u}(t)))_{\mathcal{H}} \\ & + (\mathcal{E}^*\nabla\varphi(t), \varepsilon(v) - \varepsilon(\dot{u}(t)))_{L^2(\Omega)^d} + j_1(u(t), \varphi(t), v) - j_1(u(t), \varphi(t), \dot{u}(t)) \\ & + j_2(\sigma(t), v) - j_2(\sigma(t), \dot{u}(t)) \geq (f(t), v - \dot{u}(t))_V \quad \text{for all } v \in V \text{ a.e. } t \in (0, T), \end{aligned} \quad (29)$$

$$\begin{aligned} & (\beta\nabla\varphi(t), \nabla\xi)_{L^2(\Omega)^d} - (\mathcal{E}\varepsilon(u)(t), \nabla\xi)_{L^2(\Omega)^d} + j_3(\dot{u}(t), \varphi(t), \xi) \\ & = (q_e(t), \xi)_W \quad \text{for all } \xi \in W \text{ a.e. } t \in (0, T). \end{aligned} \quad (30)$$

We are now able to state our main result that we will prove in the next section.

Theorem 3.1 Assume assumptions (h_1) - (h_9) hold. Then there exists a unique solution (u, φ) of Problem (PV), which satisfies the following regularities:

$$\ddot{u} \in L^2(0, T; V'), \quad u \in C^1(0, T; V), \quad \varphi \in C(0, T; W).$$

4 Proof of Theorem 3.1

We assume that (h_1) - (h_9) hold. The proof will be carried out in several steps. First, let $\eta = (\eta_1, \eta_2, \eta_3) \in L^2(0, T; \mathcal{H} \times L^2(\Gamma_3) \times \mathcal{H})$ be given, we define the following functionals:

$$j_1^\eta(v) = \int_{\Gamma_3} \mu |R\eta_{3\nu}| \|v_\tau\| da \quad \text{for all } v \in V, \quad (31)$$

$$j_2^\eta(v) = \int_{\Gamma_3} \eta_2 v_\nu da \quad \text{for all } v \in V. \quad (32)$$

For $\eta \in L^2(0, T; \mathcal{H} \times L^2(\Gamma_3) \times \mathcal{H})$ known, we construct the following intermediate problem.

Problem (PV₁^η). Find $u_\eta : (0, T) \rightarrow V$ such that for all $v \in V$, a.e. $t \in (0, T)$, we have

$$\begin{aligned} & \langle \ddot{u}_\eta(t), v - \dot{u}_\eta(t) \rangle_{V' \times V} + (\mathcal{A}\varepsilon(\dot{u}_\eta)(t), \varepsilon(v) - \varepsilon(\dot{u}_\eta(t)))_{\mathcal{H}} + (\eta_1, \varepsilon(v) - \varepsilon(\dot{u}_\eta(t)))_{\mathcal{H}} \\ & + j_1^\eta(v) - j_1^\eta(\dot{u}_\eta(t)) + j_2^\eta(v) - j_2^\eta(\dot{u}_\eta(t)) \geq (f(t), v - \dot{u}_\eta(t))_V, \end{aligned} \quad (33)$$

$$\dot{u}(0) = 0, \quad u(0) = 0. \quad (34)$$

The unique solvability of Problem (PV₁^η) follows from the following lemma.

Lemma 4.1 For a given $\eta = (\eta_1, \eta_2, \eta_3) \in C(0, T; \mathcal{H} \times L^2(\Gamma_3) \times \mathcal{H})$, Problem (PV₁^η) has a unique solution u_η , which satisfies $\ddot{u} \in L^2(0, T; V')$ and $u \in C^1(0, T; V)$.

Proof. We consider the operator $A : V \rightarrow V'$ and the function $f_\eta : (0, T) \rightarrow V'$ defined, for all $u, v \in V$ and $t \in (0, T)$, by

$$\langle Au, v \rangle_{V' \times V} = (\mathcal{A}\varepsilon(u), \varepsilon(v))_{\mathcal{H}}, \quad (35)$$

$$\langle f_\eta(t), v \rangle_{V' \times V} = (f(t), v)_V - (\eta_1(t), \varepsilon(v))_{\mathcal{H}} - j_2^\eta(v). \quad (36)$$

Hence, the inequality (33) can be rewritten, for all $v \in V$ and $t \in (0, T)$, as follows:

$$\begin{aligned} & \langle \dot{u}_\eta(t), v - \dot{u}_\eta(t) \rangle_{V' \times V} + \langle A\dot{u}_\eta(t), v - \dot{u}_\eta(t) \rangle_{V' \times V} \\ & + j_1^\eta(v) - j_1^\eta(\dot{u}_\eta(t)) \geq \langle f_\eta(t), v - \dot{u}_\eta(t) \rangle_{V' \times V}. \end{aligned} \tag{37}$$

By assumption (h_1) (21), the operator A is strongly monotone and Lipschitz continuous. Moreover, it follows from (31) that j_1^η is convex and Lipschitz continuous and then it is lower semi-continuous. From (36) it is easy to see that $f_\eta \in C(0, T; V')$. Then, by standard arguments on the first order nonlinear evolutionary inequalities (see [10]), there exists a unique solution u_η for Problem (PV_1^η) , which satisfies

$$\ddot{u}_\eta \in L^2(0, T; V'), \quad u_\eta \in C^1(0, T; V).$$

We use the solution u_η of Problem (PV_1^η) to consider the following auxiliary problem.

Problem (PV_2^η) . Let $\eta \in C(0, T; \mathcal{H} \times L^2(\Gamma_3) \times \mathcal{H})$ be given, find $\varphi_\eta : (0, T) \rightarrow W$ such that

$$\begin{aligned} & (\beta \nabla \varphi_\eta(t), \nabla \xi)_{L^2(\Omega)^d} - (\mathcal{E}\varepsilon(u_\eta)(t), \nabla \xi)_{L^2(\Omega)^d} \\ & + j_3(\dot{u}_\eta(t), \varphi_\eta(t), \xi) = (q_e(t), \xi)_W \quad \text{for all } \xi \in W, \text{ a.e. } t \in (0, T). \end{aligned} \tag{38}$$

The unique solvability of Problem (PV_2^η) follows from the following lemma.

Lemma 4.2 Let $\eta = (\eta_1, \eta_2, \eta_3) \in L^2(0, T; \mathcal{H} \times L^2(\Gamma_3) \times \mathcal{H})$ be known, then Problem (PV_2^η) has a unique solution φ_η which satisfies $\varphi_\eta \in C(0, T; W)$.

Proof. Let $t \in (0, T)$, we use the Riesz representation theorem to introduce the element $q_\eta(t) \in W$ and the operator $A_\eta(t) : W \rightarrow W$, defined as follows:

$$(q_\eta(t), \xi)_W = (q_e(t), \xi)_W + (\mathcal{E}\varepsilon(u_\eta)(t), \nabla \xi)_{L^2(\Omega)^d} \quad \text{for all } \xi \in W, \tag{39}$$

$$(A_\eta(t)\varphi, \xi)_W = (\beta \nabla \varphi(t), \nabla \xi)_{L^2(\Omega)^d} + j_3(\dot{u}_\eta(t), \varphi, \xi) \quad \text{for all } \xi \in W. \tag{40}$$

From hypotheses (h_1) (23), (h_3) (a), (h_4) (d) and (h_6) (b), it follows that $A_\eta(t)$ is a strongly monotone, Lipschitz continuous operator on W , and therefore, there exists a unique element $\varphi_\eta(t) \in W$ such that

$$(A_\eta(t)\varphi_\eta(t), \xi)_W = (q_\eta(t), \xi)_W \quad \text{for all } \xi \in W, t \in (0, T). \tag{41}$$

We combine (39) and (41) to find that $\varphi_\eta(t) \in W$ is the unique solution of the nonlinear variational Problem (PV_2^η) , and by using Lemma 4.3 in [15], we deduce $\varphi_\eta \in C(0, T; W)$.

In the sequel, we will need the following result.

Lemma 4.3 Let u_η and u'_η (resp. φ_η and φ'_η) be solutions of Problem (PV_1^η) (resp. Problem (PV_2^η)) for $\eta = (\eta_1, \eta_2, \eta_3)$ and $\eta' = (\eta'_1, \eta'_2, \eta'_3)$ of $C(0, T; \mathcal{H} \times L^2(\Gamma_3) \times \mathcal{H})$. Then there exist two constants $c > 0$ and $\tilde{c} > 0$ such that for all $t \in (0, T)$, we have

$$\begin{aligned} & \|\dot{u}_\eta(t) - \dot{u}'_\eta(t)\|_V^2 + \int_0^t \|\dot{u}_\eta(s) - \dot{u}'_\eta(s)\|_V^2 ds \\ & \leq c \int_0^t \|\eta_1(s) - \eta'_1(s)\|_{\mathcal{H}}^2 + \|\eta_2(s) - \eta'_2(s)\|_{L^2(\Gamma_3)}^2 + \|\eta_3(s) - \eta'_3(s)\|_{\mathcal{H}}^2 ds, \end{aligned} \tag{42}$$

$$\|\varphi_\eta(t) - \varphi'_\eta(t)\|_W \leq \tilde{c} (\|\dot{u}_\eta(t) - \dot{u}'_\eta(t)\|_V + \|u_\eta(t) - u'_\eta(t)\|_V). \tag{43}$$

Proof. It follows from (33) that for all $v \in V$ and $t \in (0, T)$, we have

$$\begin{aligned} & \langle \ddot{u}_\eta(t), v - \dot{u}_\eta(t) \rangle_{V' \times V} + (\mathcal{A}\varepsilon(\dot{u}_\eta)(t), \varepsilon(v) - \varepsilon(\dot{u}_\eta)(t))_{\mathcal{H}} + (\eta_1(t), \varepsilon(v) - \varepsilon(\dot{u}_\eta)(t))_{\mathcal{H}} \\ & + j_1^\eta(v) - j_1^\eta(\dot{u}_\eta(t)) + j_2^\eta(v) - j_2^\eta(\dot{u}_\eta(t)) \geq (f, v - \dot{u}_\eta(t))_V, \end{aligned} \quad (44)$$

$$\begin{aligned} & \langle \ddot{u}'_\eta(t), \varepsilon(v) - \varepsilon(\dot{u}'_\eta(t)) \rangle_{V' \times V} + (\mathcal{A}\varepsilon(\dot{u}'_\eta)(t), \varepsilon(v) - \varepsilon(\dot{u}'_\eta(t)))_{\mathcal{H}} \\ & + (\eta'_1(t), \varepsilon(v) - \varepsilon(\dot{u}'_\eta(t)))_{\mathcal{H}} + j_1^{\eta'}(v) - j_1^{\eta'}(\dot{u}'_\eta(t)) + j_2^{\eta'}(v) - j_2^{\eta'}(\dot{u}'_\eta(t)) \\ & \geq (f, v - \dot{u}'_\eta(t))_V. \end{aligned} \quad (45)$$

Taking $v = \dot{u}'_\eta(t)$ in (44), $v = \dot{u}_\eta(t)$ in (45) and adding the obtained inequalities, we get

$$\begin{aligned} & \int_0^t \langle \ddot{u}_\eta(s) - \ddot{u}'_\eta(s), \dot{u}_\eta(s) - \dot{u}'_\eta(s) \rangle_{V' \times V} ds \\ & + \int_0^t (\mathcal{A}\varepsilon(\dot{u}_\eta)(s) - \mathcal{A}\varepsilon(\dot{u}'_\eta)(s), \varepsilon(\dot{u}_\eta)(s) - \varepsilon(\dot{u}'_\eta)(s))_{\mathcal{H}} ds \\ & \leq - \int_0^t (\eta_1(s) - \eta'_1(s), \varepsilon(\dot{u}_\eta)(s) - \varepsilon(\dot{u}'_\eta)(s))_{L^2(\Omega)^d} ds \\ & + \int_0^t j_1^\eta(\dot{u}'_\eta(s)) - j_1^\eta(\dot{u}_\eta(s)) + j_2^\eta(\dot{u}'_\eta(s)) - j_2^\eta(\dot{u}_\eta(s)) ds \\ & + \int_0^t j_1^{\eta'}(\dot{u}_\eta(s)) - j_1^{\eta'}(\dot{u}_\eta(s)') + j_2^{\eta'}(\dot{u}_\eta(s)) - j_2^{\eta'}(\dot{u}'_\eta(s)) ds. \end{aligned} \quad (46)$$

Using the definition of the functional j_1^η , we deduce

$$\begin{aligned} & |j_1^\eta(\dot{u}'_\eta(s)) - j_1^\eta(\dot{u}_\eta(s)) + j_1^{\eta'}(\dot{u}_\eta(s)) - j_1^{\eta'}(\dot{u}'_\eta(s))| \\ & \leq \int_{\Gamma_3} \mu |R\eta_{3\nu}| (\|\dot{u}'_{\eta\tau}(s)\| - \|\dot{u}_{\eta\tau}(s)\|) da \\ & - \int_{\Gamma_3} \mu |R\eta'_{3\nu}| (\|\dot{u}'_{\eta\tau}(s)\| - \|\dot{u}_{\eta\tau}(s)\|) da, \\ & \leq \int_{\Gamma_3} \mu (|R\eta_{3\nu}| - |R\eta'_{3\nu}|) (\|\dot{u}_{\eta\tau}(s)\| - \|\dot{u}'_{\eta\tau}(s)\|) da, \\ & \leq c_0 \|\mu\|_{L^\infty(\Gamma_3)} M_R \|\eta_3 - \eta'_3\|_{\mathcal{H}} \|\dot{u}_\eta(s) - \dot{u}'_\eta(s)\|_V. \end{aligned} \quad (47)$$

Moreover, we use the definition of the functional j_2^η to obtain

$$\begin{aligned} & |j_2^\eta(\dot{u}'_\eta(s)) - j_2^\eta(\dot{u}_\eta(s)) + j_2^{\eta'}(\dot{u}_\eta(s)) - j_2^{\eta'}(\dot{u}'_\eta(s))| \\ & \leq \int_{\Gamma_3} \eta_2 (\dot{u}'_{\eta\nu}(s) - \dot{u}_{\eta\nu}(s)) da - \int_{\Gamma_3} \eta_2 (\dot{u}'_{\eta\nu}(s) - \dot{u}_{\eta\nu}(s)) da, \\ & \leq \int_{\Gamma_3} (\eta_2 - \eta'_2) (\dot{u}_{\eta\nu}(s) - \dot{u}'_{\eta\nu}(s)) da, \\ & \leq c_0 \|\eta_2 - \eta'_2\|_{L^2(\Gamma_3)} \|\dot{u}_{\eta\tau}(s) - \dot{u}'_{\eta\tau}(s)\|_V. \end{aligned} \quad (48)$$

We combine the inequalities (46)-(48) and we use the assumption (h_1) to get

$$\begin{aligned} & \frac{1}{2} \|\dot{u}_\eta(t) - \dot{u}'_\eta(t)\|_V^2 + m_{\mathcal{A}} \int_0^t \|\dot{u}_\eta(s) - \dot{u}'_\eta(s)\|_V^2 ds \\ & \leq c_p \int_0^t \|\eta_1(s) - \eta'_1(s)\|_{L^2(\Omega)^d} \|\dot{u}_\eta(s) - \dot{u}'_\eta(s)\|_V ds \\ & + c_0 \|\mu\|_{L^\infty(\Gamma_3)} M_R \int_0^t \|\eta_3 - \eta'_3\|_{\mathcal{H}} \|\dot{u}_\eta(s) - \dot{u}'_\eta(s)\|_V ds \\ & + c_0 \int_0^t \|\eta_2(s) - \eta'_2(s)\|_{L^2(\Gamma_3)} \|\dot{u}_\eta(s) - \dot{u}'_\eta(s)\|_V ds. \end{aligned} \tag{49}$$

Finally, we apply Young’s inequality $ab \leq \epsilon a^2 + \frac{b^2}{4\epsilon}$ to get, after some simplifications, that

$$\begin{aligned} & \|\dot{u}_\eta(t) - \dot{u}'_\eta(t)\|_V^2 + \int_0^t \|\dot{u}_\eta(s) - \dot{u}'_\eta(s)\|_V^2 ds \\ & \leq c \int_0^t \|\eta_1(s) - \eta'_1(s)\|_{L^2(\Omega)^d}^2 + \|\eta_2(s) - \eta'_2(s)\|_{L^2(\Gamma_3)}^2 + \|\eta_3 - \eta'_3\|_{\mathcal{H}}^2 ds. \end{aligned} \tag{50}$$

Next, let φ_η and φ'_η be the corresponding solutions of (PV_2^η) for $\eta = (\eta_1, \eta_2, \eta_3)$ and $\eta' = (\eta'_1, \eta'_2, \eta'_3)$, respectively. From (39), we get, for all $t \in (0, T)$ and $\xi \in W$, that

$$(\beta \nabla \varphi_\eta(t), \nabla \xi)_{L^2(\Omega)^d} - (\mathcal{E}\varepsilon(u_\eta)(t), \nabla \xi)_{L^2(\Omega)^d} + j_3(\dot{u}_\eta, \varphi_\eta(t), \xi) = (q_e(t), \xi)_W, \tag{51}$$

$$(\beta \nabla \varphi'_\eta(t), \nabla \xi)_{L^2(\Omega)^d} - (\mathcal{E}\varepsilon(u'_\eta)(t), \nabla \xi)_{L^2(\Omega)^d} + j_3(\dot{u}'_\eta, \varphi'_\eta(t), \xi) = (q_e(t), \xi)_W. \tag{52}$$

Replacing ξ by $\varphi_\eta(t) - \varphi'_\eta(t)$ in (51) and (52), we subtract the obtained equations to find

$$\begin{aligned} & (\beta \nabla \varphi_\eta(t) - \beta \nabla \varphi'_\eta(t), \nabla \varphi_\eta(t) - \nabla \varphi'_\eta(t))_{L^2(\Omega)^d} \\ & - (\mathcal{E}\varepsilon(u_\eta)(t) - \mathcal{E}\varepsilon(u'_\eta)(t), \nabla \varphi_\eta(t) - \nabla \varphi'_\eta(t))_{L^2(\Omega)^d} \\ & + j_3(\dot{u}_\eta, \varphi_\eta(t), \varphi_\eta(t) - \varphi'_\eta(t)) - j_3(\dot{u}'_\eta, \varphi'_\eta(t), \varphi_\eta(t) - \varphi'_\eta(t)) = 0. \end{aligned} \tag{53}$$

Using the assumptions (h_3) - (h_5) and the definition of the functional j_3 , we obtain

$$\begin{aligned} & |j_3(\dot{u}_\eta, \varphi_\eta(t), \varphi_\eta(t) - \varphi'_\eta(t)) - j_3(\dot{u}'_\eta, \varphi'_\eta(t), \varphi_\eta(t) - \varphi'_\eta(t))| \\ & = \int_{\Gamma_3} (p_e(\dot{u}_\eta(t)) h_e(\varphi_\eta(t) - \varphi_F) - p_e(\dot{u}'_\eta(t)) h_e(\varphi'_\eta(t) - \varphi_F)) (\varphi_\eta(t) - \varphi'_\eta(t)) da, \\ & = \int_{\Gamma_3} p_e(\dot{u}_\eta(t)) (h_e(\varphi_\eta(t) - \varphi_F) - h_e(\varphi'_\eta(t) - \varphi_F)) (\varphi_\eta(t) - \varphi'_\eta(t)) da \\ & + \int_{\Gamma_3} h_e(\varphi'_\eta(t) - \varphi_F) (p_e(\dot{u}_\eta(t)) - p_e(\dot{u}'_\eta(t))) (\varphi_\eta(t) - \varphi'_\eta(t)) da, \\ & \leq c_0 c_1 M_{h_e} \|\dot{u}_\eta(t) - \dot{u}'_\eta(t)\|_V \|\varphi_\eta(t) - \varphi'_\eta(t)\|_W. \end{aligned} \tag{54}$$

By virtue of hypotheses (h_1) (23) and (h_2) , it follows from (53) and (54) that

$$\|\varphi_\eta(t) - \varphi'_\eta(t)\|_V \leq \tilde{c} (\|\dot{u}_\eta(s) - \dot{u}'_\eta(s)\|_V + \|u_\eta(s) - u'_\eta(s)\|_V). \tag{55}$$

Hence, inequalities (42) and (43) of Lemma 4.3 are obtained.

In the next step, we consider the following operator:

$$\Lambda : C(0, T; \mathcal{H} \times L^2(\Gamma_3) \times \mathcal{H}) \rightarrow C(0, T; \mathcal{H} \times L^2(\Gamma_3) \times \mathcal{H}),$$

defined for $t \in (0, T)$ by $\Lambda\eta(t) = (\Lambda_1\eta(t), \Lambda_2\eta(t), \Lambda_3\eta(t))$, where

$$\Lambda_1\eta(t) = \mathfrak{F}\varepsilon(u_\eta)(t) + \mathcal{E}^*\nabla\varphi_\eta(t), \quad (56)$$

$$\Lambda_2\eta(t) = h_\nu(\varphi_\eta(t) - \varphi_f(t))p_\nu(u_{\eta\nu}(t) - g), \quad (57)$$

$$\Lambda_3\eta(t) = \mathcal{A}\varepsilon(\dot{u}_\eta(t)) + \mathfrak{F}\varepsilon(u_\eta(t)) - \mathcal{E}^*E(\varphi_\eta(t)). \quad (58)$$

We have the following fixed point result.

Lemma 4.4 *There exists a unique $\eta^* \in C(0, T; \mathcal{H} \times L^2(\Gamma_3) \times \mathcal{H})$ such that*

$$\Lambda\eta^* = \eta^*.$$

Proof. Let $\eta = (\eta_1, \eta_2, \eta_3)$, $\eta' = (\eta'_1, \eta'_2, \eta'_3) \in C(0, T; \mathcal{H} \times L^2(\Gamma_3) \times \mathcal{H})$. The definition of Λ_1 and Λ_3 , and the assumptions (h_1) and (h_2) imply, after some algebras, that

$$\|\Lambda_1\eta(t) - \Lambda_1\eta'(t)\|_{\mathcal{H}} \leq M_{\mathfrak{F}}\|u_\eta(t) - u'_{\eta}(t)\|_V + M_{\mathcal{E}}\|\varphi_\eta(t) - \varphi'_{\eta}(t)\|_W, \quad (59)$$

$$\begin{aligned} \|\Lambda_3\eta(t) - \Lambda_3\eta'(t)\|_{\mathcal{H}} &\leq M_{\mathcal{A}}\|\dot{u}_\eta(t) + \dot{u}'_{\eta}(t)\|_V + M_{\mathfrak{F}}\|u_\eta(t) - u'_{\eta}(t)\|_V \\ &\quad + M_{\mathcal{E}}\|\varphi_\eta(t) - \varphi'_{\eta}(t)\|_W. \end{aligned} \quad (60)$$

Using the definition of Λ_2 and the properties of h_ν and p_ν , it is easy to verify that

$$\|\Lambda_2\eta(t) - \Lambda_2\eta'(t)\|_{\mathcal{H}} \leq M_{h_\nu}L_{p_\nu}c_0\|u_\eta(t) + u'_{\eta}(t)\|_V + M_{p_\nu}L_{h_\nu}c_1\|\varphi_\eta(t) - \varphi'_{\eta}(t)\|_W. \quad (61)$$

Then, from the inequalities (59)-(61), (42) and (43), there exists $c > 0$ such that

$$\|\Lambda\eta(t) - \Lambda\eta'(t)\|_{\mathcal{H} \times L^2(\Gamma_3) \times \mathcal{H}}^2 \leq c \int_0^t \|\eta(s) - \eta'(s)\|_{\mathcal{H} \times L^2(\Gamma_3) \times \mathcal{H}}^2 ds. \quad (62)$$

Reiterating the previous inequality n times, we get

$$\|\Lambda^n\eta - \Lambda^n\eta'\|_{C([0, T]; \mathcal{H} \times L^2(\Gamma_3) \times \mathcal{H})} \leq \sqrt{\frac{c^n T^n}{n!}} \|\eta(s) - \eta'(s)\|_{C([0, T]; \mathcal{H} \times L^2(\Gamma_3) \times \mathcal{H})}. \quad (63)$$

Since $\lim_{n \rightarrow \infty} \frac{c^n T^n}{n!} = 0$, the inequality (63) shows that for n sufficiently large, the operator Λ^n is a contraction on the Banach space $C(0, T; \mathcal{H} \times L^2(\Gamma_3) \times \mathcal{H})$. Thus, according to the Banach fixed point theorem, there exists a unique $\eta^* \in C(0, T; \mathcal{H} \times L^2(\Gamma_3) \times \mathcal{H})$ such that $\Lambda^n\eta^* = \eta^*$. Moreover, since $\Lambda^n(\Lambda\eta^*) = \Lambda(\Lambda^n\eta^*) = \Lambda\eta^*$, we deduce that $\Lambda\eta^*$ is also a fixed point of Λ^n , and by the uniqueness of the fixed point, we obtain $\Lambda\eta^* = \eta^*$. Therefore, η^* is a unique fixed point of Λ too.

Now, we have all the ingredients needed to prove Theorem 3.1. Indeed, let η^* be the unique fixed point of the operator Λ and let $u = u_{\eta^*}$ and $\varphi = \varphi_{\eta^*}$ be the unique solutions of the Problems $(PV_1^{\eta^*})$ and $(PV_2^{\eta^*})$, respectively. Therefore, (u, φ) is a solution of Problem (PV) and then the existence part is proved. The uniqueness part results from the uniqueness of the fixed point of the operator Λ . Then Theorem 3.1 is established.

5 Convergence Result

We are interested here in the dependence of the solution of Problem (PV) on the perturbations of the data. In the sequel, we assume that the assumptions (h₁)-(h₇) hold and let (u, φ) be the solution of Problem (PV) obtained in Theorem 3.1. For each ε > 0, let f₀^ε, q₀^ε, f₂^ε, q₂^ε and φ_F^ε denote the perturbations of f₀, q₀, f₂, q₂ and φ_F, respectively. We consider the operators f^ε : (0, T) → V and q_e^ε : (0, T) → W defined as follows:

$$(f^\epsilon(t), v)_V = \int_\Omega f_0^\epsilon(t) \cdot v \, dx + \int_{\Gamma_2} f_2^\epsilon(t) \cdot v \, da \quad \text{for all } v \in V, \text{ a.e. } t \in (0, T), \quad (64)$$

$$(q_e^\epsilon(t), \xi)_W = \int_\Omega q_0^\epsilon(t) \xi \, dx - \int_{\Gamma_b} q_2^\epsilon(t) \xi \, da \quad \text{for all } \xi \in W, \text{ a.e. } t \in (0, T). \quad (65)$$

We consider the functionals j₁^ε : V × W × V → ℝ and j₃^ε : V × W × W → ℝ given by

$$j_1^\epsilon(u, \varphi, v) = \int_{\Gamma_3} h_\nu(\varphi - \varphi_F^\epsilon) p_\nu(u_\nu - g) v_\nu \, da, \quad (66)$$

$$j_3^\epsilon(u, \varphi, \xi) = \int_{\Gamma_3} p_e(u_\nu) h_e(\varphi - \varphi_F^\epsilon) \xi \, da. \quad (67)$$

Next, we introduce the following perturbation of the variational Problem (PV).

Problem (PV^ε). Find a displacement u^ε : (0, T) → V and an electric potential φ^ε : (0, T) → W such that for all ξ ∈ W, v ∈ V and a.e. t ∈ (0, T), we have

$$\begin{aligned} & \langle \ddot{u}^\epsilon(t), \varepsilon(v) - \varepsilon(\dot{u}^\epsilon)(t) \rangle_{V' \times V} + (\mathcal{A}\varepsilon(\dot{u}^\epsilon)(t), \varepsilon(v) - \varepsilon(\dot{u}^\epsilon)(t))_{\mathcal{H}} \\ & + (\mathfrak{F}\varepsilon(u^\epsilon)(t), \varepsilon(v) - \varepsilon(\dot{u}^\epsilon)(t))_{\mathcal{H}} + (\mathcal{E}^*\nabla\varphi^\epsilon(t), \varepsilon(v) - \varepsilon(\dot{u}^\epsilon)(t))_{L^2(\Omega)^d} \\ & + j_1^\epsilon(u^\epsilon(t), \varphi^\epsilon(t), v) - j_1^\epsilon(u^\epsilon(t), \varphi^\epsilon(t), \dot{u}^\epsilon(t)) \\ & + j_2(\sigma^\epsilon, v) - j_2(\sigma^\epsilon, \dot{u}^\epsilon(t)) \geq (f^\epsilon(t), v - \dot{u}^\epsilon(t))_V, \end{aligned} \quad (68)$$

$$(\beta\nabla\varphi^\epsilon(t), \nabla\xi)_{L^2(\Omega)^d} - (\mathcal{E}\varepsilon(u^\epsilon)(t), \nabla\xi)_{L^2(\Omega)^d} + j_3(\dot{u}^\epsilon(t), \varphi^\epsilon(t), \xi) = (q_e^\epsilon(t), \xi)_W. \quad (69)$$

For each ε > 0, Theorem 3.1 implies that Problem (PV^ε) has a unique solution (u^ε, φ^ε). On the other hand, we state the following convergence assumptions:

$$f_0^\epsilon \rightarrow f_0 \text{ in } C(0, T; L^2(\Omega)^d) \text{ as } \epsilon \rightarrow 0, \quad (70)$$

$$q_0^\epsilon \rightarrow q_0 \text{ in } C(0, T; L^2(\Omega)) \text{ as } \epsilon \rightarrow 0, \quad (71)$$

$$f_2^\epsilon \rightarrow f_2 \text{ in } C(0, T; L^2(\Gamma_2)^d) \text{ as } \epsilon \rightarrow 0, \quad (72)$$

$$q_2^\epsilon \rightarrow q_2 \text{ in } C(0, T; L^2(\Gamma_b)) \text{ as } \epsilon \rightarrow 0, \quad (73)$$

$$\varphi_F^\epsilon \rightarrow \varphi_F \text{ in } C(0, T; L^2(\Gamma_3)) \text{ as } \epsilon \rightarrow 0. \quad (74)$$

Let c > 0 be a generic constant which may depend on data, but does not depend on ε, and whose value may vary from place to place. We have the following convergence result.

Theorem 5.1 Under assumptions (70)-(74), the solution (u^ε, φ^ε) of Problem (PV^ε) converges strongly to the solution (u, φ) of Problem (PV), i.e.,

$$(u^\epsilon, \varphi^\epsilon) \rightarrow (u, \varphi) \text{ as } \epsilon \rightarrow 0. \quad (75)$$

Proof. Using inequalities (29) and (68), we obtain

$$\begin{aligned}
& \langle \ddot{u}(t) - \ddot{u}^\epsilon(t), \dot{u}(t) - \dot{u}^\epsilon(t) \rangle_{V' \times V} + (\mathcal{A}\varepsilon(\dot{u})(t) - \mathcal{A}\varepsilon(\dot{u}^\epsilon)(t), \varepsilon(\dot{u})(t) - \varepsilon(\dot{u}^\epsilon)(t))_{\mathcal{H}} \\
& \leq -(\mathfrak{F}\varepsilon(u)(t) - \mathfrak{F}\varepsilon(u^\epsilon)(t), \varepsilon(\dot{u})(t) - \varepsilon(\dot{u}^\epsilon)(t))_{\mathcal{H}} \\
& \quad - (\mathcal{E}^* \nabla \varphi(t) - \mathcal{E}^* \nabla \varphi^\epsilon(t), \varepsilon(\dot{u})(t) - \varepsilon(\dot{u}^\epsilon)(t))_{L^2(\Omega)^d} \\
& \quad + \underbrace{j_1^\epsilon(u^\epsilon(t), \varphi^\epsilon(t), \dot{u}(t)) - j_1(u^\epsilon(t), \varphi^\epsilon(t), \dot{u}^\epsilon(t))}_{=J_1^\epsilon} + \underbrace{j_2(\sigma^\epsilon, (\dot{u})(t)) - j_2(\sigma^\epsilon, \dot{u}^\epsilon(t))}_{=J_2^\epsilon} \\
& \quad + \underbrace{j_1(u(t), \varphi(t), \dot{u}(t)) - j_1(u(t), \varphi(t), \dot{u}^\epsilon(t))}_{=J_1} + \underbrace{j_2(\sigma, \dot{u}(t)) - j_2(\sigma, \dot{u}^\epsilon(t))}_{=J_2} \\
& \quad + (f(t) - f^\epsilon(t), \dot{u}(t) - \dot{u}^\epsilon(t))_V.
\end{aligned} \tag{76}$$

From the definition of the functionals j_1 and j_1^ϵ , we have

$$\begin{aligned}
& |J_1^\epsilon + J_1| \\
& \leq \int_{\Gamma_3} |(p_\nu(u_\nu^\epsilon(t) - g) h_\nu(\varphi^\epsilon(t) - \varphi_F^\epsilon(t)) - p_\nu(u_\nu(t) - g) h_\nu(\varphi(t) - \varphi_F(t))) (\dot{u}_\nu(t) - \dot{u}_\nu^\epsilon(t))| da.
\end{aligned}$$

Taking in mind the hypotheses (h_3) and (h_4) , we find

$$\begin{aligned}
|J_1^\epsilon + J_1| & \leq M_{p_\nu} L_{h_\nu} c_1 c_0 \|\varphi(t) - \varphi^\epsilon(t)\|_W \|\dot{u}(t) - \dot{u}^\epsilon(t)\|_V \\
& \quad + M_{p_\nu} L_{h_\nu} c_0 \|\varphi_F(t) - \varphi_F^\epsilon(t)\|_{L^2(\Gamma_3)} \|\dot{u}(t) - \dot{u}^\epsilon(t)\|_V \\
& \quad + M_{h_\nu} L_{p_\nu} c_0^2 \|u(t) - u^\epsilon(t)\|_V \|\dot{u}(t) - \dot{u}^\epsilon(t)\|_V.
\end{aligned} \tag{77}$$

Moreover, it follows from the definition of the functionals j_2 and j_2^ϵ that

$$\begin{aligned}
|J_2^\epsilon + J_2| & = \int_{\Gamma_3} \mu (|R\sigma_\nu| - |R\sigma_\nu^\epsilon|) (\|\dot{u}\tau\| - \|\dot{u}^\epsilon\tau\|) da, \\
& \leq c_0 \|\mu\|_{L^\infty(\Gamma_3)} M_R \|\sigma - \sigma^\epsilon\|_{\mathcal{H}} \|\dot{u}(t) - \dot{u}^\epsilon(t)\|_V, \\
& \leq c_0 \|\mu\|_{L^\infty(\Gamma_3)} M_R M_A \|\dot{u}(t) - \dot{u}^\epsilon(t)\|_V^2 \\
& \quad + c_0 \|\mu\|_{L^\infty(\Gamma_3)} M_R M_{\mathfrak{F}} \|u(t) - u^\epsilon(t)\|_V \|\dot{u}(t) - \dot{u}^\epsilon(t)\|_V \\
& \quad + c_0 \|\mu\|_{L^\infty(\Gamma_3)} M_R M_{\mathcal{E}} \|\varphi(t) - \varphi^\epsilon(t)\|_W \|\dot{u}(t) - \dot{u}^\epsilon(t)\|_V.
\end{aligned} \tag{78}$$

We integrate (76) and use the assumptions (h_1) - (h_2) and the inequalities (77)-(78) to get

$$\begin{aligned}
& \frac{1}{2} \|\dot{u}(t) - \dot{u}^\epsilon(t)\|_V^2 + \frac{1}{2} m_{\mathfrak{F}} \|u(t) - u^\epsilon(t)\|_V^2 + m_{\mathcal{A}} \int_0^t \|\dot{u}(s) - \dot{u}^\epsilon(s)\|_V^2 ds \\
& \leq (M_{\mathcal{E}} + c_0 \|\mu\|_{L^\infty(\Gamma_3)} M_R M_{\mathcal{E}} + M_{p_\nu} L_{h_\nu} c_1 c_0) \int_0^t \|\varphi(s) - \varphi^\epsilon(s)\|_W \|\dot{u}(s) - \dot{u}^\epsilon(s)\|_V ds \\
& \quad + M_{p_\nu} L_{h_\nu} c_0 \int_0^t \|\varphi_F(s) - \varphi_F^\epsilon(s)\|_{L^2(\Gamma_3)} \|\dot{u}(s) - \dot{u}^\epsilon(s)\|_V ds \\
& \quad + (M_{h_\nu} L_{p_\nu} c_0^2 + c_0 \|\mu\|_{L^\infty(\Gamma_3)} M_R M_{\mathfrak{F}}) \int_0^t \|u(s) - u^\epsilon(s)\|_V \|\dot{u}(s) - \dot{u}^\epsilon(s)\|_V ds \\
& \quad + c_0 \|\mu\|_{L^\infty(\Gamma_3)} M_R M_A \int_0^t \|\dot{u}(s) - \dot{u}^\epsilon(s)\|_V^2 ds + \int_0^t \|f(s) - f^\epsilon(s)\|_V \|\dot{u}(s) - \dot{u}^\epsilon(s)\|_V ds.
\end{aligned}$$

Then we apply the α -inequality $ab < \alpha^2 a^2 + \frac{b^2}{\alpha^2}$ and the Gronwall inequality to find

$$\begin{aligned} & \|\dot{u}(t) - \dot{u}^\epsilon(t)\|_V^2 + \|u(t) - u^\epsilon(t)\|_V^2 + \int_0^t \|\dot{u}(s) - \dot{u}^\epsilon(s)\|_V^2 ds \\ & \leq c \int_0^t (\|\varphi(s) - \varphi^\epsilon(s)\|_W^2 + \|\varphi_F(s) - \varphi_F^\epsilon(s)\|_{L^2(\Gamma_3)}^2 + \|f(s) - f^\epsilon(s)\|_V^2) ds. \end{aligned} \tag{79}$$

Furthermore, it follows from equations (30) and (69) that

$$\begin{aligned} & (\beta \nabla \varphi(t) - \beta \nabla \varphi^\epsilon(t), \nabla \varphi(t) - \nabla \varphi^\epsilon(t))_{L^2(\Omega)^d} \\ & - (\mathcal{E}\mathcal{E}(u)(t) - \mathcal{E}\mathcal{E}(u^\epsilon)(t), \nabla \varphi(t) - \nabla \varphi^\epsilon(t))_{L^2(\Omega)^d} + j_3(\dot{u}(t), \varphi(t), \varphi(t) - \varphi^\epsilon(t)) \\ & - j_3^\epsilon(\dot{u}^\epsilon(t), \varphi^\epsilon(t), \varphi(t) - \varphi^\epsilon(t)) = (q_e(t) - q_e^\epsilon(t), \varphi(t) - \varphi^\epsilon(t))_W. \end{aligned} \tag{80}$$

Using the definitions of j_3^ϵ and j_3 and the assumptions (h_3) and (h_4) , we have

$$\begin{aligned} & |j_3(\dot{u}(t), \varphi(t), \varphi(t) - \varphi^\epsilon(t)) - j_3^\epsilon(\dot{u}^\epsilon(t), \varphi^\epsilon(t), \varphi(t) - \varphi^\epsilon(t))| \\ & \leq M_{h_e} L_{p_e} c_0 c_1 \|\dot{u}(t) - \dot{u}^\epsilon(t)\|_V \|\varphi(t) - \varphi^\epsilon(t)\|_W \\ & + M_{h_e} L_{p_e} c_1 \|\varphi_F(t) - \varphi_F^\epsilon(t)\|_{L^2(\Gamma_3)} \|\varphi(t) - \varphi^\epsilon(t)\|_W. \end{aligned} \tag{81}$$

Keeping in mind (80) and (81) and hypotheses (h_1) and (h_2) , we deduce

$$\begin{aligned} \|\varphi(t) - \varphi^\epsilon(t)\|_W & \leq c \{ \|u(t) - u^\epsilon(t)\|_V + \|\dot{u}(t) - \dot{u}^\epsilon(t)\|_V + \|q_e(t) - q_e^\epsilon(t)\|_W^2 \\ & + \|\varphi_F(t) - \varphi_F^\epsilon(t)\|_{L^2(\Gamma_3)} \} \text{ for all } t \in (0, T). \end{aligned} \tag{82}$$

Next, we combine (79) and (82) and we apply the Gronwall inequality to find

$$\begin{aligned} & \|\dot{u}(t) - \dot{u}^\epsilon(t)\|_V^2 + \|u(t) - u^\epsilon(t)\|_V^2 + \int_0^t \|\dot{u}(s) - \dot{u}^\epsilon(s)\|_V^2 ds \\ & \leq c \int_0^t (\|q_e(t) - q_e^\epsilon(t)\|_W^2 + \|\varphi_F(s) - \varphi_F^\epsilon(s)\|_{L^2(\Gamma_3)}^2 + \|f(s) - f^\epsilon(s)\|_V^2) ds. \end{aligned} \tag{83}$$

Remembering the definitions (24), (25), (64) and (65) of f , q_e , f^ϵ and q_e^ϵ , we obtain

$$\|f(t) - f^\epsilon(t)\|_V \leq c_p \|f_0(t) - f_0^\epsilon(t)\|_{L^2(\Omega)} + c_0 \|f_2(t) - f_2^\epsilon(t)\|_{L^2(\Gamma_2)}, \quad \forall t \in (0, T), \tag{84}$$

$$\|q_e(t) - q_e^\epsilon(t)\|_W \leq c'_p \|q_0(t) - q_0^\epsilon(t)\|_{L^2(\Omega)} + c_1 \|q_2(t) - q_2^\epsilon(t)\|_{L^2(\Gamma_b)}, \quad \forall t \in (0, T). \tag{85}$$

Finally, we use the assumptions (70)-(74) together with (83)-(85) to establish (75).

6 Conclusion

Real applications in contact mechanics, where the dynamic behavior is linear, are rare. Usually, the contact phenomena involve largely nonlinearities due to the nature of the material (with a coupling constitutive law; here, an electro-elastic materials), and the friction and electrical conduction effects accompanying the mechanical contact process. Hence, the previous parameters can change the dynamic behavior of the whole mechanical system, and the modeling of this type of problem is therefore important to predict, for

instance, the effects of friction and the electrical conduction on the material's body, and then to predict the evolution of the material state, particularly in the contact zone (wear and adhesion ..). Also, it is essential to correct prediction of the critical cases (for example, introduce lubrication effects to control friction wear and adhesion before the damage of the body).

In this paper, we presented a mathematical model for the dynamic contact problem of a nonlinear electro-elastic body and a conductive foundation. The unique weak solvability of this problem was established using arguments of evolutionary variational inequalities and a fixed point theorem. The obtained results represent an improvement of those existing in literature and will facilitate future research of other open problems arising from mathematical modeling in industrial engineering when it is necessary to take into account both the mechanical and the electrical properties. An interesting continuation of the current results would be their natural extensions to complicated piezoelectric contact problems with nontrivial electrical contact conditions. Moreover, such models lead to new evolutionary variational and hemi-variational inequalities.

Acknowledgements

The authors would like to thank the anonymous reviewers for their comments and suggestions, which significantly contributed to improving the quality of the publication.

References

- [1] A. Bachmar, B. Souraya and T. Serrar. Variational Analysis of a Dynamic Electroviscoelastic Problem with Friction. *Journal of Siberian Federal University. Mathematics & Physics* **12** (1) (2019) 68–78.
- [2] M. Barboteu and M. Sofonea. Modelling and analysis of the unilateral contact of a piezoelectric body with a conductive support. *J. Math. Anal. Appl.* **358** (1) (2009) 110–124.
- [3] M. Barboteu, J.R. Fernández and Y. Ouafik. Numerical analysis of a frictionless viscoelastic piezoelectric contact problem. *ESAIM Mathematical Modelling and Numerical Analysis* **42** (4) (2008) 667–682.
- [4] M. Barboteu, J.R. Fernández, and R. Tarraf. Numerical analysis of a dynamic piezoelectric contact problem arising in viscoelasticity. *Comput. Methods Appl. Mech. Engrg.* **197** (45-48) (2008) 3724–3732.
- [5] H. Brézis. *Functional analysis, Sobolev Spaces and Partial Differential Equations*. Universitext, Springer, New York, 2011.
- [6] M. Cocu and R. Rocca. Existence results for unilateral quasistatic contact problems with friction and adhesion. *Mathematical Modelling and Numerical Analysis* **34**(5) (2000) 981–1001.
- [7] Z. Denkowski, S. Migòrski and A. Ochal. A class of optimal control problems for piezoelectric frictional contact models. *N. Analysis: Real Wor. Appl.* **12** (3) (2011) 1883–1895.
- [8] Z. Denkowski, S. Migòrski and A. Ochal. Existence and uniqueness to a dynamic bilateral frictional contact problem in viscoelasticity. *Acta Appl. Math.* **94** (2006) 251–276.
- [9] G. Duvaut. Loi de frottement non locale. *J. Méc. Th. et Appl.* (1982) 73–78.
- [10] G. Duvaut and J.L. Lions. *Inequalities in Mechanics and Physics*. Springer-Verlag, Berlin, 1976.
- [11] P. Gamorski and S. Migòrski. Hemivariational inequalities modeling electro-elastic unilateral frictional contact problem. *Mathematics and Mechanics of Solids* **23** (2018) 329–347.

- [12] S. Hübner, A. Matei and B.I. Wohlmuth. A mixed variational formulation and an optimal a priori error estimate for a frictional contact problem in elasto-piezoelectricity. *Bull. Math. Soc. Sci. Math. Roumanie* **48** (96) (2005) 209–232.
- [13] M. Kabbaj and El-H. Essoufi. Slip-dependent friction in dynamic electroviscoelasticity. *Glasnik Matematički* **45**(65) (2010) 125–137.
- [14] M. Kabbaj and El-H. Essoufi. Existence of solutions of a dynamic Signorini’s problem with nonlocal friction for viscoelastic piezoelectric materials. *Bull. Math. Soc. Sc. Math. de Roumanie* **48** (2) (2005) 181–195.
- [15] Z. Lerguet, M. Shillor and M. Sofonea. A frictional contact problem for an electroviscoelastic body. *Electronic Journal of Differential Equations* **170** (2007) 1–16.
- [16] F. Maceri and P. Bisegna. The unilateral frictionless contact of a piezoelectric body with a rigid support. *Math. Comp. Modelling* **28** (4-8) (1998) 19–28.
- [17] S. Migòrski. Hemivariational inequality for a frictional contact problem in elastopiezoelectricity. *Discrete Contin. Dyn. Syst. Ser. B* **6** (6) (2006) 1339–1356.
- [18] S. Migòrski. A class of hemivariational inequality for electroelastic contact problems with slip dependent friction. *Discrete Contin. Dyn. Syst. Ser. S* **1** (1) (2008) 117–126.
- [19] S. Migòrski, A. Ochal and M. Sofonea. Weak solvability of a piezoelectric contact problem. *European Journal of Applied Mathematics* **20** (2) (2009) 145–167.
- [20] S. Migòrski, A. Ochal and M. Sofonea. Variational analysis of fully coupled electro-elastic frictional contact problems. *Mathematische Nachrichten* **283** (2010) 1314–1335.
- [21] W. Nowacki. Foundations of linear piezoelectricity. In: *Electromagnetic Interactions in Elastic Solids*. Springer, Wein, Chapter 1, 1979.
- [22] M. Shillor, M. Sofonea and J.J. Telega. *Models and Analysis of Quasistatic Contact*. Springer, Berlin, 2004.
- [23] M. Sofonea, W. Han and M. Shillor. *Analysis and Approximation of Contact Problems with Adhesion or Damage*. Pure and Applied Mathematics, 276, Chapman & Hall/CRC press, Boca Raton, Florida, 2005.
- [24] M. Sofonea and El-H. Essoufi. Quasistatic frictional contact of a viscoelastic piezoelectric body. *Adv. Math. Sci. Appl.* **14** (1) (2004) 613–631.
- [25] E. Zeidler. *Nonlinear Functional Analysis and Applications II A/B*. Springer, New York, 1990.



Model-Based Iterative Learning Control for the Trajectory Tracking of Disturbed Robot Manipulators

Chems Eddine Boudjedir^{1*}, Djamel Boukhetala¹ and Mohamed Bourri²

¹ *Laboratory of Process Control (LCP), Ecole Nationale Polytechnique (ENP), 10 Rue des Freres OUDEK, El-Harrach 16200, Algiers, Algeria.*

² *Labs of Biorobotics (BIOROB) and Translational Neural Engineering (TNE), Ecole Polytechnique Federale de Lausanne (EPFL), Station 9, Lausanne CH-1015, Switzerland.*

Received: April 27, 2018; Revised: March 11, 2021

Abstract: This paper proposes a model-based iterative learning control (ILC) for the trajectory tracking problem of robot manipulators performing repetitive tasks and subjected to external disturbances. The proposed scheme consists of a model-based controller to compensate as much as possible the coupled robot dynamics, a PD-type ILC to improve the tracking performances through the repetitive trajectory as well as a robust term to reject the effects of the disturbances. The convergence analysis is driven using Lyapunov theory. It is shown that the tracking error converges to zero when the iteration number increases to infinity. Simulations are performed on the parallel Delta robot to demonstrate the feasibility of the proposed approach and to highlight its tracking performances. A comparative study between the proposed ILC, the conventional PID controller, and the traditional PD plus PD-type ILC is conducted to point out the effectiveness of the model-based ILC.

Keywords: *iterative learning control; model-based control; Lyapunov theory; delta robot.*

Mathematics Subject Classification (2010): 37B25, 70E60, 93D09.

* Corresponding author: <mailto:chemseddine.boudjedir@g.enp.edu.dz>

1 Introduction

Over the years, many robot manipulators have been invented to satisfy industrial needs, for example, the Stewart platform [1] and the Delta robot [2]. The conventional control methods like PD/PID are often used to achieve the required tasks of these robots. However, robot manipulators are subject to external disturbances and their dynamics are characterised by strong coupling between the joints, which has an important effect at high dynamic movements. Therefore, PD/PID controllers are not satisfactory for applications that require high tracking accuracy at high cadence. This is due to the fact that the controller gains are selected without considering the coupling effects and external disturbances. To overcome these problems, many advanced controllers have been successfully implemented. One of the interesting techniques is the model-based controller [3]. This centralized strategy integrates the nonlinear robot dynamics in the control design to stabilise and to compensate a large part of the coupled dynamics. However, the lack of very accurate knowledge of the system may decrease the tracking performance, especially for robot manipulators that move at high speed. Other advanced controllers have been developed by considering in their objective the disturbances and coupling effects, for instance, the nonlinear PD plus sliding mode control [4], robust H-infinity control [5, 6], and neural network controllers [7, 8].

Robot manipulators are usually used for repetitive tasks such as laser cutting [9] and pick and place operations [10], where the desired trajectory is repeated over a finite time interval. Unfortunately, the most well-known controllers are not able to benefit from the task repeatability which yields the same performance without improvement. In order to exploit these repetitions, the idea of iterative learning control approach has emerged. The ILC controller takes into account the information of the previous cycles in order to improve the tracking performances of the current cycle.

In the early 1990s, Arimoto proposed a series of learning laws such as the PD-type and PID-type ILC [11]. After that, the ILC has been extensively studied, where several ILC schemes for robot manipulators have been proposed [12, 13]. Other strategies, based on adaptive and robust learning have been developed to overcome parametric and non-parametric uncertainties effects, they are: the adaptive ILC [14], adaptive switching PD control strategy [15], and robust ILC [16]. For a comprehensive review on the ILC, the readers may refer to the survey given in [17] and [18]. It is noted that the ILC has been successfully applied in many areas such as robotics [19, 20] and biological systems [21].

The main contribution of this work is to develop a model-based ILC for the trajectory tracking problem of perturbed robot manipulators performing repetitive tasks. In contrary to the traditional ILC [11], the proposed controller allows to compensate the unknown uncertainties of robot manipulators as well as the external disturbances. Moreover, the model-based ILC is more practical than the adaptive ILC [22], [15] that assumes the dynamic model can be expressed by a pre-multiplication of two separate knowing matrices and unknowing vector, which can not be the case for a complex robot like our application of the "Delta robot". Thus, the proposed control law consists of two terms. The first item is a model-based controller represented by the pre-multiplication between the PD controller and the inertia matrix. The second item is a learning control scheme that consists of a PD-type ILC with an additional robust term. Compared to the existing works related to the application of ILC, the proposed controller can be applied to uncertain nonlinear dynamic, unlike [16, 23, 24], where the controller is designed to discrete-time linear systems. Unlike [13, 15, 25], where the ILC schemes are specifically

developed for repetitive disturbances, the controller in this work can deal with nonrepetitive disturbances. The stability of the proposed control is proved using the Lyapunov method. It is shown that the tracking error converges to zero in a finite time interval when the number of iterations approaches infinity. To demonstrate the feasibility and the performances of the proposed controller, simulations have been performed on a parallel Delta robot and followed by a comparative study between the proposed controller, the conventional PID controller and the traditional PD plus PD-type ILC controller.

Throughout this paper, we use the notation $\lambda_{min}(A)$ and $\lambda_{max}(A)$ to indicate the minimum and the maximum eigenvalue of matrix A , and for any $x \in \mathbb{R}^n$, the norm of vector x is defined as $\|x\| = \sqrt{x^T x}$, while the norm of matrix A is defined as follows: $\|A\| = \sqrt{\lambda_{max}(A^T A)}$.

2 Problem Formulation

Consider the actual dynamic model for a rigid robot with n -degrees of freedom described by

$$M(q_k)\ddot{q}_k + C(q_k, \dot{q}_k)\dot{q}_k + G(q_k) + w_k(t) = \tau_k, \quad (1)$$

where $q_k \in \mathbb{R}^n$ is the generalized joint vector, $M(q_k)$ is the inertia matrix, $C(q_k, \dot{q}_k)\dot{q}_k$ is a vector resulting from Coriolis and centrifugal forces, $G(q_k)$ is the gravity torque vector, τ_k is the control input vector containing the torques to be applied at each joint and $w_k(t)$ is the vector containing external disturbances. The index k denotes the iteration number.

The actual robot dynamics (1) can be written using the nominal model as follows:

$$M_n(q_k)\ddot{q}_k + C_n(q_k, \dot{q}_k)\dot{q}_k + G_n(q_k) + d_k(t) = \tau_k, \quad (2)$$

where

$$d_k(t) = \Delta M(q_k)\ddot{q}_k + \Delta C(q_k, \dot{q}_k)\dot{q}_k + \Delta G(q_k) + w_k(t). \quad (3)$$

Our objective is to design an iterative control law τ_k , which allows the robot to track any given trajectory q_d as k tends to infinity, i.e., $\lim_{k \rightarrow \infty} \tilde{q}_k(t) = q_d(t) - q_k(t) = 0$, $\lim_{k \rightarrow \infty} \dot{\tilde{q}}_k(t) = \dot{q}_d(t) - \dot{q}_k(t) = 0, \forall t \in [0, T]$.

The dynamic motion equation (2) has the following fundamental properties, which facilitate the convergence analysis of the proposed control law [22]:

(P1) The inertia matrix $M_n(q_k)$ is symmetric, positive and satisfies

$$0 < \alpha \leq \|M_n(q_k)\| \leq \beta,$$

where α , and β are known positive constants.

(P2) There exists a positive constant K_M such that the inertia matrix $M_n(q_k)$ is globally Lipschitz continuous in its arguments

$$\|M_n(q_{k+1}) - M_n(q_k)\| < K_{M_n} \|q_{k+1} - q_k\|.$$

(P3) $G_n(q_k)$ is globally Lipschitz continuous in its arguments

$$\|G_n(q_{k+1}) - G_n(q_k)\| \leq K_g \|q_{k+1} - q_k\|,$$

where K_g is a known positive constant.

(P4) The following upper bounds are valid:

$$\|C_n(q_k, \dot{q}_k)\| \leq K_{c1} \|\dot{q}_k\|, \quad \|G_n(q_k)\| \leq K_G, \quad \forall q_k, \dot{q}_k \in \mathbb{R}^n,$$

where K_{c1} and K_G are known positive constants.

(P5) For robots having exclusively revolute joints, there exist constants $K_{c1} > 0$ and $K_{c2} > 0$ such that

$$\|C_n(q_{k+1}, \dot{q}_{k+1})\dot{q}_{k+1} - C_n(q_k, \dot{q}_k)\dot{q}_{k+1}\| \leq K_{c1}\|\dot{q}_{k+1} - \dot{q}_k\|\|\dot{q}_{k+1}\| + K_{c2}\|q_{k+1} - q_k\|\|\dot{q}_{k+1}\|^2.$$

The following assumptions are made:

(A1) The reference trajectory and its first and second time-derivatives, namely, q_d , \dot{q}_d , and \ddot{q}_d are bounded $\forall t \in [0, T]$ and $\forall k \in Z_+$.

(A2) The resetting condition is satisfied:

$$q_k(0) = q_d(0), \quad \dot{q}_k(0) = \dot{q}_d(0), \quad \forall k \in Z_+.$$

(A3) The robot velocity is bounded by a known constant V_m such that

$$\|\dot{q}_k\| \leq V_m.$$

(A4) The external disturbances and the model uncertainty are bounded by a known constant l_d such that

$$\|d_k(t)\| \leq l_d.$$

In this paper, the following lemma is used.

Lemma [26]: *The inertia matrix $M_n(q_k)$ has the following property:*

$$\|M_n(q_{k+1})^{-1} - M_n(q_k)^{-1}\| \leq K_{M_n}\alpha^{-2}\|q_{k+1} - q_k\|.$$

Proof.

$$M_n(q_{k+1})^{-1} - M_n(q_k)^{-1} = -M_n(q_{k+1})^{-1}(M_n(q_{k+1}) - M_n(q_k))M_n(q_k)^{-1}.$$

From (P1) and (P2) we can obtain

$$\|M_n(q_{k+1})^{-1} - M_n(q_k)^{-1}\| \leq K_{M_n}\alpha^{-2}\|q_{k+1} - q_k\|.$$

3 Iterative Learning Control

3.1 Controller design

The model-based ILC is given below

$$\tau_k = M_n(q_k)[K_p\tilde{q}_k + K_d\dot{\tilde{q}}_k + u_k], \tag{4}$$

and the ILC expression is given by

$$u_{k+1} = u_k + \Lambda\tilde{q}_k + \Gamma\dot{\tilde{q}}_k + \mu\text{sgn}(\tilde{z}_k), \tag{5}$$

where the variables \tilde{z}_k and z_k are defined as

$$\tilde{z}_k = z_{k+1} - z_k, \tag{6}$$

$$z_k(t) = \dot{\tilde{q}}_k(t) + \zeta\tilde{q}_k(t). \tag{7}$$

K_p, K_d, Γ , and Λ are diagonal matrices, and μ, ζ are positive constants.

The scheme of the proposed controller is illustrated in Fig. 1, where x_d represents the desired trajectory in the task space and the IGM indicates the inverse geometric model.

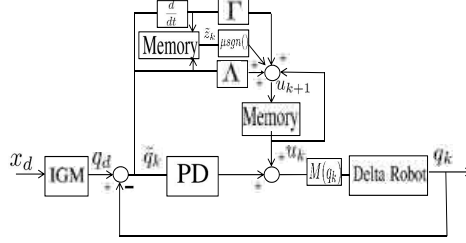


Figure 1: The proposed control scheme.

3.2 Convergence analysis

To simplify the notation, let

$$M_n(q_k) = M_{n,k}, C_n(q_k, \dot{q}_k) = C_{n,k}, G_n(q_k) = G_{n,k}, d_k(t) = d_k.$$

In the k -th iteration, equation (2) can be rewritten as

$$\ddot{q}_k = k_p \tilde{q}_k + k_d \dot{\tilde{q}}_k + u_k - M_{n,k}^{-1} C_{n,k} \dot{q}_k - M_{n,k}^{-1} G_{n,k} - M_{n,k}^{-1} d_k. \quad (8)$$

Similarly, in the $(k+1)$ -th iteration, we have

$$\begin{aligned} \ddot{q}_{k+1} = & k_p \tilde{q}_{k+1} + k_d \dot{\tilde{q}}_{k+1} + u_{k+1} - M_{n,k+1}^{-1} C_{n,k+1} \dot{q}_{k+1} \\ & - M_{n,k+1}^{-1} G_{n,k+1} - M_{n,k+1}^{-1} d_{k+1}. \end{aligned} \quad (9)$$

For the purpose of convergence proof, we assume that

$$K_p = \zeta K_d \quad \text{and} \quad \Lambda = \zeta \Gamma. \quad (10)$$

We also define the variable δq_k as

$$\delta q_k = \tilde{q}_{k+1} - \tilde{q}_k. \quad (11)$$

Theorem. Consider the system (2) under assumptions (A1-A4), properties (P1-P5), and control law (4). Then the position and velocity tracking errors converge to zero as k approaches infinity over a finite-time interval $[0, T]$, i.e., $\lim_{k \rightarrow \infty} q_k(t) = q_d(t)$ and $\lim_{k \rightarrow \infty} \dot{q}_k(t) = \dot{q}_d(t)$, $\forall t \in [0, T]$, if the gains of the controller are selected as:

$$2\lambda_{\min}(K_d - \zeta I) \geq \lambda_{\max}(\Gamma) - 2\zeta + \frac{a_1 + a_2}{\zeta} \geq 0, \quad (12)$$

$$2\lambda_{\min}(K_d - \zeta I) \geq \lambda_{\max}(\Gamma) + a_3 \geq 0, \quad (13)$$

$$4AB \geq C^2, \quad (14)$$

$$\mu - 2l_d \alpha^{-1} > \gamma, \quad (15)$$

where

$$A = \zeta^2 \lambda_{\max}(\Gamma) - 2\zeta^2 \lambda_{\min}(K_d - \zeta I) - 2\zeta^3 + \zeta(a_1 + a_2), \quad (16)$$

$$B = \lambda_{\max}(\Gamma) - 2\lambda_{\min}(K_d - \zeta I) + a_3, \quad (17)$$

$$C = a_1 + a_2 + \zeta a_3, \quad (18)$$

and

$$a_1 = 2(\alpha^{-1}K_g + K_M\alpha^{-2}K_G), \tag{19}$$

$$a_2 = 2(\alpha^{-1}K_{c2}V_m^2 + \alpha^{-2}K_MK_{c1}V_m^2), \tag{20}$$

$$a_3 = 4\alpha^{-1}K_{c1}V_m, \tag{21}$$

γ is a positive constant.

Proof: Consider the following Lyapunov function:

$$V_k(t) = \int_0^t z_k^T \Gamma z_k d\sigma. \tag{22}$$

Hence

$$\Delta V_k = V_{k+1} - V_k = \int_0^t z_{k+1}^T \Gamma z_{k+1} d\sigma - \int_0^t z_k^T \Gamma z_k d\sigma = \int_0^t \tilde{z}_k^T \Gamma \tilde{z}_k + 2\tilde{z}_k^T \Gamma z_k d\sigma. \tag{23}$$

We have $\ddot{q}_{k+1} - \ddot{q}_k = \ddot{q}_d - \ddot{q}_{k+1} - \ddot{q}_d + \ddot{q}_k$. By subtracting (9) from (8), we obtain

$$\begin{aligned} \ddot{q}_{k+1} - \ddot{q}_k = & -K_p(\tilde{q}_{k+1} - \tilde{q}_k) - K_d(\dot{\tilde{q}}_{k+1} - \dot{\tilde{q}}_k) - u_{k+1} + u_k \\ & + M_{n,k+1}^{-1}G_{n,k+1} - M_{n,k}^{-1}G_k + M_{n,k+1}^{-1}C_{n,k+1}\dot{q}_{k+1} \\ & - M_{n,k}^{-1}C_{n,k}\dot{q}_k + M_{n,k+1}^{-1}d_{k+1} - M_{n,k}^{-1}d_k. \end{aligned} \tag{24}$$

By combining the equations (5), (6), (7), (10) and (11) we get

$$\begin{aligned} \dot{\tilde{z}}_k + (K_d - \zeta I)\tilde{z}_k + \zeta^2\delta q_k - (M_{n,k+1}^{-1}G_{n,k+1} - M_{n,k}^{-1}G_{n,k}) - \\ (M_{n,k+1}^{-1}C_{n,k+1}\dot{q}_{k+1} - M_{n,k}^{-1}C_{n,k}\dot{q}_k) - (M_{n,k+1}^{-1}d_{k+1} - M_{n,k}^{-1}d_k) + \mu \operatorname{sgn}(\tilde{z}_k) = -\Gamma z_k. \end{aligned} \tag{25}$$

Replacing (25) in (23) gives us

$$\begin{aligned} \Delta V_k = & \int_0^t \tilde{z}_k^T \Gamma \tilde{z}_k - 2\tilde{z}_k^T \dot{\tilde{z}}_k - 2\tilde{z}_k^T (K_d - \zeta I)\tilde{z}_k - \\ & 2\zeta^2 \tilde{z}_k^T \delta q_k + 2\tilde{z}_k^T (M_{n,k+1}^{-1}G_{n,k+1} - M_{n,k}^{-1}G_{n,k}) + \\ & 2\tilde{z}_k^T (M_{n,k+1}^{-1}C_{n,k+1}\dot{q}_{k+1} - M_{n,k}^{-1}C_{n,k}\dot{q}_k) + \\ & 2\tilde{z}_k^T (M_{n,k+1}^{-1}d_{k+1} - M_{n,k}^{-1}d_k - \mu \operatorname{sgn}(\tilde{z}_k)) d\sigma. \end{aligned} \tag{26}$$

Therefore

$$\begin{aligned} \Delta V_k = & \int_0^t \tilde{z}_k^T \Gamma \tilde{z}_k - 2\tilde{z}_k^T \dot{\tilde{z}}_k - 2\tilde{z}_k^T (K_d - \zeta I)\tilde{z}_k - \\ & 2\zeta^2 \tilde{z}_k^T \delta q_k + 2\tilde{z}_k^T [M_{n,k+1}^{-1}(G_{n,k+1} - G_{n,k}) + \\ & (M_{n,k+1}^{-1} - M_{n,k}^{-1})G_{n,k}] + 2\tilde{z}_k^T [M_{n,k+1}^{-1}((C_{n,k+1} - C_{n,k})\dot{q}_{k+1} \\ & + C_{n,k}(\dot{q}_{k+1} - \dot{q}_k)) + (M_{n,k+1}^{-1} - M_{n,k}^{-1})C_{n,k}\dot{q}_k] + \\ & 2\tilde{z}_k^T (M_{n,k+1}^{-1}d_{k+1} - M_{n,k}^{-1}d_k - \mu \operatorname{sgn}(\tilde{z}_k)) d\sigma. \end{aligned} \tag{27}$$

With assumption (A4) and property (P1) we can obtain $\tilde{z}_k^T (M_{n,k+1}^{-1}d_{k+1} - M_{n,k}^{-1}d_k) \leq \|\tilde{z}_k^T\| (2l_d\alpha^{-1})$, thus

$$\int_0^t \tilde{z}_k^T (M_{n,k+1}^{-1}d_{k+1} - M_{n,k}^{-1}d_k - \mu \operatorname{sgn}(\tilde{z}_k)) d\sigma \leq \int_0^t \|\tilde{z}_k^T\| (2l_d\alpha^{-1} - \mu) d\sigma. \tag{28}$$

Properties (P1-P5), (28) and assumption (A3) lead to

$$\begin{aligned} \Delta V_k \leq & \int_0^t \tilde{z}_k^T \Gamma \tilde{z}_k - 2\tilde{z}_k^T \dot{\tilde{z}}_k - 2\tilde{z}_k^T (K_d - \zeta I) \tilde{z}_k - \\ & 2\zeta^2 \tilde{z}_k^T \delta q_k + 2\|\tilde{z}_k^T\|(\alpha^{-1}K_g + K_M \alpha^{-2}K_G)\|\delta q_k\| + \\ & 2\|\tilde{z}_k^T\|(\alpha^{-1}K_{c2}V_m^2 + \alpha^{-2}K_M K_{c1}V_m^2)\|\delta q_k\| + \\ & 2\|\tilde{z}_k^T\|(2\alpha^{-1}K_{c1}V_m)\|\delta \dot{q}_k\| + 2\|\tilde{z}_k^T\|(2l_d\alpha^{-1} - \mu)d\sigma. \end{aligned} \quad (29)$$

By replacing (7), (19), (20) and (21) in (29) we obtain

$$\begin{aligned} \Delta V_k \leq & \int_0^t \delta \dot{q}_k^T \Gamma \delta \dot{q}_k + \zeta^2 \delta q_k^T \Gamma \delta q_k + 2\zeta \delta \dot{q}_k^T \Gamma \delta q_k - 2\tilde{z}^T \dot{\tilde{z}}_k - \\ & 2\zeta^2 \delta q_k^T (K_d - \zeta I) \delta q_k - 2\delta \dot{q}_k^T (K_d - \zeta I) \delta \dot{q}_k - \\ & 4\zeta \delta \dot{q}_k^T (K_d - \zeta I) \delta q_k - 2\zeta^2 \delta \dot{q}_k^T \delta q_k - 2\zeta^3 \|\delta q_k\|^2 + \\ & \zeta a_1 \|\delta q_k\|^2 + a_1 \|\delta q_k\| \|\delta \dot{q}_k\| + \zeta a_2 \|\delta q_k\|^2 + \\ & a_2 \|\delta q_k\| \|\delta \dot{q}_k\| + a_3 \|\delta \dot{q}_k\|^2 + \zeta a_3 \|\delta q_k\| \|\delta \dot{q}_k\| + \\ & 2\|\tilde{z}_k^T\|(2l_d\alpha^{-1} - \mu)d\sigma. \end{aligned} \quad (30)$$

Using assumption (A2) one can get

$$\begin{aligned} \Delta V_k \leq & -\|\tilde{z}_k\|^2 - \zeta^2 \|\delta q_k\|^2 - \zeta \delta q_k^T (2K_d - 2\zeta I - \Gamma) \delta q_k + \\ & \int_0^t \delta \dot{q}_k^T \Gamma \delta \dot{q}_k + \zeta^2 \delta q_k^T \Gamma \delta q_k - 2\zeta^3 \|\delta q_k\|^2 - \\ & 2\zeta^2 \delta q_k^T (K_d - \zeta I) \delta q_k - 2\delta \dot{q}_k^T (K_d - \zeta I) \delta \dot{q}_k + \\ & \zeta a_1 \|\delta q_k\|^2 + a_1 \|\delta q_k\| \|\delta \dot{q}_k\| + \zeta a_2 \|\delta q_k\|^2 + \\ & a_2 \|\delta q_k\| \|\delta \dot{q}_k\| + a_3 \|\delta \dot{q}_k\|^2 + \zeta a_3 \|\delta q_k\| \|\delta \dot{q}_k\| + \\ & 2\|\tilde{z}_k^T\|(2l_d\alpha^{-1} - \mu)d\sigma. \end{aligned} \quad (31)$$

Hence

$$\begin{aligned} \Delta V_k \leq & -\|\tilde{z}_k\|^2 - \zeta^2 \|\delta q_k\|^2 - \zeta \lambda_{\min}(2K_d - 2\zeta I - \Gamma) \|\delta q_k\|^2 \\ & + \int_0^t [\lambda_{\max}(\Gamma) - 2\lambda_{\min}(K_d - \zeta I) + a_3] \|\delta \dot{q}_k\|^2 + \\ & [\zeta^2 \lambda_{\max}(\Gamma) - 2\zeta^3 - 2\zeta^2 \lambda_{\min}(K_d - \zeta I) \\ & + \zeta(a_1 + a_2)] \|\delta q_k\|^2 + [a_1 + a_2 + \zeta a_3] \|\delta q_k\| \|\delta \dot{q}_k\| + \\ & 2\|\tilde{z}_k^T\|(2l_d\alpha^{-1} - \mu)d\sigma. \end{aligned} \quad (32)$$

Using (16), (17), and (18) we obtain

$$\begin{aligned} \Delta V_k \leq & -\|\tilde{z}_k\|^2 - \zeta^2 \|\delta q_k\|^2 - \zeta \lambda_{\min}(2K_d - 2\zeta I - \Gamma) \|\delta q_k\|^2 \\ & + \int_0^t A \|\delta q_k\|^2 + B \|\delta \dot{q}_k\|^2 + C \|\delta q_k\| \|\delta \dot{q}_k\| + 2\|\tilde{z}_k^T\|(2l_d\alpha^{-1} - \mu)d\sigma. \end{aligned} \quad (33)$$

Hence, from (15) we can get

$$\begin{aligned} \Delta V_k < & -\|\tilde{z}_k\|^2 - \zeta^2 \|\delta q_k\|^2 - \zeta \lambda_{\min}(2K_d - 2\zeta I - \Gamma) \|\delta q_k\|^2 \\ & + \int_0^t A(\|\delta q_k\| + \frac{C}{2A} \|\delta \dot{q}_k\|)^2 + (B - \frac{C^2}{4A}) \|\delta \dot{q}_k\|^2 - 2\gamma \|\tilde{z}_k^T\| d\sigma. \end{aligned} \quad (34)$$

From (12), (13), (14) and (15) we can get

$$\Delta V_k < 0, \quad i.e., \quad V_{k+1} < V_k. \quad (35)$$

From (35) we conclude that when k tends to infinity, V_k tends to zero, which implies that $z_k \rightarrow 0$, and from the definition of z_k (7), we can obtain

$$\lim_{k \rightarrow \infty} \tilde{q}_k(t) = \lim_{k \rightarrow \infty} \dot{\tilde{q}}_k = 0, \forall t \in [0, T]. \quad (36)$$

Remark: It is worth noting that the sign function used in the proposed control (5) might lead to the chattering phenomenon in the control input. In order to reduce the effects of this phenomenon in practical applications, saturation function can be introduced instead of the sign function. As a consequence, the tracking error converges to a domain around zero with a smooth control signal.

4 Simulation

In this section, we present the simulation results obtained by applying the model-based ILC on the parallel Delta robot described by Fig. 2. Delta robot is a very fast robot designed to achieve high precision for high dynamic pick and place operations, where the traditional controllers can fail to deal with this dynamic and to reject the external disturbances.

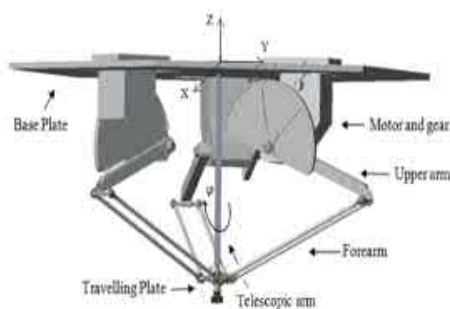


Figure 2: The Delta robot.

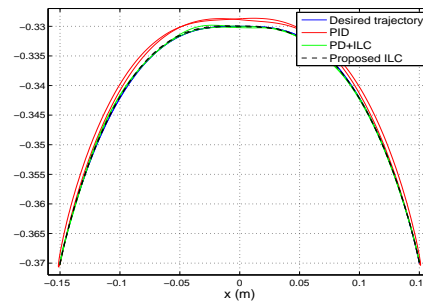


Figure 3: The trajectory tracking in the task space.

The matrices of the robot are given as follows:

$$M(q) = I_b + m_{nt} J^T J, \quad C(q, \dot{q}) = J^T m_{nt} \dot{J}, \quad G(q) = -\tau_{Gn} - \tau_{Gb},$$

where τ_{Gn} is the torque produced by the inertial force, τ_{Gb} is the torque produced by the gravitational force of the arms, J represents the Jacobian matrix and \dot{J} is its time derivative, m_{nt} represents the total mass which is the sum of the travelling plate mass, the mass of the payload and the 3 reported masses contributed each of the 3 forearms. For the detailed expressions of the Jacobian, τ_{Gn} , τ_{Gb} and m_{nt} , please, refer to [27]. The geometrical and dynamic parameters of the Delta robot are described in Table 1. The constants are given as follows: $K_{c1} = 0.44 \text{ kgm}^2$, $K_{c2} = 2.675 \text{ kgm}^2$, $K_g = 0.354 \text{ kg.m}^2/\text{s}^2$, $K_G = 0.442 \text{ kg.m}^2/\text{s}^2$, $V_m = 5 \text{ rad/s}$, $\alpha = 0.3 \text{ kgm}^2$, $K_M = 0.09 \text{ kgm}^2$. The modelling errors are set as follows: $\Delta M(q_k) = 0.1 * M(q_k)$, $\Delta C(q_k, \dot{q}_k) = 0.1 * C(q_k, \dot{q}_k)$, $\Delta G(q_k) = 0.1 * G(q_k)$. Whereas, the disturbances are assumed to be time-varying and also varying from iteration to iteration as follows: $d1(t)=d2(t)=d3(t)=0.2.rand(k)sin(2\pi t)$ (in Newton meters), where $rand(k)$ is a random function taking its values between 0 and 1.

Table 1: Geometric and dynamic parameters.

Parameter	Value
Length of the upper arm	0.380 m
Length of the forearm	0.205 m
Mass of the travelling plate	0.042 kg
Mass of the upper arm	0.098 kg
Masses of the forearms	0.028 kg
Mass of the elbow	0.015 kg

The desired trajectory used along the x-axis and the z-axis is a polynomial of degree five with an initial and final velocity and acceleration equal to zero. Its expression is given by

$$x(t) = x_i + (x_f - x_i) \left(6 \frac{t^5}{t_f^5} - 15 \frac{t^4}{t_f^4} + 10 \frac{t^3}{t_f^3} \right), \quad (37)$$

where x_i and x_f are the initial and final positions, and t_f is the duration of the movement.

To evaluate the performance of the controllers, the Root Mean Square Error (RMSE) criteria and the Maximum Absolute Error (MaxAE) criteria are used. Their expressions are given as follows:

$$RMSE = \sqrt{\frac{1}{n} \sum_{i=1}^n (y_i - y_{d_i})^2}, \quad (38)$$

$$MaxAE = \text{Max}(|y_i - y_{d_i}|), \quad (39)$$

where y_d is the desired trajectory, y_i is the actual response, and n is the total number of samples in one iteration. The controller gains matrices were selected so that the minimum performance criteria specified by the RMSE and the MaxAE are obtained after 90 iterations. The proposed controller gains were set to: $K_p = \text{diag}\{600\}$, $K_d = \text{diag}\{40\}$, $\Lambda = \text{diag}\{18.3\}$, $\Gamma = \text{diag}\{1.22\}$, and $\zeta = 15$, while the PID controller gains were selected as: $K_{p(PID)} = \text{diag}\{12\}$, $K_{d(PID)} = \text{diag}\{0.18\}$, $K_{I(PID)} = \text{diag}\{2\}$, and the PD plus ILC controller gains were chosen as: $K_{p(PD-ILC)} = \text{diag}\{8\}$, $K_{d(PD-ILC)} = \text{diag}\{0.08\}$, $\Lambda_{PD-ILC} = \text{diag}\{0.5\}$, $\Gamma_{PD-ILC} = \text{diag}\{0.02\}$. We give the simulation study in two cases.

Case 1: The desired trajectory starts from the initial position $(-0.15, 0, -0.37)$ m to the final position $(0.15, 0, -0.37)$ m with a height of transit equal to 0.04 m, then returns to the initial position during 0.4 second.

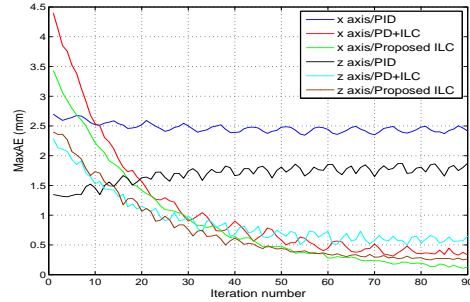
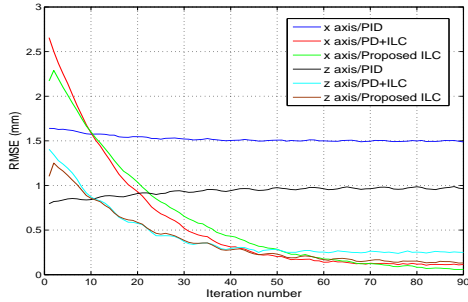


Figure 4: The RMSE along the iteration axis. **Figure 5:** The MaxAE along the iteration axis.

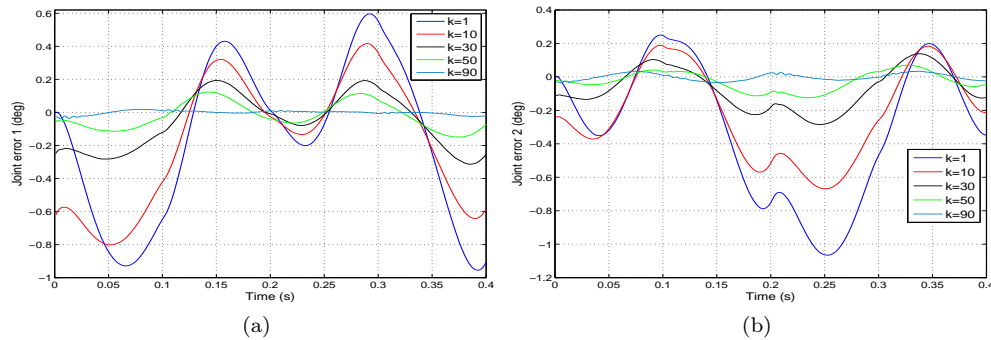


Figure 6: Tracking error for iteration $k=1,10,30,50,90$. (a) joint 1, (b) joint 2.

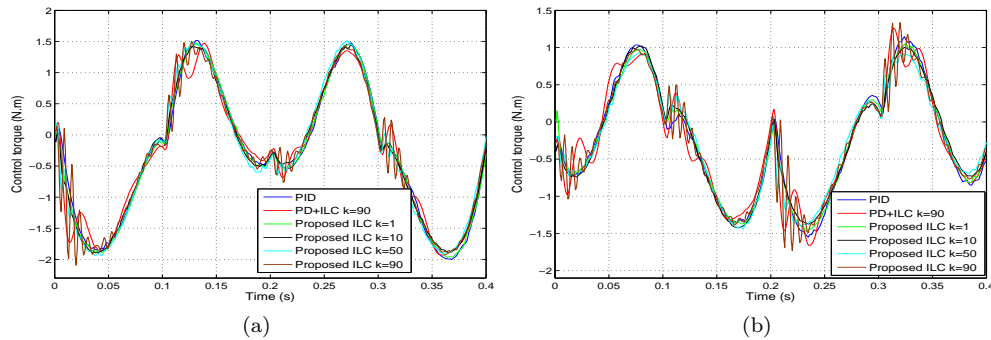


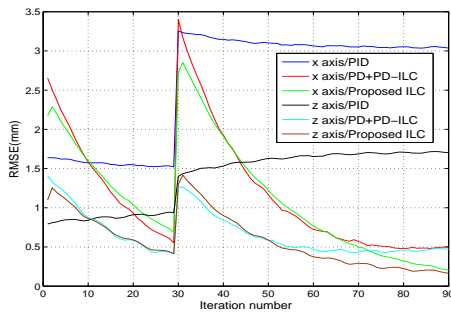
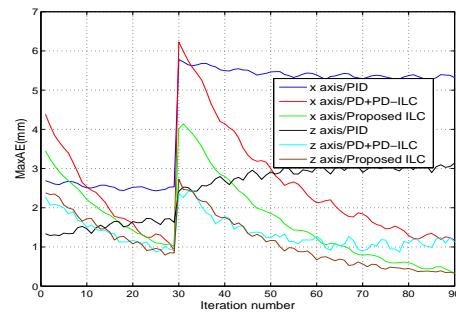
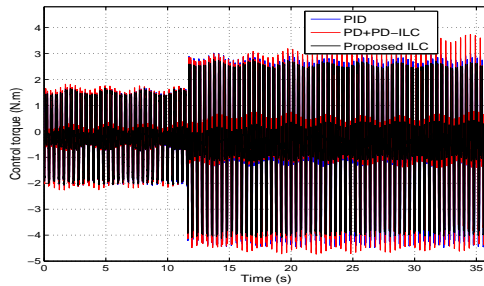
Figure 7: Control torque for iteration $k=1,10,30,50,90$. (a) joint 1, (b) joint 2.

Figure 3 presents the trajectory tracking in the operational space after 90 iterations under the proposed controller, the PID controller and the PD plus PD-type ILC. Fig. 4 and Fig. 5 indicate the progress of the RMSE and the MaxAE, respectively, through the iterations. It can be observed that the tracking performance improves from iteration to iteration, where, for instance, the RMSE decreased from 2.17 mm at the first iteration along the x-axis to 0.06 mm at the 90th iteration, while the PID and the PD plus PD-type ILC controller lead to an RMSE along the x-axis equal to 1.48 mm and 0.12 mm, respectively. Fig. 6 shows the tracking error of joint 1 and joint 2, respectively, (the tracking error of joint 3 is similar to that of joint 2 due to the nature of the trajectory), for the 1st, 10th, 30th, 50th and the 90th iteration. It is observed that the desired trajectory has been obtained successfully with the increase of the iteration number despite the existence of the model uncertainty and the external disturbances. Fig. 7 represents the torque control of joint 1 and joint 2, respectively. It is shown that the torque profile remains nearly the same from the first iteration to the 90th iteration, which provides an advantage of the proposed controller where the tracking performances are enhanced through the iteration without requiring more control energy.

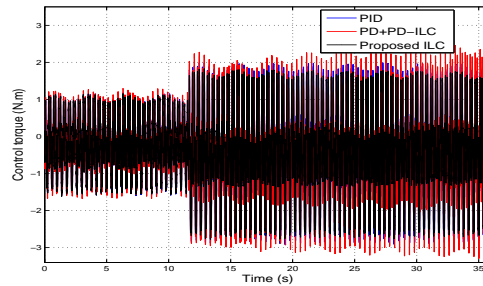
Case 2: In order to evaluate the ability to track the desired trajectory in the presence of payloads, an additional load of 200 g is introduced on the travelling plate of the Delta robot, from 30 iterations to 90 iterations.

Table 2: Tracking performance through iterations under additional load of 200 g.

Iteration	1	10	30	50	90
RMSE x-axis (mm)	2.17	1.60	2.76	1.22	0.20
MaxAE x-axis (mm)	3.43	2.21	4.02	1.85	0.33
RMSE z-axis (mm)	1.10	0.85	1.30	0.58	0.16
MaxAE z-axis (mm)	2.40	1.73	2.73	1.16	0.33

**Figure 8:** The RMSE along the iteration axis-Case 2.**Figure 9:** The RMSE along the iteration axis-Case 2.

(a)



(b)

Figure 10: The control torque-Case 2. (a) joint 1, (b) joint 2.

The simulation results are presented in Fig. 8 to Fig. 10. It is observed that the PID controller lost its performances after the introduction of the additional load, while the performances of the PD plus PD-type became constant between the 60th and the 70th iterations, then start diverging after that. Meanwhile, the proposed ILC is still the one giving us better performances, where, on one hand, the RMSE and the MaxAE decrease with a rate faster than the traditional ILC and continue to decrease even at the 90th iteration. On the other hand, the control torque of the proposed controller is smaller than the PID and the PD plus PD-type ILC, which provides a significant importance to the proposed approach. Table 2 summarises the tracking performance obtained under an additional load of 200 g.

5 Conclusion

In this work, a model-based iterative learning scheme has been proposed for the trajectory tracking of robot manipulators with model uncertainty and subjected to external disturbances. In order to decrease the coupling effect, a model-based controller has been introduced and combined with an ILC and a robust control term to benefit from the repetition of the task and to reject the model uncertainty and external disturbances. The asymptotic convergence has been demonstrated using the Lyapunov method. It has been shown that the tracking position and velocity errors decrease through the iterations regardless of the influence of the model uncertainty and the external disturbances. Simulation results confirm the feasibility and the effectiveness of the proposed control scheme compared to the PID and the PD plus PD-type ILC. Otherwise, the control energy is still limited and does not increase with the number of iterations.

References

- [1] B. Andrievsky, D.V. Kazunin, D.M. Kostygova, N.V. Kuznetsov, G.A. Leonov, P. Lobanov and A.A. Volkov. Differential equations of controlled pneumatic actuators for 6-DOF Stewart platform. *Nonlinear Dynamics and Systems Theory* **15** (1) (2015) 14–24.
- [2] C. E. Boudjedir, M. Bouri and D. Boukhetala. Iterative learning control for trajectory tracking of a parallel delta robot. *at - Automatisierungstechnik* **67** (2) (2019) 145–156.
- [3] A. Dumlu, K. Erenturk, A. Kaleli and K. K. Ayten. A comparative study of two model-based control techniques for the industrial manipulator. *Robotica* **35** (10) (2016) 2036–2055.
- [4] C. E. Boudjedir, D. Boukhetala and M. Bouri. Nonlinear PD plus sliding mode control with application to a parallel delta robot. *Journal of Electrical Engineering* **69** (5) (2018) 329–336.
- [5] M. Rachedi, B. Hemici and M. Bouri. Design of an H_∞ controller for the Delta robot: experimental results. *Advanced Robotics* **29** (18) (2015) 1165–1181.
- [6] A. G. Mazko. Robust output feedback stabilization and optimization of discrete-time control systems. *Nonlinear Dynamics and Systems Theory* **18** (1) (2018) 92–106.
- [7] H. Ait Abbas, M. Belkheiri and B. Zegnini. Robust neural output feedback tracking control for a class of uncertain nonlinear systems without time-delay. *Nonlinear Dynamics and Systems Theory* **16** (2) (2016) 115–128.
- [8] H. Ait Abbas, A. Seghiour, M. Belkheiri and M. Rahmani. Robust output feedback stabilization and boundedness of highly nonlinear induction motors systems using single-hidden-layer neural-networks. *Nonlinear Dynamics and Systems Theory* **19** (3) (2019) 331–347.
- [9] C. H. Tsai and C. J. Chen. Application of iterative path revision technique for laser cutting with controlled fracture. *Opt. Laser Eng* **41** (1) (2004) 189–204.
- [10] C. E. Boudjedir, M. Bouri and D. Boukhetala. Model-free Iterative Learning Control with Nonrepetitive Trajectories for Second-Order MIMO Nonlinear Systems – Application to a Delta Robot. *IEEE Transactions on Industrial Electronics* (2020) 1-1.
- [11] S. Arimoto, S. Kawamura and F. Miyazaki. Can mechanical robots learn by themselves? In: *H. Hanafusa, H. Inoue (Eds.) Robotics Research*. Second International Symposium, MIT Press, Cambridge, 1984, 127–134.
- [12] C. E. Boudjedir, D. Boukhetala and M. Bouri. Iterative learning control of multivariable uncertain nonlinear systems with nonrepetitive trajectory. *Nonlinear Dynamics* **95** (3) (2019) 2197–2208.

- [13] F. Bouakrif, D. Boukhetala and F. Boudjema. Iterative learning control schemes for robot manipulators. *The Mediterranean Journal of Measurement and Control* **3** (3) (2007) 104–112.
- [14] C. E. Boudjedir and D. Boukhetala. Adaptive robust iterative learning control with application to a Delta robot. *Proceedings of the Institution of Mechanical Engineers, Part I: Journal of Systems and Control Engineering* **235** (2) (2021) 207–221.
- [15] P.R. Ouyang, W.J. Zhang and M. Gupta. An adaptive switching learning control method for trajectory tracking of robot manipulators. *Mechatronics* **16** (1) (2006) 51–61.
- [16] D. Meng and K. L. Moore. Robust Iterative Learning Control for Nonrepetitive Uncertain Systems. *IEEE Trans. on Automatic Control* **62** (2) (2017) 907–913.
- [17] Jian-Xin Xu. A survey on iterative learning control for nonlinear systems. *International Journal of Control* **84** (7) (2011) 1275–1294.
- [18] D. Shen. Iterative learning control with incomplete information: a survey. *IEEE/CAA Journal of Automatica Sinica* **5** (5) (2018) 885–901.
- [19] P. Chirarattananon, K. Y. Ma and R. J. Wood. Perching with a robotic insect using adaptive tracking control and iterative learning control. *The International Journal of Robotics Research* **35** (10) (2016) 1185–1206.
- [20] L. Zhang, W. Chen, J. Liu and C. Wen. A robust adaptive iterative learning control for trajectory tracking of permanent-magnet spherical actuator. *IEEE Transactions on Industrial Electronics* **63** (1) (2016) 291–301.
- [21] M.A. Márquez-Vera, L.E. Ramos-Velasco, J. Suárez-Cansino and C.A. Márquez-Vera. Iterative learning control applied in a biological reactor using a reduced number of measures. *Appl. Math. Comput.* **46** (2014) 608–618.
- [22] R. Kelly, V. Santibáñez and A. Loria. Control of Robot Manipulators in Joint Space. *Advanced Textbooks in Control and Signal Processing*. Springer, Berlin, 2005.
- [23] H. Abdellatif, M. Feldt and B. Heimann. Application study on iterative learning control of high speed motions for parallel robotic manipulator. In: *Proceedings of IEEE International Conference on Control Applications*, Munich, Germany, 2006, 2528–2533.
- [24] B. Altın, J. Willems, T. Oomen and K. Barton. Iterative Learning Control of Iteration-Varying Systems via Robust Update Laws with Experimental Implementation. *Control Engineering Practice* **62** (2017) 36–45.
- [25] C. E. Boudjedir, D. Boukhetala and M. Bouri. Fuzzy logic iterative learning control for trajectory tracking of parallel kinematic manipulators. In: *5th International Conference on Electrical Engineering*. Bumerdes, Algeria, 2017, 1–6.
- [26] F. Bouakrif, D. Boukhetala and F. Boudjema. Velocity observer-based iterative learning control for robot manipulators. *International Journal of Systems Science* **44** (2) (2013) 214–222.
- [27] A. Codourey. Dynamic modelling and mass matrix evaluation of the delta parallel robot for axes decoupling control. In: *The International Conference on Intelligent Robots and Systems*. Osaka, Japan, 1996, 1211–1218.



Convective Stability of CO_2 Sequestration in a Porous Medium

M. H. DarAssi*

Department of Basic Sciences, Princess Sumaya University for Technology, Amman, Jordan.

Received: September 9, 2020; Revised: March 22, 2021

Abstract: We considered an incompressible fluid-saturated porous layer bounded by two infinite parallel plates. The Boussinesq approximation and Darcy's law are applied. The permeability is assumed to be a linear function of the depth z . The linear stability is investigated. The long wavelength expansion method is applied to conduct the weakly nonlinear stability analysis. The evolution equation is derived and analyzed. A uniformly valid periodic solution of the evolution equation is obtained by the application of the Poincaré-Lindstedt method. Some numerical simulations are presented.

Keywords: *stability analysis; long wavelength method; Poincaré-Lindstedt method; periodic solution; carbon sequestration.*

Mathematics Subject Classification (2010): 76E20, 76E15, 76S05, 76-10, 76E06.

1 Introduction

The greenhouse effect of carbon dioxide is one of the most urgent problems that face the humanity. The greenhouse gas emissions can be reduced through the geological carbon dioxide sequestration in deep rock formations. Geological carbon dioxide sequestration is the process of trapping CO_2 that is produced by burning fossil fuels or any other chemical or biological processes and placing it in a deep rock formation (thousands of feet deep) for a long-term storage so that it will not affect the atmosphere. This process is comprised of three stages: capturing, transporting, and injecting CO_2 into the geological formation such as gas reservoirs, unmineable coal seams, and basalt formations [1–4]. The capacity of such formations is estimated worldwide to be between 675–900 Gt of carbon in the gas reservoirs, between 1000–10000 Gt for saline aquifers, and for unmineable coal it

* Corresponding author: <mailto:m.assi@psut.edu.jo>

is between 3-200 Gt of carbon. Depending on the geothermal gradient and the fluid properties, CO_2 migrates and reacts with the rock formation. Hence, many trapping mechanisms such as structure trapping, residual-phase trapping, solubility trapping, and mineral trapping have been contributing to retention of the CO_2 sequestration for a very long period [5].

In the past few decades, the interest in the understanding of the convection in porous media has been increased. Vast studies have been made in several branches of engineering and science [6–23]. Natural convection in porous media has been explored in numerous papers. Horton and Rogers in 1945 and Lapwood in 1948, carried out the stability analysis of the convection of a fluid in a porous medium for a horizontal fluid layer problem. The critical Rayleigh number was $4\pi^2$ [6, 7]. Foster [8, 9] applied the amplification theory to study time dependent coefficients of a system of partial differential equations. They determined the onset of instability in terms of critical time. King et. al. use the amplification method to study the carbon dioxide sequestration problem in anisotropic porous media [10, 11]. The problem of convection of carbon dioxide storage in saline aquifers has been investigated by Hassanzadeh et. al. [12–14] and Emami-Meybodi et. al. [15, 16]. A step-function base profile has been considered by Wanstall and Hadji [17]. They conducted the stability analysis by applying the normal modes approach. They investigated the linear and nonlinear stability to obtain the minimum thickness of the layer of the saturated brine that is required for the fluid motion.

Neufeld et. al. [18] performed laboratory experiments to study the convective behavior of CO_2 brine. Their numerical simulations depicted the relation between the convective flux and the Rayleigh number. To study the dissolution of CO_2 into brine, Neufeld et. al. [19] used mixtures of methanol and ethylene-glycol solutions in water in their laboratory experiments. Batchelor and Nitsche [20] considered the small disturbance of a stationary stratified fluid. They showed numerically that the growth rate is a function of the Rayleigh number, the Prandtl number, and the horizontal wavenumber of the disturbance. A nonlinear stability analysis of a convection in porous layer with finite conducting boundaries has been conducted by Riahi [21]. Hill and Morad [22] have studied the convective stability in an anisotropic porous medium. They considered a water-saturated porous layer bounded by two horizontal parallel plates. The Darcy equation with variable permeability is used to govern the fluid motion.

Vo and Hadji [23] investigated the linear and weakly nonlinear stability of the convection induced by sequestration of CO_2 in a perfectly impervious geological formation. They considered a horizontal layer of brine saturated porous medium confined between two horizontal planes that are impermeable to mass flow. They used the classical normal modes to investigate the linear stability. The weakly nonlinear stability is studied by applying the long wavelength asymptotic expansion method that is valid for small Damköhler numbers. They determined that the Rayleigh number and its corresponding wavenumber are independent of the depth of the formation.

Vo and Hadji [23] described the model that mimics the Rayleigh-Taylor instability to study the carbon sequestration. They considered the heavy carbon-saturated layer (Z_0 1) on the top of the light free-carbon layer (0 Z_0). This situation leads to a very thin unstable stratified layer at $z = Z_0$ across which buoyancy diffuses. The stratified basic profile is defined as a step function and the reference carbon concentration in porous

media is defined by

$$C_{ref}(z) = \begin{cases} 0, & 0 < z < Z_0, \\ \frac{z - Z_0}{1 - Z_0}, & Z_0 < z < 1. \end{cases}$$

The basic temperature profile is defined by $T_B = T_1 + (T_2 - T_1)\mathcal{H}(z - Z_0)$, where T_1 and T_2 are temperature values at the lower region and the upper region, respectively, and \mathcal{H} is the Heaviside function.

In this paper, we considered the same model as that proposed by Hill and Morad [22], where the instability is quantified in terms of the long time evolution with the Dirichlet and Neumann boundary conditions at the upper and lower walls, respectively. This paper is organized as follows: In Section 2, a full description of the problem is presented and the problem is governed by a mathematical model. Moreover, the basic profile of the concentration is derived. In Section 3, the steady-state linear stability is studied. The weakly nonlinear stability is investigated by the application of the long wavelength expansion method in Section 4. In Section 5, the Poincaré-Lindstedt method is used to obtain a uniformly valid periodic solution. Numerical simulations are introduced and the results are concluded in Section 6.

2 Mathematical Formulation

In this section we considered the mathematical model that has been discussed by Hill and Morad [22], Wanstall and Hadji [17], and Vo and Hadji [23]. That is, we considered an incompressible fluid-saturated porous layer bounded by two infinite horizontal parallel plates. We assumed that the Boussinesq approximation and Darcy’s law are applied and the fluid motion is governed by the Darcy equation. Therefore, the nondimensionalized governing system of equations comprised of the Darcy equation, the continuity equation, the conservation of carbon dioxide equation, and the equation of solute balance is given by

$$\nabla \cdot \mathbf{u} = 0, \tag{1a}$$

$$\frac{1}{\mathcal{F}(z)} \mathbf{u} = \nabla p - c \mathbf{k}, \tag{1b}$$

$$\frac{\partial c}{\partial \hat{t}} + \mathbf{u} \cdot \nabla c + \left(\frac{dM(z)}{dz} \right) w = \frac{\xi}{R} \nabla_H^2 c + \frac{1}{R} \left(\frac{\partial^2 c}{\partial z^2} - Da c \right), \tag{1c}$$

$$\rho = \rho_0 [1 + \gamma_c (c - C_0)], \tag{1d}$$

where $M(z)$ is the basic profile of concentration, p is the pressure, \mathbf{k} is the vertical unit vector, ρ_0 is the reference density, $\xi = \frac{\kappa_h}{\kappa_v}$ is the ratio of the horizontal and vertical solutal diffusion, $\mathcal{F}(z)$ is the z -dependent dimensionless permeability, $Da = \frac{\beta H^2}{\psi_p \kappa_v}$ is the Damökhler number, β is the reaction rate and the control parameter, namely, the Rayleigh-Darcy number $R = \frac{\gamma_c g H K_0 C_0}{\phi_p \nu \kappa_v}$, where γ_c is the solutal expansion, g is the gravitational constant, H is the distance between the two plates, K_0 is the reference permeability value, C_0 is the reference concentration of CO_2 , ϕ_p is the porosity, ν is the kinematic viscosity, and κ_v is the vertical CO_2 diffusion coefficient. The system is subject to the following boundary conditions:

$$\mathbf{u} = \mathbf{0}, \quad \text{at } z = 0, z = 1,$$

and

$$\frac{\partial c}{\partial z} = 0, \quad \text{at } z = 0, z = 1.$$

For more details about this model, please, refer to [22], [17] and [23]. Figure 1 describes the problem with its boundary conditions.

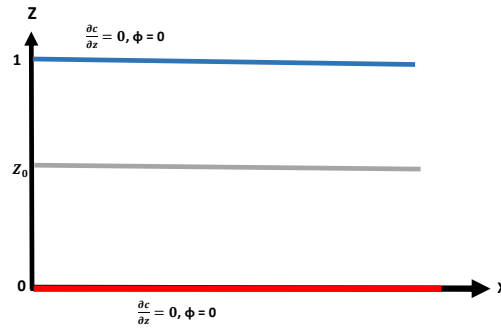


Figure 1: An incompressible fluid-saturated porous layer bounded by two infinite horizontal parallel plates.

The step function base state is modeled by the partial differential equation

$$\frac{\partial C_B}{\partial t} = \frac{1}{R} \left(\frac{\partial^2 C_B}{\partial z^2} - Da C_B \right), \quad 0 \leq z \leq 1, \quad t > 0, \quad (2)$$

subject to the boundary conditions

$$\frac{\partial C_B}{\partial z} = 0 \quad \text{at } z = 0, \quad z = 1,$$

and the initial condition

$$C_B(z, 0) = \begin{cases} 0, & 0 \leq z < Z_0, \\ 1, & Z_0 \leq z \leq 1. \end{cases}$$

The solution of equation (2) is given by

$$C_B(z, \hat{t}) = 1 - Z_0 - 2 \sum_{n=1}^{\infty} \frac{\sin(n\pi Z_0)}{n\pi} \cos(n\pi z) \exp\left(-\frac{Da + n^2 \pi^2}{R} \hat{t}\right). \quad (3)$$

Figure 2 below shows the plot of the concentration basic profile as a function of z for some values of t .

Following [17], the basic concentration profile consists of a light layer $0 < z < Z_0$ under a heavier one, $Z_0 < z < 1$, which can be described by the Heaviside function, i.e.,

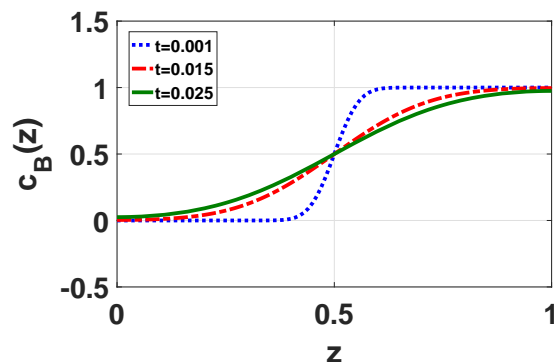


Figure 2: The plot of the concentration profile $c_B(z)$ as a function of the depth of the fluid layer z and $t = 0.001$ (dotted line), $t = 0.015$ (dashed line) and $t = 0.025$ (solid line).

$M(z) = \mathcal{H}(z - Z_0)$. Upon subtracting the basic state profiles, introducing the poloidal representation for the velocity field $\mathbf{u} = \nabla \times (\nabla \times \phi \mathbf{k})$, and considering the vertical component of the velocity, we removed the pressure term and the system of equations (1a)-(1d) reduced to

$$\mathcal{F}(z)\nabla^2\phi - \mathcal{F}'(z)\frac{d\phi}{dz} = -\mathcal{F}^2(z)c, \tag{4a}$$

$$c_t + (\nabla_H\phi_z) \cdot (\nabla_H c) - \nabla_H^2\phi c_z = -\nabla_H^2\phi\delta(z - Z_0) + \frac{\xi}{R}\nabla_H^2c + \frac{1}{R}\left(\frac{\partial^2c}{\partial z^2} - Da c\right), \tag{4b}$$

where ϕ is the poloidal representation for the divergence velocity field, $\delta(z - Z_0)$ is the Dirac delta function, c is the deviation of the concentration in volume fraction from the diffusive state, R is the Rayleigh-Decay number, and $\nabla_H = (\partial/\partial x, \partial/\partial y)$. It is subject to the following boundary conditions:

$$\phi = 0 \text{ at } z = 0, 1, \text{ and } \frac{\partial c}{\partial z} = 0 \text{ at } z = 0, z = 1. \tag{5}$$

Upon introducing the transformation $\Phi = R\phi$ and $\frac{\partial}{\partial t} = R\frac{\partial}{\partial \hat{t}}$, the equations (4a) and (4b) reduced to

$$\mathcal{F}(z)\nabla^2\Phi - \mathcal{F}'(z)\frac{d\Phi}{dz} = -R\mathcal{F}^2(z)c, \tag{6a}$$

$$c_t + (\nabla_H\Phi_z) \cdot (\nabla_H c) - \nabla_H^2\Phi c_z = -\nabla_H^2\Phi\delta(z - Z_0) + \xi\nabla_H^2c + \left(\frac{\partial^2c}{\partial z^2} - Da c\right) \tag{6b}$$

subject to the following boundary conditions:

$$\Phi = 0 \text{ at } z = 0, 1, \text{ and } \frac{\partial c}{\partial z} = 0 \text{ at } z = 0, z = 1. \tag{7}$$

To investigate the linear and weakly nonlinear stability, we will assume $\xi = 1$, the convection effect dominates over the reaction effect, i.e., $Da = 0$ and $\mathcal{F}(z) = 1 + \lambda z$, $|\lambda| < 1$, see [22]. Hence, equations (6a) and (6b) become

$$(1 + \lambda z)\nabla^2\Phi - \lambda\frac{d\Phi}{dz} = -R(1 + \lambda z)^2c, \tag{8a}$$

$$c_t + (\nabla_H \Phi_z) \cdot (\nabla_H c) - \nabla_H^2 \Phi c_z = -\nabla_H^2 \Phi \delta(z - Z_0) + \nabla_H^2 c + \frac{\partial^2 c}{\partial z^2} \quad (8b)$$

subject to the following boundary conditions:

$$\Phi = 0 \text{ at } z = 0, 1, \text{ and } \frac{\partial c}{\partial z} = 0 \text{ at } z = 0, z = 1. \quad (9)$$

3 Steady-State Linear Stability Analysis

Following the standard procedure used in [24], we obtained the following linearized system of equations governing the convective perturbations:

$$(1 + \lambda z) \nabla^2 \phi - \lambda \frac{d\Phi}{dz} = -(1 + \lambda z)^2 R c, \quad (10a)$$

$$\nabla^2 c = -\nabla_H^2 \phi \delta(z - Z_0) \quad (10b)$$

subject to the following boundary conditions:

$$\Phi = 0 \text{ at } z = 0, 1, \text{ and } \frac{\partial c}{\partial z} = 0 \text{ at } z = 0, z = 1. \quad (11)$$

To investigate the linear stability, we will introduce the normal modes

$$\Phi = e^{i\alpha \cdot \mathbf{x}} W(z), \quad c = e^{i\alpha \cdot \mathbf{x}} S(z), \quad (12)$$

where $\mathbf{x} = (x, y)$ and $|\alpha| = \alpha$, we obtained

$$(1 + \lambda z)(D^2 W(z) - \alpha^2 W(z)) = -(1 + \lambda z)^2 R S(z), \quad (13a)$$

$$(D^2 - \alpha^2) S(z) = \alpha^2 W(z) \delta(z - Z_0), \quad (13b)$$

where $D = \frac{d}{dz}$. The corresponding Dirichlet and Neumann boundary conditions are $W = 0$ at $z = 0, 1$, $DS = 0$ at $z = 0, 1$.

Expand W, S and R in terms of the small wave number α and keep λ of order 1. $W = W_0 + \alpha^2 W_2 + \dots$, $S = S_0 + \alpha^2 S_2 + \dots$ and $R = R_0 + \alpha^2 R_2$. The $O(1)$ problem is given by

$$D \left[\frac{1}{1 + \lambda z} DW_0 \right] = -R_0 S_0, \quad (14a)$$

$$D^2 S_0 = 0 \quad (14b)$$

subject to the boundary conditions $W_0(0) = W_0(1) = 0$ and $DS_0(0) = DS_0(1) = 0$. The solution of the equations (14a) and (14b) is given by

$$S_0 = 1,$$

$$W_0 = -\frac{R_0 G}{6} [(3z^2 + 2\lambda z^3) - L_1(2z + \lambda z^2)],$$

where $L_1 = ((3/2) + \lambda)(1 - \lambda/2)$.

When proceeding to the next order $O(\alpha^2)$, the equation of the concentration becomes

$$D^2 S_2 - S_0 = W_0 \delta(z - Z_0). \quad (15)$$

It has a unique solution if and only if the following condition is satisfied:

$$\int_0^1 S_0^* [S_0 + W_0 \delta(z - Z_0)] dz = 0,$$

where S_0^* is the solution of the adjoint problem of equation (14b), namely, $D^2 S_0^* = 0$ with the corresponding boundary conditions $DS_0^*(0) = DS_0^*(1) = 0$ to get $S_0^* = 1$. Upon applying the Fredholm alternative at $O(\alpha^2)$ we obtain the critical Rayleigh-Darcy number

$$R_0 = \frac{6}{L_1(2Z_0 + \lambda Z_0^2) - (3Z_0^2 + 2\lambda Z_0^3)}.$$

As $\lambda \rightarrow 0$, the critical Rayleigh-Darcy number becomes $R_0 = \frac{2}{Z_0 - Z_0^2}$, which is consistent with what has been obtained in [17]. Figure 3 depicts that the plot of the critical Rayleigh-Darcy number R_0 is decreased as the values of λ have increased in the right figure and the left figure shows that the minimum value of the critical Rayleigh-Darcy number R_0 is at $Z_0 = 0.5$ and it goes to infinity as Z_0 approaches 0 or 1.

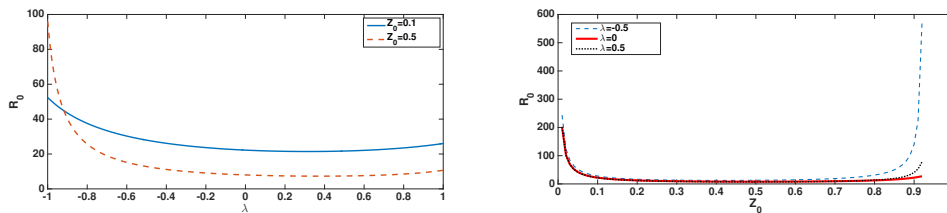


Figure 3: (Right) Plot of the critical Rayleigh-Darcy number R_0 as a function of λ for $Z_0 = 0.1$ (solid line) and $Z_0 = 0.5$ (dashed line). (Left) Plot of the critical Rayleigh-Darcy number R_0 as a function of Z_0 for $\lambda = 0$ (solid line), $\lambda = -0.5$ (dashed line) and $\lambda = 0.5$ (dotted line).

4 Weakly Nonlinear Stability

In this section we will investigate the weakly nonlinear stability by deriving the evolution equation. Following the long wavelength analysis procedure used in [25] and [26] we introduce the small parameter $\epsilon \ll 1$ and we scale $X = \epsilon x$, $Z = z$, $\tau = \epsilon^4 t$ and keep λ of $O(1)$ quantity in equations (8a) and (8b). Moreover, we expand

$$\Phi = \Phi_0 + \epsilon^2 \Phi_2 + \dots, \quad c = c_0 + \epsilon^2 c_2 + \epsilon^4 c_4 + \dots$$

and $R = R_0 + \epsilon^2 \hat{\mu}^2$. The solution of the leading order problem that is described by

$$(1 + \lambda Z)D^2 \Phi_0 - \lambda D \Phi_0 = -(1 + \lambda Z)^2 R_0 c_0, \tag{16a}$$

$$D^2 c_0 = 0, \tag{16b}$$

with boundary conditions $\Phi_0(0) = \Phi_0(1) = 0$ and $Dc_0(0) = Dc_0(1) = 0$ is given by

$$\Phi_0 = -\frac{R_0 h}{6} [(3Z^2 + 2\lambda Z^3) - L_1 (2Z + \lambda Z^2)],$$

$$c_0 = h(X, \tau),$$

where $L_1 = (1.5 + \lambda)(1 - \lambda/2)$.

When proceeding to the next order, the $O(\epsilon^2)$ problem is described by

$$D^2\Phi_2 - \lambda D\Phi_2 + (\Phi_0)_{XX} = -(1 + \lambda Z)[R_0 c_2 + \hat{\mu}^2 c_0], \quad (18a)$$

$$(D\Phi_0)_X (c_0)_X = -(\Phi_0)_{XX} \delta(Z - Z_0) + D^2 c_2 + (c_0)_{XX}. \quad (18b)$$

Application of the solvability condition to equation (18b) yields

$$R_0 = \frac{6 + 3\lambda}{(3 + 2\lambda)(Z_0 + (\lambda/2)Z_0^2) - (3Z_0^2 + 2\lambda Z_0^3)(1 + \lambda/2)}. \quad (19)$$

As $\lambda \rightarrow 0$, the critical Raleigh-Dracy number becomes $R_0 = \frac{2}{Z_0 - Z_0^2}$, which is consistent with what has been obtained in [17]. Proceeding to solve $O(\epsilon^2)$ problem and because of the appearance of the $\delta(Z - Z_0)$ term, we will divide the problem in two cases and equation (18b) will be divided into two equations:

$$\text{the light layer when } 0 < Z < Z_0: D^2 c_2^- = -R_0 (c_0)_X^2 (Z + \lambda Z^2) - (c_0)_{XX}, \quad (20a)$$

$$\text{the heavy layer when } 0 < Z < Z_0: D^2 c_2^+ = -R_0 (c_0)_X^2 (Z + \lambda Z^2) - (c_0)_{XX}, \quad (20b)$$

with boundary conditions $Dc_2^-(0) = 0$ and $Dc_2^+(1) = 0$. Thus, the solutions of equations (20a) and (20b) are

$$c_2^- = -\frac{R_0 (h_X)^2}{36} [6Z^3 + 3\lambda Z^4 - L_1(3Z^2 + \lambda Z^3)] - \frac{h_{XX}}{2} Z^2 + A^-,$$

$$c_2^+ = -\frac{R_0 (h_X)^2}{36} [6Z^3 + 3\lambda Z^4 - L_1(3Z^2 + \lambda Z^3)] - \frac{h_{XX}}{2} (Z^2 - 2Z) + A^+,$$

where $A^- = Z_0 h_{XX} + A^+$ and

$A^+ = \frac{R_0 (h_X)^2}{720} [(30 + 12\lambda) - 5L_1(4 + \lambda)] - \frac{h_{XX}}{6} (2 + 3Z_0^2)$. Similarly, the solution of equation (18a) is given by

$$\begin{aligned} \Phi_2^- = & -\frac{R_0 h_{XX}}{10080} [92\lambda^3 Z^7 + (182 - 35L_1)\lambda^2 Z^6 - (588\lambda + 98\lambda^2 L_1) Z^5 \\ & - (840 + 140\lambda L_1) Z^4 + L_1 - ((1680 Z_0^2 - 3360 Z_0 + 1120)\lambda - 280 L_1) Z^3 \\ & - (2520 Z_0^2 - 5040 Z_0 + 1680) Z^2] + \frac{R_0^2 (h_X)^2}{30240} [72\lambda^2 Z^7 + (294\lambda - 35L_1) Z^6 \\ & + (252 - 210\lambda L_1) Z^5 - 210 L_1 Z^4 - (168\lambda^2) + 420\lambda - 70 L_1(4\lambda + \lambda^2)) Z^3 \\ & - (252\lambda + 630 - 105 L_1(4 + \lambda)) Z^2] - \frac{\hat{\mu}^2 h}{6} (2\lambda Z^3 + 3Z^2) + \frac{B^-}{2} (\lambda Z^2 + 2Z), \\ \Phi_2^+ = & -\frac{R_0 h_{XX}}{10080} [92\lambda^3 Z^7 + (182 - 35L_1)\lambda^2 Z^6 - (588\lambda + 98\lambda^2 L_1) Z^5 \\ & + (1260\lambda - 3360 - 70\lambda L_1) Z^4 - ((1680 Z_0^2 + 1120)\lambda - 1680 - 280 L_1) Z^3 \\ & - (2520 Z_0^2 + 1680) Z^2] + \frac{R_0^2 (h_X)^2}{30240} [72\lambda^2 Z^7 + (294\lambda - 35L_1) Z^6 + (252 - 210\lambda L_1) Z^5 \end{aligned}$$

$$-210 L_1 Z^4 - (168 \lambda^2) + 420 \lambda - 70 L_1(4\lambda + \lambda^2)) Z^3 - (252\lambda + 630 - 105 L_1 (4 + \lambda)) Z^2] \\ - \frac{\hat{\mu}^2 h}{6} (2\lambda Z^3 + 3 Z^2) + \frac{B^+}{2} (\lambda Z^2 + 2 Z) + A^{++},$$

where

$$B^+ = \frac{R_0 h_{XX}}{15120(2 + \lambda)} [288\lambda^3 - 546\lambda^2 - (1260 Z_0^4 + 5040 Z_0^2 + 1344)\lambda + 5040 Z_0^3 \\ + 7560 Z_0^2 + 2520 - L_1(105\lambda^3 + 294\lambda^2 - 420\lambda - 840)] \\ + \frac{R_0^2 (h_X)^2}{15120(2 + \lambda)} [(96\lambda^2 + 378\lambda - 378 - L_1 (35\lambda^2 + 175\lambda + 210))] + \frac{L_1 \hat{\mu}^2 h}{3}, \\ B^- = \frac{Z_0^2 R_0 h_{XX}}{2} + B^+$$

$$A^{++} = \frac{R_0 h_{XX}}{10080} [96\lambda^3 + 182\lambda^2 - (1680 Z_0^2 + 448)\lambda + (840 - 1260\lambda) - 2520 Z_0^2 - 840 \\ - L_1(35\lambda^3 + 98\lambda^2 - 140\lambda - 280)] + \frac{R_0^2 (h_X)^2}{30240} [(96\lambda^2 + 378\lambda + 378 \\ - L_1 (35\lambda^2 + 175\lambda + 210))] + \frac{\hat{\mu}^2 h}{6} (2\lambda + 3) - \frac{B^+}{2} (2 + \lambda).$$

Proceeding to the next order $O(\epsilon^4)$, we have

$$D^2 c_4 = h_\tau + h_X (D\Phi_2)_X - (\Phi_0)_{XX} Dc_2 + (D\Phi_0)_X (c_2)_X + (\Phi_2)_{XX} \delta(Z - Z_0) - (c_2)_{XX} \tag{22}$$

with boundary conditions $Dc_4(0) = Dc_4(1) = 0$. Integrating equation (22) with respect to Z from $Z = 0$ to $Z = 1$, yields the sought evolution equation

$$h_\tau = -\mathcal{A} h_{XXXX} - \hat{\mu}^2 \mathcal{B} h_{XX} + \mathcal{C} (h_X)_{XX}^2 + \mathcal{E} h_X^2 h_{XX}, \tag{23}$$

where

$$\mathcal{A} = -\frac{R_0 (Z_0 - Z_0^2)}{10080(2 + \lambda)} \{ [35(Z_0^4 + Z_0^3 + Z_0^2 + Z_0) L_1 - 96(Z_0^5 + Z_0^4 + Z_0^3 + Z_0^2 + Z_0)] \lambda^4 \\ + [(70Z_0^4 + 168Z_0^3 + 168Z_0^2 + 168Z_0 + 70) L_1 - (192Z_0^5 + 374Z_0^4 + 374Z_0^3 + 374Z_0^2 \\ + 374Z_0 + 192)] \lambda^3 + [(196Z_0^3 + 56Z_0^2 + 56Z_0 + 196) L_1 - (784Z_0^4 - 1484Z_0^2 - 84Z_0 \\ + 364)] \lambda^2 - [280(Z_0^2 + 2Z_0 + 1) L_1 - 56(36Z_0^3 + 21Z_0^2 + Z_0 + 16)] \lambda - 560(Z_0 + 1) L_1 \\ - 1680(2Z_0^2 - Z_0 + 1) \},$$

$$\mathcal{B} = \frac{1}{3} (Z_0 - Z_0^2) (\lambda Z_0 + L_1),$$

$$\mathcal{C} = \frac{R_0^2 (Z_0 - Z_0^2)}{30240(2 + \lambda)} \{ [(72Z_0^5 + 72Z_0^4 + 72Z_0^3 + 72Z_0^2 - 96Z_0) - 35(Z_0^4 + Z_0^3 + Z_0^2 \\ + Z_0) L_1] \lambda^3 + [(144Z_0^5 + 438Z_0^4 + 438Z_0^3 + 438Z_0^2 - 318Z_0 - 192) - (70Z_0^4 + 280Z_0^3 \\ + 280Z_0^2 - 140Z_0 - 70) L_1] \lambda^2 + [(588Z_0^4 + 840Z_0^3 + 840Z_0^2 - 756) - (420Z_0^3 + 630Z_0^2 \\ + 70Z_0 - 350) L_1] \lambda + 504Z_0^3 + 504Z_0^2 + 504Z_0 - 756 - 420(Z_0^2 + Z_0 - 1) L_1 \},$$

$$\mathcal{E} = \frac{R_0^2}{30240} [96\lambda^2 + 504\lambda + 756 - (84\lambda^2 + 476\lambda + 870)L_1 + (21\lambda^2 + 140\lambda + 280)L_1^2].$$

The evolution equation (23) is of parabolic type which is well-posed whenever the coefficient of the fourth derivative, $-\mathcal{A}$, is negative. Figure 4 shows that $-\mathcal{A}$ is negative for all values of λ and Z_0 .

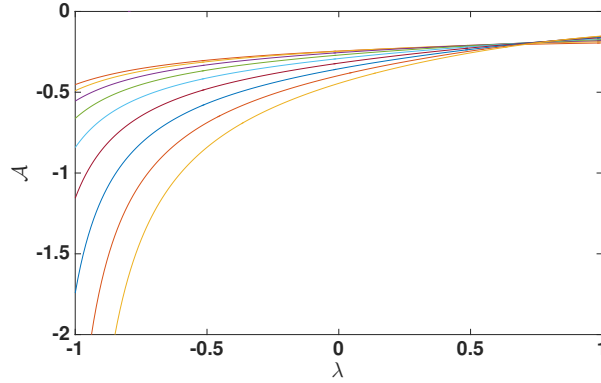


Figure 4: The plot of \mathcal{A} as a function of λ , where $|\lambda| < 1$ and $0 \leq Z_0 \leq 1$.

5 Uniformly Valid Periodic Solution

Upon using the general procedure of the Biot number [27], the term $-\hat{\gamma}h$ will be added to equation (23) to obtain

$$h_\tau = -\mathcal{A}h_{XXXX} - \hat{\mu}^2\mathcal{B}h_{XX} - \hat{\gamma}h + \mathcal{C}(h_X)_{XX}^2 + \mathcal{E}h_X^2 h_{XX}. \quad (24)$$

Upon introducing the following scales and transformations: $h = af$, $\xi = bX$, $\tau = e\hat{\tau}$, $\gamma = a\hat{\gamma}$ and $e = 1/a$, we have

$$f_\tau = -f_{\xi\xi\xi\xi} - 2\mu^2 f_{\xi\xi} - \gamma f + \Gamma(f_\xi)_{\xi\xi}^2 + (f_\xi)^2 f_{\xi\xi}, \quad (25)$$

where

$$a = \sqrt{\frac{\mathcal{A}}{\mathcal{E}}}, \quad b = \left(\frac{1}{\mathcal{A}} \sqrt{\frac{\mathcal{E}}{\mathcal{A}}} \right)^{1/4}, \quad \Gamma = \frac{\mathcal{C}}{\sqrt{\mathcal{A}\mathcal{E}}} \quad \text{and} \quad \mu^2 = \frac{\hat{\mu}^2 a b^2}{2}.$$

To investigate the stability of the static solution of equation (25) we consider the linear part

$$f_\tau = -f_{\xi\xi\xi\xi} - 2\mu^2 f_{\xi\xi} - \gamma f. \quad (26)$$

By introducing the normal modes $f(\xi, \tau) = e^{\sigma\tau + i\theta\xi}$, the following dispersion relation is obtained:

$$\sigma = -(\theta^2 - \mu^2) + \mu^4 - \gamma. \quad (27)$$

Therefore, the trivial static solution, $f = 0$, is unstable when $\gamma < \mu^4$. Upon introducing the small parameter $\epsilon \ll 1$, the weakly nonlinear stability of the evolution equation can

be investigated. To conduct the perturbation analysis around the linear solution, we expand

$$\gamma = \mu^4 - \epsilon \gamma_1 - \epsilon^2 \gamma_2, \quad \tau = \epsilon^2 \eta$$

and

$$f = \epsilon f_1 + \epsilon^2 f_2 + \epsilon^3 f_3 + \dots$$

The $O(\epsilon)$ problem of equation (25) is described by

$$(f_1)_{\xi\xi\xi\xi} + 2\mu^2 (f_1)_{\xi\xi} + \gamma f_1 = 0 \tag{28}$$

whose period solution on the interval $\left(\frac{-\pi}{\mu}, \frac{\pi}{\mu}\right)$ is $f_1 = \cos(\mu\xi)$. Because of the secular terms that are expected due to the linear part and the nonlinear terms, we will apply the Poincaré-Lindstedt method [28] to obtain a uniformly valid periodic solution. Substituting $\nu = \omega\xi$ and expanding $\omega = 1 + \epsilon\omega_1 + \epsilon^2\omega_2 + \dots$ in equation (25) we obtain

$$\omega^4 f_{\nu\nu\nu\nu} + 2\mu^2 \omega^2 f_{\nu\nu} + \gamma f = \omega^4 [\Gamma (f_\nu)_{\nu\nu}^2 + (f_\nu)^2 f_{\nu\nu}]. \tag{29}$$

Define the operator $\mathcal{L}(f) = f_{\nu\nu\nu\nu} + 2\mu^2 f_{\nu\nu} + \mu^4 f$. The leading order problem is described by

$$\mathcal{L}(f_1) = (f_1)_{\nu\nu\nu\nu} + 2\mu^2 (f_1)_{\nu\nu} + \mu^4 f_1 = 0 \tag{30}$$

whose solution is $f_1 = \cos(\mu\nu)$. The $O(\epsilon^2)$ problem is described by

$$\mathcal{L}(f_2) = \gamma_1 \cos(\mu\nu) + \mu^4 \cos(2\mu\nu). \tag{31}$$

To remove the mixed-secular terms, we set $\gamma_1 = 0$, that is, there is no subcritical instability. Thus, the solution of $\mathcal{L}(f_2) = \mu^4 \cos(2\mu\nu)$ is $f_2 = \frac{1}{9} \cos(2\mu\nu)$. When proceeding to the next order, the $O(\epsilon^3)$ problem is described by

$$\begin{aligned} \mathcal{L}(f_3) = & \left[\gamma_2 - 4\omega_1^2 \mu^4 - \frac{\Gamma \mu^4}{4} - \frac{5\mu^4}{9} \right] \cos(\mu\nu) - \frac{20\omega_1 \mu^4}{9} \cos(2\mu\nu) \\ & + \left[\frac{\Gamma \mu^4}{4} + \frac{5\mu^4}{9} \right] \cos(3\mu\nu). \end{aligned} \tag{32}$$

To remove the secular term, we set $\gamma_2 - 4\omega_1^2 \mu^4 - \frac{\Gamma \mu^4}{4} - \frac{5\mu^4}{9} = 0$ and then we solve for ω_1 to get

$$\omega_1 = \pm \sqrt{\frac{\gamma_2}{4\mu^4} - \frac{\Gamma}{16} - \frac{5}{36}}.$$

Therefore, the solution of equation (32) is given by

$$f_3 = -\frac{5\omega_1}{36} \cos(2\mu\nu) + \frac{9\Gamma + 20}{2916} \cos(3\mu\nu). \tag{33}$$

Thus, a uniformly valid steady state of equation (25) is given by

$$\begin{aligned} f = & \epsilon \cos((1 + \epsilon\omega_1)\xi\mu) + \epsilon^2 \frac{1}{9} \cos(2(1 + \epsilon\omega_1)\xi\mu) \\ & + \epsilon^3 \left[-\frac{5\omega_1}{36} \cos(2(1 + \epsilon\omega_1)\xi\mu) + \frac{9\Gamma + 20}{2916} \cos(3(1 + \epsilon\omega_1)\xi\mu) \right]. \end{aligned} \tag{34}$$

Figure 5 shows the plot of the uniformly valid periodic solution of equation (25) as a function of ξ for $\gamma_2 = 10$ and $\mu = 0.7$.

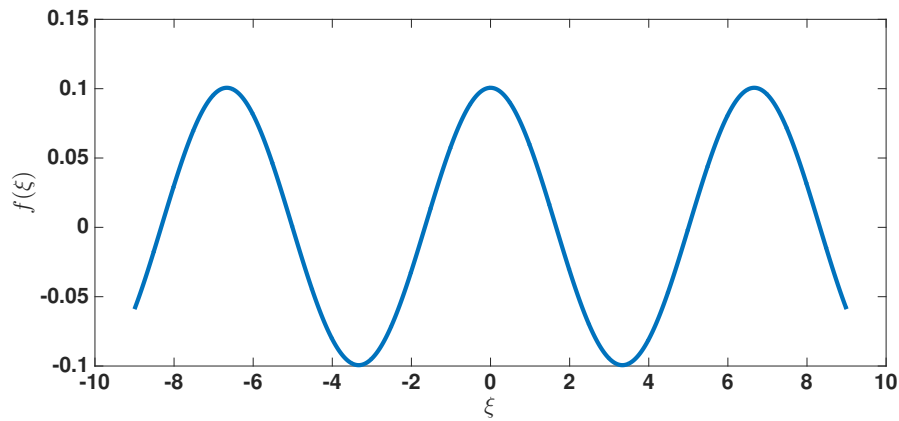


Figure 5: A plot of the periodic solution of equation (25) as a function of ξ with $\gamma_2 = 10$ and $\mu = 0.7$.

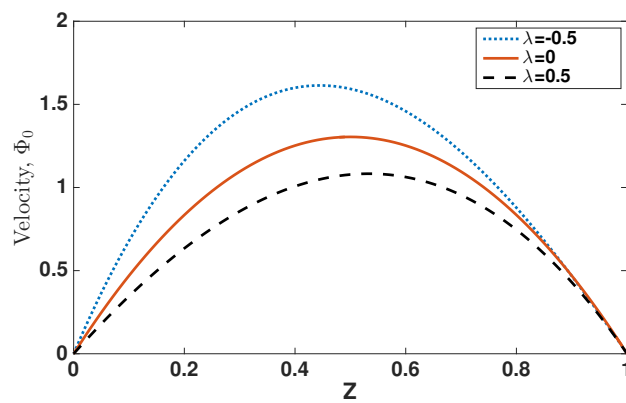


Figure 6: The plot of the velocity Φ_0 as a function of the depth Z with $\lambda = -0.5$ (dotted line), $\lambda = 0$ (solid line) and $\lambda = 0.5$ (dashed line).

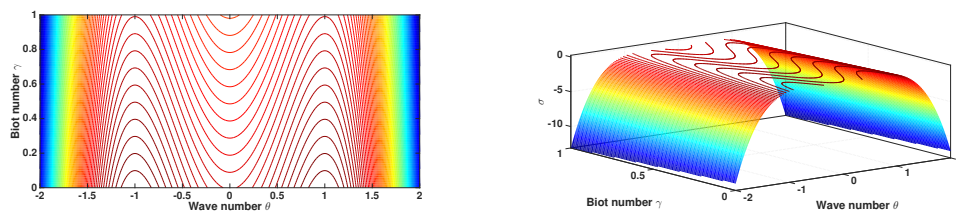


Figure 7: The 2D plot of the growth rate σ as a function of the wave number θ and the Biot number γ (left figure) and the 3D plot (right figure) with $\mu = 0.7$.

6 Discussion and Conclusion

In this paper, we studied the mathematical model that was proposed by Hill and Morad [22]. That is, we considered an incompressible fluid-saturated porous layer bounded by two infinite parallel plates. The Boussinesq approximation and Darcy's law are applied. The permeability is assumed to be a linear function of the depth z , namely, $\mathcal{F}(z) = 1 + \lambda z$. The base state of the model consists of a light free-carbon layer, $[0, Z_0)$, at the bottom and a heavier carbon-saturated layer, $(Z_0, 1]$, at the top, Figures 1 and 2 illustrate the problem. Steady-state linear stability analysis is conducted and the critical Rayleigh-Darcy number is obtained, namely, $R_0 = \frac{6}{L_1(2Z_0 + \lambda Z_0^2) - (3z^2 + 2\lambda Z_0^3)}$. If we let $\lambda \rightarrow 0$, then the

critical Rayleigh-Darcy number becomes $R_0 = \frac{2}{Z_0 - Z_0^2}$, which is consistent with the value obtained in [17]. The relation between the critical Rayleigh-Darcy number and the permeability coefficient λ is depicted in Figure 3.

The weakly nonlinear stability analysis is conducted by the long wavelength expansion method and the evolution equation (23) is derived and analyzed. Figure 6 shows the velocity, Φ_0 , as a function of the depth Z for different values of the permeability coefficient λ .

Moreover, the dispersion equation is obtained and the relation between the growth rate, the Biot number and the wave number is depicted in Figure 7 and a uniformly valid periodic solution is obtained by the application of the Poincaré-Lindstedt method. The plot of this periodic solution is shown in Figure 5.

References

- [1] R. Sedjo and B. Sohngen. Carbon Sequestration in Forests and Soils. *Annual Reviews* **4** (2012) 127–144.
- [2] S. Bachu. Sequestration of CO_2 in geological media in response to climate change: road map for site selection using the transform of the geological space into the CO_2 phase space. *Energy Convers Mgmt.* **43** (2002) 87–102.
- [3] S. Bachu. Sequestration of CO_2 in geological media: criteria and approach for site selection in response to climate change. *Energy Convers Mgmt.* **41** (2000) 953–970.
- [4] U.S. Department of Energy. Carbon Sequestration Key R&D Programs and Initiatives. <https://www.energy.gov/fe/science-innovation/carbon-capture-and-storage-research>.
- [5] International Panel on Climate Change. Carbon Dioxide Capture and Storage. *Cambridge University Press*, 2005.
- [6] C. W. Horton and F. T. Rogers. Convection currents in porous media. *J. Appl. Phys.* **16** (1945) 367–369.
- [7] E. R. Lapwood. Convection of a fluid in porous medium. *Proc. Cambridge Phil. Soc.* **44** (1948) 508–521.
- [8] T. Foster. Onset of convection in a layer of fluid cooled from above. *Phys. Fluids* **8** (1965) 1770–1774.
- [9] T. Foster. Onset of manifest convection in a layer of fluid with time-dependent surface temperature. *Phys. Fluids* **12** (1969) 2482–2487.
- [10] J. P. Ennis-King and L. Paterson. Role of convective mixing in the long-term storage of carbon dioxide in deep saline formulations. *Soc. Pet. Eng.* **10** (2005) 349–356.

- [11] J. P. Ennis-King, I. Preston and L. Paterson. Onset of convection in anisotropic porous media subject to a rapid change in boundary conditions. *Phys. Fluids* **17** 084107 (2005) 1–15.
- [12] H. Hassanzadeh, M. Poolladi-Darvish and D. W. Keith. Modelling of Convective Mixing in CO_2 Storage. *J. Can. Petrol. Technol.* **44** (2005) 43–51.
- [13] H. Hassanzadeh, M. Poolladi-Darvish, and D. W. Keith. Stability of a fluid in a horizontal saturated porous layer: effect of non-linear concentration profile, initial, and boundary conditions. *Transp Porous Med.* **64** (2006) 193–211.
- [14] H. Hassanzadeh, M. Poolladi-Darvish, and D. W. Keith. Scaling Behavior of Convective Mixing, with Application to Geological Storage of CO_2 . *AIChEJ* **53** (2007) 1121–1131.
- [15] H. Emami-Meybodi, H. Hassanzadeha, C. P. Greenb and J. Ennis-King. Convective dissolution of CO_2 in saline aquifers: Progress in modeling and experiments. *International Journal of Greenhouse Gas Control* **40** (2015) 238–266.
- [16] H. Emami-Meybodi, H. Hassanzadeha, and J. Ennis-King. CO_2 dissolution in the presence of background flow of deep saline aquifers. *Water Resources Research* **51** (2015) 2595–2615.
- [17] C. T. Wanstall and L. Hadji. A step function density profile model for the convective stability of CO_2 geological sequestration. *J. Eng. Math.* **108** (2018) 53–71.
- [18] J. Neufeld, M. Hesse, A. Riaz, M. Hallworth, H. Techelepi, and H. Huppert. Convective dissolution of carbon dioxide in saline aquifers. *Geophysical Research Letters* **37** L22404 (2010).
- [19] J. Neufeld, D. Vella and H. Huppert. The effect of a fissure on storage in a porous medium. *J. Fluid Mech.* **639** (2009) 239–259.
- [20] G. Batchelor and J. Nitsche. Instability of stationary unbounded stratified fluid. *J. Fluid Mech.* **227** (1991) 357–391.
- [21] N. Riahi. Nonlinear convection in a porous layer with finite conducting boundaries. *J. Fluid Mech.* **129** (1983) 153–171.
- [22] A. Hill and M. Morad. Convective stability of carbon sequestration in anisotropic porous media. *Proceedings of the Royal Society A* **470** (2014) 2170.
- [23] L. Vo and L. Hadji. Weakly nonlinear convection induced by the sequestration of CO_2 in a perfectly impervious geological formation. *Physics of Fluids* **29** 127101 (2017).
- [24] P. G. Drazin and W. H. Reid. *Hydrodynamic Stability*. Cambridge University Press: Cambridge, UK, 2004.
- [25] F. H. Busse and N. Riahi. Nonlinear thermal convection with poorly conducting boundaries. *J. Fluid Mech.* **96** (1980) 243–256.
- [26] C. J. Chapman and M. R. E. Proctor. Nonlinear Rayleigh-Bénard convection between poorly conducting boundaries. *J. Fluid Mech.* **101** (1980) 759–782.
- [27] M. R. E. Proctor. Planform selection by finite-amplitude thermal convection between poorly conducting slabs. *J. Fluid Mech.* **113** (1981) 469–485.
- [28] A. H. Nayfeh. *Introduction to Perturbation Techniques*. Wiley, New Yourk, 2004.



System Reliability of Ailamujia Model and Additive Failure Rate Models

M. M. Smadi ^{1*} and A. A. Jaradat ²

¹ *Department of Mathematics and Statistics, Jordan University of Science and Technology, Jordan.*

² *Department of Family and Community Medicine, Arabian Gulf University, Bahrain.*

Received: October 25, 2020; Revised: March 28, 2021

Abstract: Dynamic and non-dynamic reliability systems play an important role in industry, manufacturing, safety engineering and quality. The most commonly used models in the parametric statistical reliability analysis are the exponential, Weibull, inverted Weibull, lognormal, Lindley and Raleigh ones as well as their generalizations. In certain engineering applications such as the distribution of repair time and the distribution of delay time, it is found that the Ailamujia model is a suitable alternative compared to other models. This work considers system reliability analysis of the Ailamujia model, in which different reliability measures were computed. The combinations of additive failure rate models associated with the Ailamujia distribution were derived, they include the exponential, Weibull, Frechet and Raleigh distributions.

Keywords: *Ailamujia distribution; stress strength model; reliability; additive rate model.*

Mathematics Subject Classification (2010): 62N05, 68M15, 90B25.

1 Introduction

The lifetime of equipment or apparatus is a random time from the beginning of the operation until the appearance of a complete failure. Reliability is the ability of a system to perform its stated purpose adequately for a specified period of time under specified operational conditions. The system defined here could be an electronic or mechanical hardware product, a software product, a manufacturing process or even a service. For example, in case of a mechanical system, a failure is a breakdown of some of its parts or an increase in vibration above the permitted level. One of the most dangerous failures

* Corresponding author: <mailto:smadi@just.edu.jo>

of a nuclear reactor is a leak of radioactive material. The reliability characteristics are usually expressed in terms of the lifetime.

Modeling and analyzing lifetime data are important issues in many disciplines including medicine, engineering, industry, quality control and finance, etc. Different lifetime data can be represented by several well-known continuous probability distributions such as exponential, Lindley, Weibull, lognormal, and Frechet as well as their generalizations. The Ailamujia distribution is a newly proposed lifetime model that has many engineering applications [1]. In some practical applications such as the distribution of repair time and the distribution of delay time, it is found that the Ailamujia model is a convenient one compared to other models. Lv *et. al.* [2] studied the different properties including mean, variance, and median and maximum likelihood estimators. This distribution has also been investigated for the interval estimation and the hypothesis [3]. The minimax estimation of the Ailamujia model parameter has been discussed under a non-informative prior using three loss functions [4].

The probability density function of the Ailamujia distribution is given by

$$f(x, \theta) = 4\theta^2 x e^{-2\theta x}; \quad x \geq 0, \theta > 0, \quad (1)$$

while the corresponding cumulative distribution function is given as

$$F(x, \theta) = 1 - (1 + 2\theta x)e^{-2\theta x}; \quad x \geq 0, \theta > 0, \quad (2)$$

where θ is the unknown parameter. It can be easily concluded that

$$E(X) = \frac{1}{\theta} \quad \text{and} \quad \sigma^2 = \frac{1}{2\theta}.$$

The maximum likelihood estimator for θ is given by

$$\hat{\theta} = \frac{n}{\sum_{i=1}^n x_i}. \quad (3)$$

The survival function and failure rate are, respectively, given by

$$r(x) = (1 + 2\theta x)e^{-2\theta x}, \quad (4)$$

$$h(x) = \frac{4\theta^2 x}{1 + 2\theta x}. \quad (5)$$

The reliability of the system is given by

$$R(t) = \exp \left\{ - \int_0^t h(x) dx \right\}. \quad (6)$$

Having in mind that

$$\int_0^t h(x) dx = \int_0^t \frac{4\theta^2 x}{1 + 2\theta x} dx = 2\theta t - \ln(2\theta t + 1), \quad (7)$$

the reliability can be expressed as

$$R(t) = e^{-\int_0^t \frac{4\theta^2 x}{1+2\theta x} dx} = (2\theta t + 1)e^{-2\theta t}. \quad (8)$$

The time to failure can be expressed as

$$F(t) = 1 - (1 + 2\theta x)e^{2\theta x}. \tag{9}$$

There is a wide application of the mean residual life function in reliability and survival analysis (see [5–8]). The mean residual life function for the Aijamujia distribution is given by

$$e(t) = \frac{\int_t^\infty R(x)dx}{R(t)} \tag{10}$$

$$= \frac{\int_t^\infty (1 + 2\theta x)e^{-2\theta x} dx}{R(t)} \tag{11}$$

$$= \frac{te^{-2\theta t} + \frac{(1+\theta t)}{\theta}e^{-2\theta t}}{(1 + 2\theta t)e^{-2\theta t}} = \frac{1 + \theta t}{\theta(1 + 2\theta t)}. \tag{12}$$

The following section explains the stress-strength model using the Ailamujia model, while the derivation of additive failure rate models is followed, where the Ailamujia failure rate model is combined with every one of the Ailamujia, exponential, Weibull, Frechet, and Raleigh distributions.

2 Stress-Strength Reliability

The stress-strength reliability describes the life of a component which has a random strength subjected to a random stress. When the stress applied to the component exceeds the strength, the component fails instantly and the component will not function satisfactorily. Therefore, there is a measure of component reliability known as a stress-strength parameter. The stress-strength reliability has wide applications in almost all areas, especially in engineering including structures, deterioration of rocket motors, static fatigue of ceramic components, aging of concrete pressure vessels etc. Beg and Singh [9] gave estimation of $P(X > Y)$ for the Pareto distribution. Maroof and Islam [10] studied the Bayesian estimation of a system reliability when the stress and strength follow the Lomax distribution. Nandi and Aich [11] have shown that Reliability (R) can be obtained as the Laplace transform of the stress. Also, Kotz *et. al.* [1] investigated the generalization of the stress-strength model. Their main findings are summarized as follows.

Let X and Y be two non-negative and continuous random variables having densities $f(x)$ and $g(y)$, respectively. If X and Y are independent, then the probability that Y exceeds X is given as [1]

$$R = P(Y > X) = \int_0^\infty xf(x) \left[\int_1^\infty g(vx)dv \right] dx. \tag{13}$$

Theorem 2.1 *Let the random stress X and the random strength Y be two independent Ailamujia distributions with probability density functions given by*

$$f(x, \theta) = 4\theta_1^2xe^{-2\theta_1x}; x \geq 0, \theta_1 > 0,$$

$$f(y, \theta) = 4\theta_2^2ye^{-2\theta_2x}; y \geq 0, \theta_2 > 0,$$

then the system reliability, $R = P(Y > X)$, is

$$R = P(Y > X) = \frac{\theta_1^2(\theta_1 + 3\theta_2)}{(\theta_1 + \theta_2)}.$$

Proof: It is given that

$$R = P(Y > X) = \int_0^{\infty} xf(x) \left[\int_1^{\infty} 4x\theta_2^2 ve^{-2\theta_2 xv} dv \right] dx \quad (14)$$

$$= P(Y > X) = \int_0^{\infty} xf(x)[I]dx, \quad (15)$$

where

$$I = \int_1^{\infty} 4x\theta_2^2 ve^{-2\theta_2 xv} dv.$$

Then we evaluate the integral I:

$$I = 2\theta_2 \int_1^{\infty} 2\theta_2 xve^{-2\theta_2 xv} dv.$$

Integration by parts can be used which gives

$$I = 2\theta_2 \int_0^{\infty} 2\theta_2 xve^{-2\theta_2 xv} dx \quad (16)$$

$$= 2\theta_2 \left\{ \left[-ve^{-2\theta_2 xv} \right]_1^{\infty} - \int_1^{\infty} e^{-2\theta_2 xv} dv \right\} \quad (17)$$

$$= 2\theta_2 \left\{ \left[-ve^{-2\theta_2 xv} \right]_1^{\infty} - \left[\frac{1}{-2\theta_2 x} e^{-2\theta_2 xv} \right]_1^{\infty} \right\} \quad (18)$$

$$= 2\theta_2 \left\{ e^{-2\theta_2 x} + \frac{1}{2\theta_2 x} e^{-2\theta_2 x} \right\} \quad (19)$$

$$= \frac{1 + 2\theta_2 x}{x} e^{-2\theta_2 x}. \quad (20)$$

Substitute (20) into (15):

$$\begin{aligned} R &= P(Y > X) = \int_0^{\infty} xf(x) \left[\frac{(1 + 2\theta_2 x)e^{-2\theta_2 x}}{x} \right] dx \\ &= \int_0^{\infty} x(4\theta_1^2 xe^{-2\theta_1 x}) \left[\frac{(1 + 2\theta_2 x)e^{-2\theta_2 x}}{x} \right] dx \\ &= 4\theta_1^2 \int_0^{\infty} xe^{-2\theta_1 x} \left((1 + 2\theta_2 x)e^{-2\theta_2 x} \right) dx \\ &= 4\theta_1^2 \left[\int_0^{\infty} xe^{-2(\theta_1 + \theta_2)x} dx + 2\theta_2 \int_0^{\infty} x^2 e^{-2(\theta_1 + \theta_2)x} dx \right] \\ &= 4\theta_1^2 \left[\frac{1}{2(\theta_1 + \theta_2)} \int_0^{\infty} 2(\theta_1 + \theta_2)x e^{-2(\theta_1 + \theta_2)x} dx \right. \\ &\quad \left. + \frac{2\theta_2}{2(\theta_1 + \theta_2)} \int_0^{\infty} 2(\theta_1 + \theta_2)x^2 e^{-2(\theta_1 + \theta_2)x} dx \right] \\ &= 4\theta_1^2 \left[\frac{1}{2(\theta_1 + \theta_2)} \frac{1}{2(\theta_1 + \theta_2)} + \frac{2\theta_2}{(\theta_1 + \theta_2)} \frac{2}{4(\theta_1 + \theta_2)^2} \right] \\ &= \theta_1^2 \left[\frac{1}{(\theta_1 + \theta_2)^2} + \frac{2\theta_2}{(\theta_1 + \theta_2)^3} \right] = \frac{\theta_1^2(\theta_1 + \theta_2)}{(\theta_1 + \theta_2)^3}. \end{aligned}$$

3 Additive Failure Rate Models

More attention is given to the reliability of a combination of two failure rate models for a system with two components that function independently. Assume X_1 and X_2 with respective failure densities, failure probabilities and failure rates being $f_1(x), f_2(x); F_1(x), F_2(x); h_1(x), h_2(x)$, then the system reliability is given by

$$R(t) = \text{Exp} \left\{ - \int_0^t [h_1(x) + h_2(x)] dx \right\}.$$

It is then possible to obtain the failure density and the failure rate of the series system whose reliability is given by (1). Different options have been considered in the literature regarding $h_1(x)$ and $h_2(x)$ [12–15].

The following subsections describe derivation of the additive failure rate models as related to the Ailamujia distribution.

3.1 Ailamujia-Ailamujia failure rate model

The Ailamujia distribution with parameter θ_1 for $h_1(x)$ and the Ailamujia distribution with parameter θ_2 for $h_2(x)$ are selected.

$$\begin{aligned} \int_0^t h(x) dx &= \int_0^t [h_1(x) + h_2(x)] dx \\ &= \int_0^t \frac{4\theta_1^2 x}{1 + 2\theta_1 x} dx + \int_0^t \frac{4\theta_2^2 x}{1 + 2\theta_2 x} dx \\ &= 2\theta_1 t - \ln(2\theta_1 t + 1) + 2\theta_2 t - \ln(2\theta_2 t + 1) \\ &= 2(\theta_1 + \theta_2)t - \ln \frac{2\theta_1 t + 1}{2\theta_2 t + 1}. \end{aligned}$$

Then the reliability function of the system can be written as

$$R(t) = e^{-\left((2(\theta_1 + \theta_2)t - \ln \frac{2\theta_1 t + 1}{2\theta_2 t + 1}) \right)} = \frac{2\theta_1 t + 1}{2\theta_2 t + 1} e^{-2(\theta_1 + \theta_2)t}$$

and the probability density of the Ailamujia-Ailamujia failure rate model (**AAF**RM) is given by

$$f(t) = -\frac{d}{dt} R(t) = 2(\theta_1 + \theta_2) \frac{2\theta_1 t + 1}{2\theta_2 t + 1} e^{-2(\theta_1 + \theta_2)t} - \frac{2\theta_1 + \theta_2}{(2\theta_2 t + 1)^2} e^{-2(\theta_1 + \theta_2)t}.$$

3.2 Ailamujia-exponential failure rate model

The probability density, cumulative distribution, and hazard functions of the exponential distribution are respectively given by

$$\begin{aligned} f(x) &= \lambda e^{-\lambda x}; \quad x > 0, \lambda > 0, \\ F(x) &= 1 - e^{-\lambda x}; \quad x > 0, \lambda > 0, \\ R(x) &= e^{-\lambda x} \text{ and } h(x) = \lambda. \end{aligned}$$

The Ailamujia distribution is selected with parameter θ for $h_1(x)$ and the exponential distribution for $h_2(x)$.

$$\begin{aligned}\int_0^t h(x)dx &= \int_0^t [h_1(x) + h_2(x)]dx \\ &= \int_0^1 \frac{4\theta^2 x}{1 + 2\theta x} dx + \int_0^t \lambda dx \\ &= (2\theta + \lambda)t + \ln(2\theta t + 1)\end{aligned}$$

and the reliability function of the system can be written as

$$R(t) = e^{-[(2\theta + \lambda)t + \ln(2\theta t + 1)]} = (2\theta t + 1)e^{-(2\theta + \lambda)t}$$

and the probability density of the Ailamujia-Ailamujia failure rate model (**AAFRM**) is given by

$$f(t) = -\frac{d}{dt}R(t) = (4\theta^2 t + 2\theta\lambda t + \lambda)e^{-(2\theta + \lambda)t}.$$

3.3 Ailamujia-Weibull failure rate model

The probability density, cumulative distribution, and hazard functions of the Weibull distribution are respectively given by

$$\begin{aligned}f(x) &= \lambda\alpha x^{\alpha-1}; \quad x > 0, \lambda > 0, \alpha > 0, \\ F(x) &= 1 - e^{-\lambda x^\alpha}; \quad x > 0, \lambda > 0, \alpha > 0, \\ R(x) &= e^{-\lambda x^\alpha} \text{ and } h(x) = \lambda\alpha x^{\alpha-1}.\end{aligned}$$

The Ailamujia distribution was selected for $h_1(x)$ and the Weibull distribution for $h_2(x)$.

$$\begin{aligned}\int_0^t h(x)dx &= \int_0^t [h_1(x) + h_2(x)]dx \\ &= \int_0^1 \frac{4\theta^2 x}{1 + 2\theta x} dx + \int_0^t \lambda\alpha x^{\alpha-1} dx \\ &= 2\theta t - \ln(2\theta t + 1) + \lambda t^\alpha.\end{aligned}$$

Then the reliability function of the system can be written as

$$R(t) = e^{-(2\theta t - \ln(2\theta t + 1) + \lambda t^\alpha)} = (2\theta t + 1)e^{-(2\theta + \lambda t^\alpha)t}$$

and the probability density of the Ailamujia-Weibull failure rate model (**AWFRM**) is given by

$$f(t) = -\frac{d}{dt}R(t) = (4\theta^2 t + 2\theta\lambda\alpha t^\alpha + \lambda\alpha t^{\alpha-1})e^{-(2\theta + \lambda t^\alpha)t}.$$

3.4 Ailamujia-Frechet failure rate model

The probability density, cumulative distribution, and hazard functions of the Frechet distribution are respectively given by

$$\begin{aligned} f(x) &= \lambda \alpha x^{-(\alpha+1)} ; x > 0, \lambda > 0, \alpha > 0, \\ F(x) &= 1 - e^{-\lambda x^{-\alpha}} ; x > 0, \lambda > 0, \alpha > 0, \\ R(x) &= e^{-\lambda x^{-\alpha}} \text{ and } h(x) = \lambda \alpha x^{-(\alpha+1)}. \end{aligned}$$

The Ailamujia distribution was selected for $h_1(x)$ and the inverted Weibull distribution for $h_2(x)$.

$$\begin{aligned} \int_0^t h(x)dx &= \int_0^t [h_1(x) + h_2(x)]dx \\ &= \int_0^1 \frac{4\theta^2 x}{1 + 2\theta x} dx + \int_0^t \lambda \alpha x^{-(\alpha+1)} dx \\ &= 2\theta t - \ln(2\theta t + 1) - \lambda t^{-\alpha} \\ &= (2\theta t - \lambda t^{-\alpha}) - \ln(2\theta t + 1). \end{aligned}$$

Then the reliability function of the system can be written as

$$R(t) = e^{-((2\theta t - \lambda t^{-\alpha}) - \ln(2\theta t + 1))} = (2\theta t + 1)e^{-(2\theta t + \lambda t^{-\alpha})}$$

and the probability density of the Ailamujia-Frechet failure rate model (**AFFRM**) is given by

$$f(t) = -\frac{d}{dt}R(t) = (4\theta^2 t + 2\theta \lambda \alpha t^{\alpha-1} + \lambda \alpha t^{\alpha-1})e^{-(2\theta t + \lambda t^{-\alpha})}.$$

3.5 Ailamujia-Raleigh failure rate model

The probability density, cumulative distribution, and hazard functions of the Raleigh distribution are respectively given by

$$\begin{aligned} f(x) &= 2\beta^2 x e^{-(\beta x)^2} ; x > 0, \beta > 0, \\ F(x) &= 1 - e^{-(\beta x)^2} ; x > 0, \beta > 0, \\ R(x) &= e^{-(\beta x)^2} \text{ and } h(x) = \beta^2 x. \end{aligned}$$

The Ailamujia distribution was selected for $h_1(x)$ and the Raleigh distribution for $h_2(x)$.

$$\begin{aligned} \int_0^t h(x)dx &= \int_0^t [h_1(x) + h_2(x)]dx \\ &= \int_0^1 \frac{4\theta^2 x}{1 + 2\theta x} dx + \int_0^t 2\beta^2 x dx \\ &= 2\theta t - \ln(2\theta t + 1) + \beta t^2. \end{aligned}$$

Then the reliability function of the system can be written as

$$R(t) = e^{-(2\theta t - \ln(2\theta t + 1) + \beta^2 t^2)} = (2\theta t + 1)e^{-(2\theta t + \beta^2 t^2)}$$

and the probability density of the Ailamujia-Raleigh failure rate model (**ARFRM**) is given by

$$f(t) = -\frac{d}{dt}R(t) = 2(2\theta\beta^2 t^2 + 2\theta^2 t^2 + \beta^2 t)e^{-(2\theta t + \beta^2 t^2)}.$$

These findings suggest further research involving estimation of parameters of the failure rate distributions, testing of hypothesis and the power likelihood ratio criterion for the proposed models and apply the proposed failure rate models to certain real lifetime data sets.

4 Conclusion

System reliability measures were derived where the failure data follow the Ailamujia distribution. The system reliability is estimated at the conditions where the applied stress and strength follow the Ailamujia distribution. The combinations of the Ailamujia distribution and every one of well-known reliability distributions are developed. The additive failure rate model of the Ailamujia distribution and every one of the Ailamujia, exponential, Weibull, Frechet, and Raleigh distributions were derived.

References

- [1] S. Kotz and M. Pensky. *The Stress-strength Model and its Generalizations. Theory and Applications*. World Scientific, Singapore, 2003.
- [2] L. Huiqiang, G. Lianhua and C. Chunliang. Ailamujia distribution and its application in supportability data analysis. *Journal of Academy of Armored Force Engineering* **16** (3) (2002) 48–52.
- [3] U. T. Pan, C. Wang, Y. B. H. Gano and M. T. Dang. The research of interval estimation and hypothetical test of small sample of Ailamujia distribution. *Application of Statistics and Management* **28** (3) (2009) 468–472.
- [4] L. P. Li. Minimax estimation of the parameter of Ailamujia distribution under different loss functions. *Science Journal of Applied Mathematics and Statistics* **4** (5) (2016) 229–235.
- [5] M. C. Bhattacharjee. The class of residual lives and some consequences. *Journal of Discrete Algebra* **3** (1) (1982) 56–65.
- [6] C. L. Chiang. *Introduction to Stochastic Processes in Biostatistics*. Wiley, New York, 1968.
- [7] E. S. Deevey. Life tables for natural populations of animals. *Quarterly Review of Biology* **22** (1947) 283–314.
- [8] F. M. Guess, J. C. Steele, T. M. Young and R. V. Leon. Applying novel mean residual life confidence intervals. *International Journal of Reliability Applications* **7** (2) (2006) 177–186.
- [9] M. A. Beg and N. Singh. Estimation of $P(X > Y)$ for the Pareto distribution. *IEEE Trans. Reliability* **28** (1979) 411–414.
- [10] A. K. Maroof and H. M. Islam. Reliability computation and Bayesian analysis of system reliability with Lomax Model. *Safety and Reliability* **29** (1) (2009) 5–14.
- [11] S. B. Nandi and A. B. Aich. A Note on estimation of some distributions useful in life testing. *IAPQR Trans.* **19** (1) (1994) 35–44.

- [12] K. Vtsaijh, K. Maranthi Nagarauna, D. Siva Kumar and B. Srinivasa Rao. Exponential log logistic additive failure rate model. *International Journal of Scientific and Research Publications* **4**(3) (2014) 1–5.
- [13] H. Salih and H. A. Hassan. Some additive failure rate models related with MOEU distribution. *American Journal of System Science* **4**(1) (2015) 1–10.
- [14] B. Sirinvasa Rao, S. Nagendrat and K. Rosaiah. Exponential–Half logismic additive failure rate model. *International eourndl of Scientific and Research* **3**(5) (2013) 1–10.
- [15] B. Srininasa Rao, R. R. L. Kantam, K. Rosaiah and B. M. Sridhar. Exponential–gamma additive failure rate model. *Journal of Safety Engineering* **2**(2A) (2013) 1–16.



Dynamics of Nonlinear Longitudinal Vibrations in a 1D Nano-Scale Continuum Described by the Generalized Morse Potential

S. A. Surulere*, M. Y. Shatalov, A. C. Mkolesia and I. Fedotov

*Department of Mathematics and Statistics, Tshwane University of Technology, P.O. Box
X680, Pretoria, 0001, South Africa.*

Received: October 3, 2020; Revised: January 21, 2021

Abstract: A continuum which was described by a governing second-order partial differential equation (PDE), containing an infinite attachment of atoms, was detailed. We formulated the governing PDE using Hamilton's principle and derived the boundary conditions. Four different boundary conditions were formulated but we assumed that the left end of the continuum was fixed, $u(t, r = 0) = 0$, while the right end was free, $\frac{\partial u}{\partial r} \Big|_{r=l} = 0$. The method of lines was employed and used to convert the governing PDE into a coupled system of infinite ordinary differential equations (ODEs). The system of coupled ODEs was numerically integrated within the time interval, $t \in [0, 4\pi]$. It was observed that the trough of the waves became sharply triangular for lower grid points and smooth for higher grid points.

Keywords: *generalized Morse potential; Hamilton's principle; method of lines; non-linear interactions; periodic motion.*

Mathematics Subject Classification (2010): 70K25, 70H03, 70H25, 35L05.

* Corresponding author: <mailto:samuel.abayomi.sas@gmail.com>

1 Introduction

The analysis of vibrations in a mechanical system is very crucial to engineers because neglecting the vibrations in a system can result into wears, tears, and an eventual system breakdown. It can be observed that from a cell to a community of organisms, from an atom to galaxies, oscillatory processes are a fundamental characteristic of all organic and inorganic nature [1]. This makes the philosophic significance of the science of vibrations absolutely necessary [1]. The bodies in the nano-scale dimensions are not exempted from these studies. Morikazu Toda studied and proposed the well-known Toda lattice. His proposed lattice is one-dimensional and has nonlinear interactions that were described by a potential having one exponent [2]. His results and subsequent findings were later published as a book [3].

In this paper, we will construct a nanochain, described as a continuum containing an attachment of infinite atoms, using Hamilton's principle. The finite-difference scheme and Maclaurin series can also be used to formulate the governing PDE. The disadvantage of the former is that the Lagrangian formalism automatically conserves energy. The interaction potential between the atoms in the continuum is chosen as the Generalized Morse potential. The potential is one of the hybrid forms of the Morse potential [4].

The exact solution of the governing second-order PDE to be formulated, is very difficult to obtain. Hence, the method of lines (MOL) will be used to obtain a numerical solution of the governing PDE. The MOL details the conversion of a PDE into a coupled system of ODEs using the discretisation of the space variable. This conversion is necessary because most computer algebra softwares have built-in algorithms for effectively solving a system of ODEs [5,6]. The MOL was first proposed, discovered and presented by William Schiesser in [7]. Several other books have been published by him on the subject (see [5,8–12]).

2 Derivation of the Governing PDE and Boundary Conditions

Let us represent the Generalized Morse interatomic potential

$$U_{\text{GM}}(r) = \bar{A}e^{-\bar{\alpha}r} - \bar{B}e^{-\bar{\beta}r}, \quad (1)$$

where $\bar{A} > \bar{B} > 0$ and $\bar{\alpha} > \bar{\beta} > 0$ are constant parameters, in this form

$$U_{\text{GM}}(r) = Ae^{-\bar{\alpha}(r-\bar{r})} - Be^{-\bar{\beta}(r-\bar{r})}, \quad (2)$$

where A and B are new amplitude parameters. Indeed,

$$A = \bar{A}e^{-\bar{\alpha}\bar{r}} \quad \text{and} \quad B = \bar{B}e^{-\bar{\beta}\bar{r}}. \quad (3)$$

Let us assume that the coordinate \bar{r} corresponds to the minimum of $U_{\text{GM}}(r)$ as presented in Figure 1,

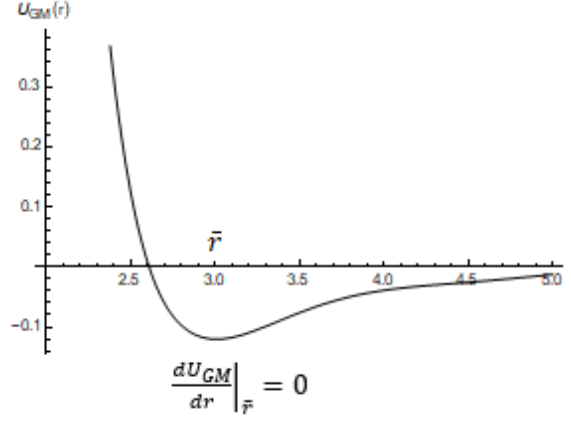


Figure 1: Potential energy curve of Generalized Morse potential for gold atom.

where $U'_{\text{GM}}(r = \bar{r}) = \frac{dU_{\text{GM}}}{dr} \Big|_{\bar{r}} = 0$. We differentiate Equation (2) with respect to r at the coordinate $r = \bar{r}$

$$\frac{dU_{\text{GM}}}{dr} \Big|_{\bar{r}} = -\bar{\alpha}A + \bar{\beta}B = 0. \quad (4)$$

From Equation (3) and Equation (4), we obtain the coordinate of \bar{r}

$$\bar{r} = \frac{1}{\bar{\alpha} - \bar{\beta}} \ln \left(\frac{\bar{\alpha}\bar{A}}{\bar{\beta}\bar{B}} \right). \quad (5)$$

By substituting Equation (5) into Equation (3), the following expressions are derived:

$$\begin{aligned} A &= \bar{A} \exp \left[-\frac{\bar{\alpha}}{\bar{\alpha} - \bar{\beta}} \ln \left(\frac{\bar{\alpha}\bar{A}}{\bar{\beta}\bar{B}} \right) \right] = \bar{A} \left(\frac{\bar{\alpha}\bar{A}}{\bar{\beta}\bar{B}} \right)^{-\frac{\bar{\alpha}}{\bar{\alpha} - \bar{\beta}}}, \\ B &= \bar{B} \exp \left[-\frac{\bar{\beta}}{\bar{\alpha} - \bar{\beta}} \ln \left(\frac{\bar{\alpha}\bar{A}}{\bar{\beta}\bar{B}} \right) \right] = \bar{B} \left(\frac{\bar{\alpha}\bar{A}}{\bar{\beta}\bar{B}} \right)^{-\frac{\bar{\beta}}{\bar{\alpha} - \bar{\beta}}}. \end{aligned} \quad (6)$$

Let us consider a nonlinear chain of identical atoms (unit mass, m) in which the atoms at equilibrium are located at the distance, \bar{r} , with respect to each other, and assume that the linear longitudinal displacement of the k^{th} atom is $u_k = u_k(t)$, where $k = 1, 2, \dots, N$ number of atoms in the chain. We only consider the interactions between the k^{th} and $(k+1)^{\text{th}}$ or $(k-1)^{\text{th}}$ and k^{th} atoms.

It is reasonable to apply the variational principles to simultaneously derive the governing PDE and possible boundary conditions. We write the kinetic energy of the continuum as

$$K = \int_0^l \frac{1}{2} m \dot{u}^2 dr, \quad (7)$$

where the stress $\dot{u} = \frac{\partial u(t, r)}{\partial t}$ and l is the length of the distributed chain. The potential energy of the continuum is

$$P = \int_0^l (Ae^{-\alpha u'} - Be^{-\beta u'}) dr, \quad (8)$$

where the strain $u' = \frac{\partial u(t, r)}{\partial r}$. It should be noted that

$$\alpha = \bar{\alpha}\bar{r}, \quad \beta = \bar{\beta}\bar{r}. \tag{9}$$

Hence, the Lagrangian of the continuum is $L = K - P = \int_0^l \Lambda dr$, where Λ is the Lagrangian density defined as

$$\Lambda = \Lambda(\dot{u}, u') = \frac{1}{2}m\dot{u}^2 - (Ae^{-\alpha u'} - Be^{-\beta u'}). \tag{10}$$

The explicit governing second-order PDE is

$$\frac{\partial^2 u}{\partial t^2} - \left[\bar{a} \exp\left(-\alpha \frac{\partial u}{\partial r}\right) - \bar{b} \exp\left(-\beta \frac{\partial u}{\partial r}\right) \right] \frac{\partial^2 u}{\partial r^2} = 0, \tag{11}$$

where

$$\bar{a} = \frac{\alpha^2 A}{m} = \frac{\bar{\alpha}^2 A}{m} \bar{r}^2, \quad \bar{b} = \frac{\beta^2 B}{m} = \frac{\bar{\beta}^2 B}{m} \bar{r}^2.$$

There are four possible different combinations of the boundary conditions, and we select one of them, which is the fixed left end and the free right end

$$r = 0 : \quad u(t, r = 0) = 0; \quad r = l : \quad \left. \frac{\partial u}{\partial r} \right|_{r=l} = 0. \tag{12}$$

See Appendix A and B for the derivation.

3 Applying the Method of Lines to Obtain the Numerical Approximation of the Solution for the Governing PDE

The method of lines (MOL) is a semi-analytical approach that involves the conversion of a PDE to a coupled system of infinite ODEs [13, 14]. The PDE is converted to a coupled system of infinite ODEs by discretizing one of the spatial variables while using an analytical solution for the other spatial variable [14]. The coupled system of infinite ODEs can then be truncated to obtain a coupled system of finite ODEs.

For simplicity, we assume that $r = l$ becomes $r = 1$. In our case, we discretize the space variable r and use an analytical solution for the time variable t . The definitions for the first-order and second-order centered-difference formulas are

$$\left. \frac{\partial u_k(t)}{\partial r} \right|_{r=r_k} = \frac{1}{2\Delta r} [u_{k+1}(t) - u_{k-1}(t)], \tag{13}$$

$$\left. \frac{\partial^2 u_k(t)}{\partial r^2} \right|_{r=r_k} = \frac{1}{\Delta r^2} [u_{k-1}(t) - 2u_k(t) + u_{k+1}(t)], \tag{14}$$

where Δr is the spacing between the discretized lines, and $k = 1, 2, \dots, N - 1$. Finally, we write $\frac{\partial^2 u(t, r)}{\partial t^2} = \frac{d^2 u_k(t)}{dt^2}$. These definitions are introduced into Equation (11) and Equation (12) to obtain the coupled system of infinite second-order ODEs and new boundary conditions (See Appendix C).

We have partially discretised the space variable, r , of the function, $u(t, r)$, into a coupled system of infinite ODEs whose unknown solutions are $u_1(t), u_2(t), u_3(t), \dots, u_{N-1}(t)$,

and we also converted the boundary conditions into initial conditions. It should be noted that $u_0(t) = 0, u_N(t) = u_{N-1}(t)$ and $k = 1, 2, \dots, N - 1$. The infinitely coupled system is truncated into a coupled system of finite ODEs, where $N = 60, 75, 150$. We select the initial conditions as $u_k(0) = A \sin \frac{\pi k}{2N}$, where A is the amplitude of the wave solution and $u'_k(0) = 0$ for $k = 1, 2, \dots, N - 1$. The value of the amplitude determines how the nonlinear terms in the continuum manifest themselves. We consider the initial conditions, corresponding to the boundary conditions, at the first mode of vibration of the linearized wave equation. The initial conditions for $A = 1.75$ are illustrated in Figure 2.

During the numerical simulations of the truncated system of ODEs, it was found that $A \in (0.0, 1.75]$. We did not consider negative values of the amplitude, A , because the negative values make the continuum oscillate in the opposite direction. The value of the amplitude to be used depends on the number of the truncated coupled system of finite ODEs to be numerically integrated. This is because the truncated coupled system of ODEs becomes a stiff system (with higher values of A) and the computer algebra software takes a lot of time in unsuccessfully integrating the problem. The time integration of the numerical analysis for the coupled system of ODEs was carried out within the interval $t \in [0, 4\pi]$ seconds.

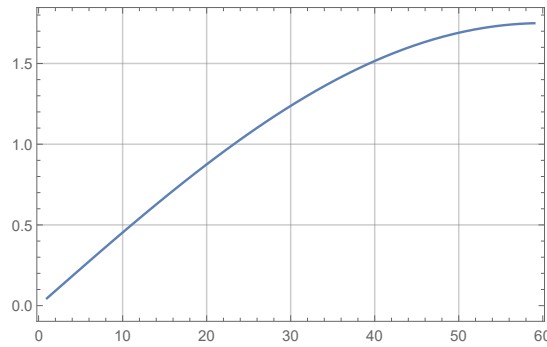


Figure 2: Graph of initial conditions, $u_k(0)$.

For convenience of numerical simulations, the parameters \bar{a}, \bar{b}, α , and β were further scaled to the new parameters

$$a = \frac{\bar{a}}{\bar{a} - \bar{b}} \Delta r^{-2}, \quad b = \frac{\bar{b}}{\bar{a} - \bar{b}} \Delta r^{-2}, \quad \check{\alpha} = \frac{\alpha}{20\bar{r}\Delta r}, \quad \check{\beta} = \frac{\beta}{20\bar{r}\Delta r}.$$

We also defined the parameter values $m = 197, A = 0.058, B = 0.174$, and $\bar{r} = 3.006174$, where we choose the molar mass of the gold atom as the unit mass. It should be noted that $\bar{\alpha}, \bar{\beta}, \bar{A}$ and \bar{B} have been calculated in [15, 16].

3.1 Numerical analysis of truncated coupled ODEs

The numerical simulations for a grid of 60 points using the amplitude value $A = 1.75$ is shown in Figure 3. Then, bearing in mind that the higher the number of lines, the more accurate the approximation, we consider the Equation (26) for higher grids, i.e., $N = 75, 150$ points, respectively. However, for higher number of lines, $N > 150$, the numerically approximated solution of the governing PDE significantly deteriorates. The

NDSolve framework of Wolfram Mathematica[®], student edition, version 12.0.0.0 was used to numerically solve the truncated coupled system of ODEs. We also invoked the “Adams” sub-method (for computational time efficiency) with no specified “AccuracyGoal” or “PrecisionGoal” values defined. The amplitude for all the numerical simulation in Figure 3(a) to (d) was 1.75 and time interval $t \in [0, 4\pi]$ seconds. In nonlinear acoustics, the trough of the wave solutions in continuum mechanics is skewed and triangle-like. This was the case in Figure 3(d), which was also observed from Figure 3(b). In Figure 3(a), we see that the approximate solution for $u_1(t)$, is substantially deteriorated. This was due to the high value of the amplitude, A , used for the numerical simulation. Figure 3(c) displays how nonlinear terms in the continuum are manifested.

See Figure 4(a) to (d) for the numerical simulations of an amplitude value 1.0 and the number of grids having 75 points. Figure 4(b) and (e) reveals the wave troughs are still triangle-like through the entire solution, although not as sharp as those in Figure 3(b) and (e). The value of the amplitude is reasonable but still high. A comparison between Figure 3(b) and Figure 4(b) implies that the higher the value of the amplitude, the more skewed the troughs become all through the wave solution. Surprisingly, Figure 4(a) presents a symmetric solution as compared to Figure 3(a). This means the number of lines chosen and the value of the amplitude used influence the reliability of the approximate solution of the governing PDE.

For the next solution, we use an amplitude value of 0.04 and show numerical simulation results for 150 grid points. The solution plots display perfect symmetric edges (from a pictorial perspective) all through the wave solution. The effect of high amplitude is clearly observed in the comparisons between Figure 3(b), Figure 4(b) and Figure 5(b). The contour plots for Figure 3(b), Figure 4(b) and Figure 5(b) are each distinct because different amplitude values were used and the number of lines was varied. The lines in the contour plots clearly detail the manifestation of the nonlinear terms and the suppression of the terms.

3.2 Analysis of the periodic motion of the wave solution

Now, we want to calculate the spectrum of a number of cosine and sine harmonics using the Fourier coefficients for the right end of the continuum. We do this by taking into consideration the solution, $u_{149}(t)$, interpolate the solution, find the zeros of the solution using the LogPlot function of the absolute value for the interpolated function (in Wolfram Mathematica[®]), then we plot one period of the solution and integrate the plotted function from 0 to 2π in order to obtain the desired coefficients. Although the Fourier series are well-known and used in longitudinal oscillations in crystals, vibrating mechanical systems or in describing physical processes in which events recur in a regular pattern [17, 18], we apply the knowledge to understand the manifestation of nonlinear terms in the continuum of atoms.

Numerical simulations yielded the following harmonics for an amplitude value of 0.04:

$$\begin{aligned}
 c_0 &= 2.674036 \times 10^{-4}, \\
 c_1 &= -3.985559 \times 10^{-4}, & s_1 &= 3.9736 \times 10^{-2}, \\
 c_2 &= 1.318224 \times 10^{-4}, & s_2 &= 2.296953 \times 10^{-6}, \\
 c_3 &= 9.509503 \times 10^{-7}, & s_3 &= -8.771975 \times 10^{-5}, \\
 c_4 &= -1.256332 \times 10^{-6}, & s_4 &= 7.783809 \times 10^{-8}, \\
 c_5 &= -1.06498 \times 10^{-6}, & s_5 &= 1.434977 \times 10^{-5}.
 \end{aligned} \tag{15}$$

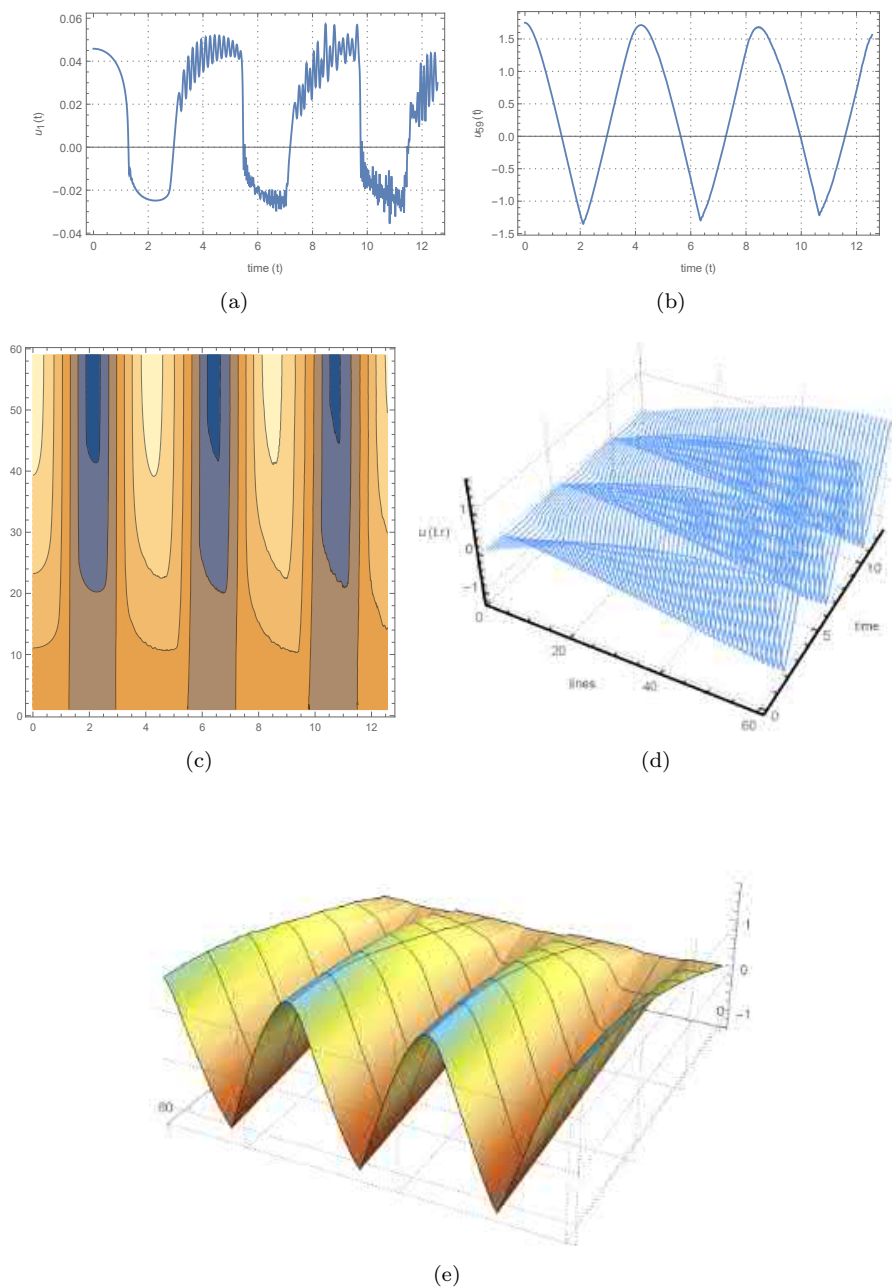


Figure 3: (a) First solution plot, $u_1(t)$, of the truncated coupled ODEs for $N = 60$ points; (b) Last solution plot, $u_{59}(t)$, of the truncated coupled ODEs for $N = 60$ points; (c) Contour plot of the truncated coupled ODEs for $N = 60$ points; (d) Parametric plot of the truncated coupled ODEs for $N = 60$ points; (e) Surface plot of the truncated coupled ODEs for $N = 60$ points.

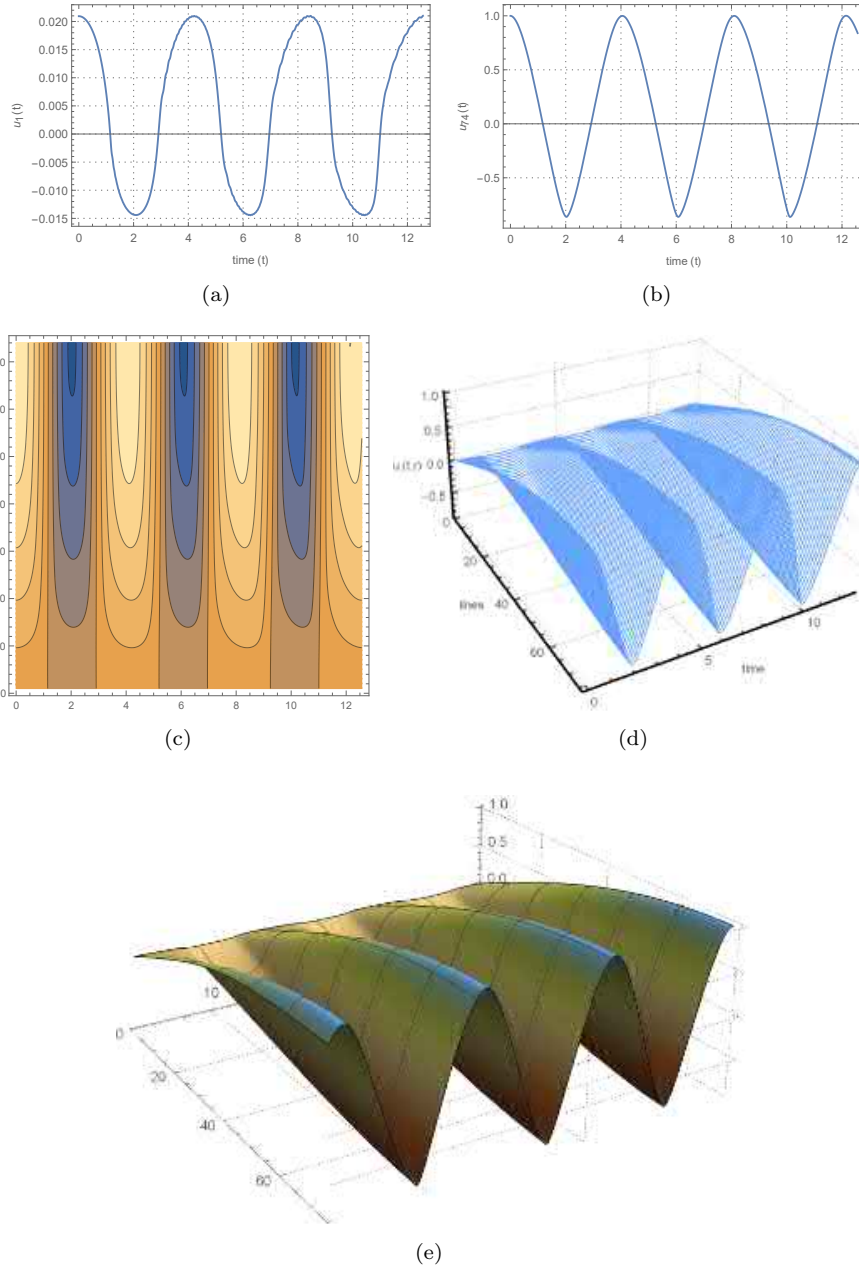


Figure 4: (a) First solution plot, $u_1(t)$, of the truncated coupled ODEs for $N = 75$ points; (b) Last solution plot, $u_{74}(t)$, of the truncated coupled ODEs for $N = 75$ points; (c) Contour plot of the truncated coupled ODEs for $N = 75$ points; (d) Parametric plot of the truncated coupled ODEs for $N = 75$ points; (e) Surface plot of the truncated coupled ODEs for $N = 75$ points.

Numerical simulations for an amplitude value of 0.25 yielded the following harmonics:

$$\begin{aligned}
 c_0 &= 9.945892 \times 10^{-3}, & s_1 &= 2.41632 \times 10^{-1}, \\
 c_1 &= -1.4423 \times 10^{-2}, & s_2 &= 5.031898 \times 10^{-4}, \\
 c_2 &= 4.65619 \times 10^{-3}, & s_3 &= -2.461517 \times 10^{-3}, \\
 c_3 &= 8.796602 \times 10^{-5}, & s_4 &= 1.930631 \times 10^{-5}, \\
 c_4 &= -2.389894 \times 10^{-4}, & s_5 &= 2.905531 \times 10^{-4}, \\
 c_5 &= -5.048646 \times 10^{-5}, & &
 \end{aligned}
 \tag{16}$$

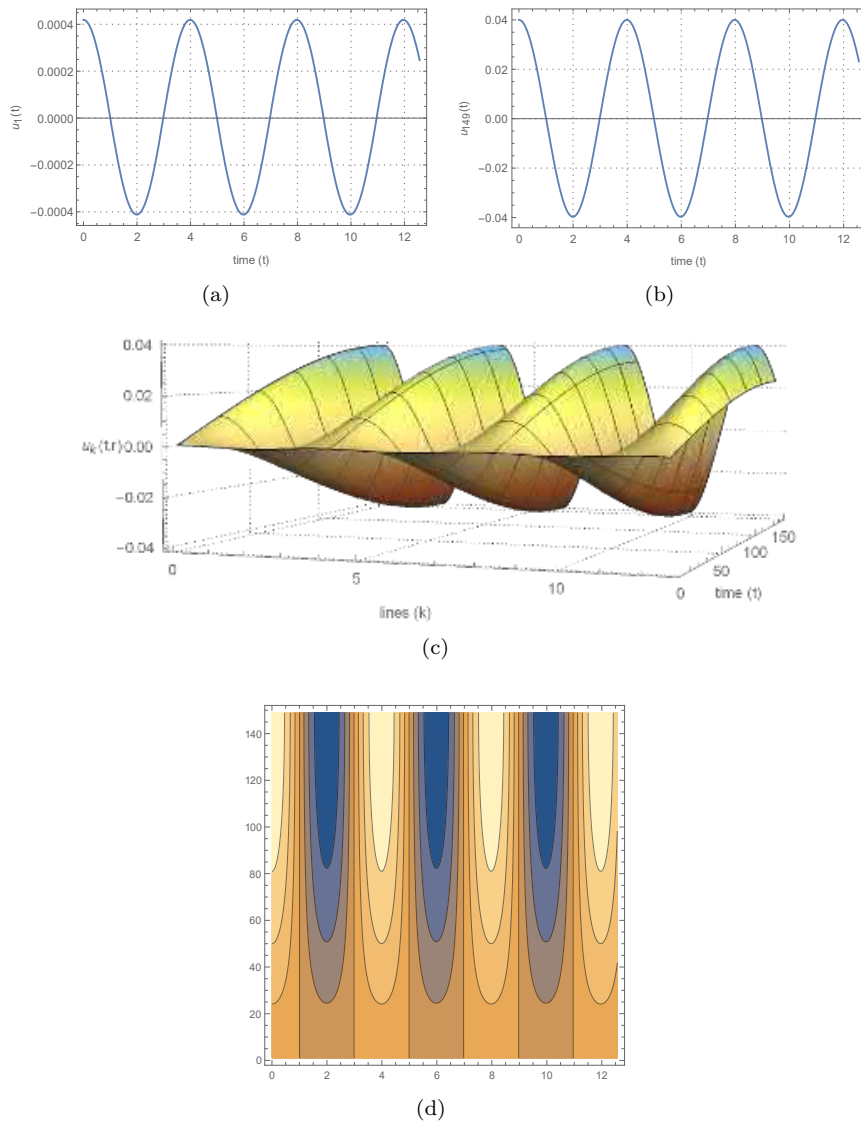


Figure 5: (a) First solution plot, $u_1(t)$, of the truncated coupled ODEs for $N = 150$ points; (b) Last solution plot, $u_{149}(t)$, of the truncated coupled ODEs for $N = 150$ points; (c) Contour plot of the truncated coupled ODEs for $N = 150$ points; (d) Surface plot of the truncated coupled ODEs for $N = 150$ points.

Numerical simulations for an amplitude value of 1.0 yielded the following harmonics:

$$\begin{aligned}
 c_0 &= 1.37004 \times 10^{-1}, & s_1 &= 8.61703 \times 10^{-1}, \\
 c_1 &= -1.81718 \times 10^{-1}, & s_2 &= 2.3806 \times 10^{-2}, \\
 c_2 &= 4.5512 \times 10^{-2}, & s_3 &= -3.7237 \times 10^{-2}, \\
 c_3 &= 1.0145 \times 10^{-2}, & s_4 &= -4.446461 \times 10^{-3}, \\
 c_4 &= -1.0638 \times 10^{-2}, & s_5 &= 8.400466 \times 10^{-3}, \\
 c_5 &= -3.749745 \times 10^{-3}, & &
 \end{aligned} \tag{17}$$

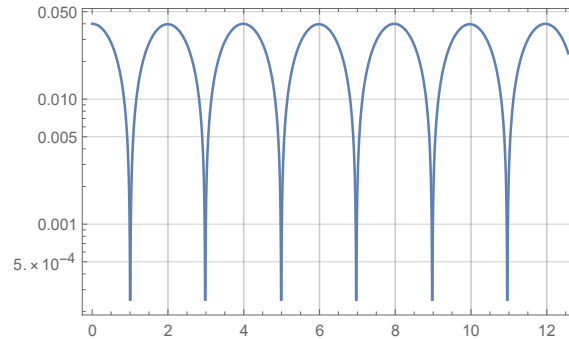


Figure 6: Zeros of interpolated function for $u_{149}(t)$ solution.

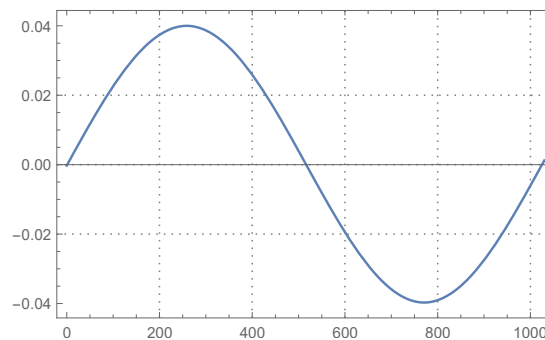


Figure 7: Plot of one period.

The numeric values in the respective harmonics for the respective amplitude show that the sine and cosine harmonics increase as the value of the amplitude is increased. This is therefore a substantial (and more reliable) measure of how nonlinear interactions in the continuum of gold atoms manifest. Although the simulation plots for amplitude values 0.25 and 0.04 will appear to be perfectly smooth, the calculation of the Fourier coefficients helps us to understand (by numerical computations) how the nonlinear terms are changing.

4 Discussion and Summary

A continuum describing an attachment of infinite atoms was theoretically investigated. The nonlinear interactions in the nanochain were described by the Generalized Morse potential energy function. A governing second-order PDE was derived using Hamilton's principle and the corresponding boundary conditions were also formulated. The MOL was employed to obtain approximate solutions of the continuum because of the PDE's complexity. The contour plots indicate how the nonlinear terms in the continuum are manifested or suppressed.

This study can be used as an example to understand the fast building of slender nanostructures/nanochain or one-dimensional lattices. This can be done by taking into consideration the dynamics which includes fast growing amplitudes and the manifestation

of nonlinear growth of nonlinear effects due to the large amplitudes of vibration as well as manifestation of nonlinear quadratic terms in the potential function.

It was generally observed that the waves motion towards the right end of the continuum became more skewed for increasing values of A . The formation of the sharp corners in longitudinal displacement (see Figures 3(b) and 4(b)) means the formation of discontinuity in the radial strain (which is equal to the derivative of displacement with respect to longitudinal coordinate). The strain discontinuity forms the stress discontinuity (Hooke's law). In continuous structures, the stresses must change continuously: "stress \times area = applied force", but "action = reaction" due to Newton's third law. This means, at fast growth and oscillations, the long nanochains demonstrate the tendency for disruption. We can interpret this to be one of fundamental properties of asymmetry of the interatomic potentials, not only for the Morse potential investigated in this study.

Acknowledgments

The authors wish to thank Tshwane University of Technology for the postgraduate bursary support of Mr Surulere. The authors also acknowledge support from the Department of Higher Education and Training, South Africa.

A Derivation of explicit governing equation for the continuum

We introduce the functional of action

$$I = \int_0^t L d\tau = \int_0^t \int_0^l \Lambda dr d\tau, \quad (18)$$

and the variation of the functional of action

$$\delta I = \int_0^t \delta L d\tau = \int_0^t \int_0^l \delta \Lambda dr d\tau. \quad (19)$$

We know that

$$\delta \Lambda(\dot{u}, u') = \frac{\partial \Lambda}{\partial \dot{u}} \delta \dot{u}(t, r) + \frac{\partial \Lambda}{\partial u'} \delta u'(t, r). \quad (20)$$

Now, we can write

$$\delta \Lambda(\dot{u}, u') = \frac{\partial}{\partial t} \left[\frac{\partial \Lambda}{\partial \dot{u}} \delta u(t, r) \right] - \frac{\partial}{\partial t} \left(\frac{\partial \Lambda}{\partial \dot{u}} \right) \delta u(t, r) + \frac{\partial}{\partial r} \left[\frac{\partial \Lambda}{\partial u'} \delta u(t, r) \right] - \frac{\partial}{\partial r} \left(\frac{\partial \Lambda}{\partial u'} \right) \delta u(t, r). \quad (21)$$

Hamilton's principle at the stationary point is applied, i.e., $\delta I = 0$ while bearing in mind that $\delta u(t, r) = 0$ at the limits of integration, $\tau \in [0, t]$

$$\delta I = \int_0^t \left[\frac{\partial \Lambda}{\partial u'} \delta u(t, r) \right]_0^l d\tau - \int_0^t \int_0^l \left[\frac{\partial}{\partial t} \left(\frac{\partial \Lambda}{\partial \dot{u}} \right) + \frac{\partial}{\partial r} \left(\frac{\partial \Lambda}{\partial u'} \right) \right] \delta u(t, r) dr d\tau = 0. \quad (22)$$

Since $\delta u(t, r)$ is arbitrary, the fundamental lemma of calculus of variations requires that $\delta I = 0$ if and only if

$$\frac{\partial}{\partial t} \left(\frac{\partial \Lambda}{\partial \dot{u}} \right) + \frac{\partial}{\partial r} \left(\frac{\partial \Lambda}{\partial u'} \right) = 0, \quad \left[\frac{\partial \Lambda}{\partial u'} \delta u(t, r) \right]_{r=0}^{r=l} = 0.$$

The Euler-Lagrange equation presented in terms of the Lagrangian density (i.e., an implicit form of the Euler-Lagrange equation) is

$$\frac{\partial}{\partial t} \left(\frac{\partial \Lambda}{\partial \dot{u}} \right) + \frac{\partial}{\partial r} \left(\frac{\partial \Lambda}{\partial u'} \right) = 0,$$

and possible boundary conditions for the continuum are

$$\begin{aligned} r = 0 : \quad & [\delta u(t, r)]_{r=0} = 0 \quad \text{or} \quad \left[\frac{\partial \Lambda}{\partial u'} \right]_{r=0} = 0, \\ r = l : \quad & [\delta u(t, r)]_{r=l} = 0 \quad \text{or} \quad \left[\frac{\partial \Lambda}{\partial u'} \right]_{r=l} = 0. \end{aligned} \tag{23}$$

We recall Equation (10) to obtain the expressions

$$\begin{aligned} \frac{\partial}{\partial r} \left(\frac{\partial \Lambda}{\partial u'} \right) &= \frac{\partial}{\partial r} [-\alpha A \exp(-\alpha u') + \beta B \exp(-\beta u')] \\ &= \left[\alpha^2 A \exp \left(-\alpha \frac{\partial u}{\partial r} \right) - \beta^2 B \exp \left(-\beta \frac{\partial u}{\partial r} \right) \right] \frac{\partial^2 u}{\partial r^2}, \\ \frac{\partial}{\partial t} \left(\frac{\partial \Lambda}{\partial \dot{u}} \right) &= \frac{\partial}{\partial t} (m\ddot{u}) = m \frac{\partial^2 u}{\partial t^2}. \end{aligned} \tag{24}$$

B Derivation of boundary conditions

Before writing the explicit boundary conditions, let us remark that

$$\frac{\partial \Lambda}{\partial u'} = -\alpha A \exp(-\alpha u') + \beta B \exp(-\beta u'),$$

but from Equation (4), $\bar{\alpha}A = \bar{\beta}B$ and hence, $\alpha A = \beta B$. This means that $\frac{\partial \Lambda}{\partial u'} = 0$ if and only if $\frac{\partial u}{\partial r} = 0$. The explicit boundary conditions are then obtained from Equation (23)

$$\begin{aligned} r = 0 : \quad & u(t, r = 0) = 0 \quad \text{or} \quad \left. \frac{\partial u}{\partial r} \right|_{r=0} = 0, \\ r = l : \quad & u(t, r = l) = 0 \quad \text{or} \quad \left. \frac{\partial u}{\partial r} \right|_{r=l} = 0. \end{aligned} \tag{25}$$

C Formulation of coupled system of infinite ODEs

Introducing definitions (13) and (14) into Equation (11) and Equation (12), we will obtain the coupled system of infinite second-order ODEs

$$\begin{aligned} \frac{d^2 u_k(t)}{dt^2} - \left\{ \bar{a} \exp \left(-\frac{\alpha}{2\Delta r} [u_{k+1}(t) - u_{k-1}(t)] \right) - \bar{b} \exp \left(-\frac{\beta}{2\Delta r} [u_{k+1}(t) - u_{k-1}(t)] \right) \right\} \\ \times \frac{1}{(\Delta r)^2} [u_{k-1}(t) - 2u_k(t) + u_{k+1}(t)] = 0, \end{aligned} \tag{26}$$

and the new boundary conditions

$$r = 0 : \quad u_k(0) = 0, \quad (27)$$

$$r = 1 : \quad \left. \frac{\partial u(t, r)}{\partial r} \right|_{r=r_N} = 0. \quad (28)$$

At the boundary, $r = 1$, Equation (13) is replaced by the backward-difference (or implicit difference) method

$$\left. \frac{\partial u_k(t)}{\partial r} \right|_{r=r_k} = \frac{1}{2\Delta r} [u_k(t) - u_{k-1}(t)]. \quad (29)$$

Evaluating Equation (29) at $r = r_N$ and comparing with Equation (26) give the expression $\frac{1}{2\Delta r} [u_N(t) - u_{N-1}(t)] = 0$. This simply means $u_N(t) = u_{N-1}(t)$.

References

- [1] B. I. Iliya. *Vibrational Mechanics: Nonlinear Dynamic Effects, General Approach, Applications*. World Scientific Publishing Co. Ptc. Ltd, 2000.
- [2] M. Toda. Vibration of a chain with nonlinear interaction. *Journal of the Physical Society of Japan* **22** (2) (1967) 431–436.
- [3] M. Toda. *Theory of Nonlinear Lattices*, Vol. 20. Springer Science & Business Media, 2012.
- [4] P. M. Morse. Diatomic molecules according to the wave mechanics. II. Vibrational levels. *Physical Review* **34** (1) (1929) 57.
- [5] W. E. Schiesser and G. W. Griffiths. *A Compendium of Partial Differential Equation Models: Method of Lines Analysis With Matlab*. Cambridge University Press, 2009.
- [6] F. Shakeri and M. Dehghan. The method of lines for solution of the one-dimensional wave equation subject to an integral conservation condition. *Computers & Mathematics with Applications* **56** (9) (2008) 2175–2188.
- [7] W. Schiesser. *The Numerical Method of Lines: Integration of Partial Differential Equations*. Academic Press, 1991.
- [8] W. E. Schiesser. *Partial Differential Equation Analysis in Biomedical Engineering: Case Studies with Matlab*. Cambridge University Press, 2012.
- [9] W. E. Schiesser. *Method of Lines Pde Analysis in Biomedical Science and Engineering*. John Wiley & Sons, 2016.
- [10] W. E. Schiesser. *Method of Lines Analysis of Turing Models*. World Scientific, 2017.
- [11] W. Schiesser. Method of lines solution of the Korteweg-de Vries equation. *Computers & Mathematics with Applications* **28** (10-12) (1994) 147–154.
- [12] P. Saucez, W. Schiesser and A. V. Wouwer. Upwinding in the method of lines. *Mathematics and Computers in Simulation* **56** (2) (2001) 171–185.
- [13] J. N. M. Bidie. An error analysis of the numerical method of lines, Master's thesis. Tshwane University of Technology, South Africa, 2011.
- [14] M. N. Sadiku and C. Obiozor. A simple introduction to the method of lines. *International journal of electrical engineering education* **37** (3) (2000) 282–296.

- [15] S. Surulere, M. Shatalov, A. Mkolesia, T. Malange and A. Adeniji. The integral-differential and integral approach for the exact solution of the hybrid functional forms for Morse potential. *IAENG International Journal of Applied Mathematics* **50** (2) (2020) 242–250.
- [16] S. A. Surulere, M. Y. Shatalov, A. C. Mkolesia and I. Fedotov. Vibrations in a growing nonlinear chain. *Discontinuity, Nonlinearity and Complexity*, in press (2020).
- [17] A. Jeffrey. *Advanced Engineering Mathematics*. Elsevier, 2001.
- [18] D. G. Duffy. *Advanced Engineering Mathematics with Matlab*. CRC Press, 2016.



Linear Chaos Control of Fractional Generalized Hénon Map

Abdelwahab Zarour¹, Adel Ouannas^{2*}, Chahla Latrous¹ and Abdelhak Berkane¹

¹ *Department of Mathematics, Faculty of Exact Sciences, Constantine University, Algeria.*

² *Department of Mathematics and Computer Science, University of Larbi Ben M'hidi, Oum El Bouaghi, Algeria.*

Received: November 24, 2020; Revised: March 13, 2021

Abstract: This paper is concerned with the topic of chaos control in fractional maps. It presents two linear control laws to stabilize the dynamics of a new three-dimensional fractional Hénon map. The chaos control has been achieved by proving a new theorem, based on a suitable Lyapunov function and a linear method. Finally, numerical simulations have been carried out to highlight the effectiveness of the proposed control method.

Keywords: *discrete fractional calculus; fractional generalized Hénon map; linear control; Lyapunov method.*

Mathematics Subject Classification (2010): 34H10, 34H15.

1 Introduction

Recently, researchers have diverted their attention to the discrete-time case of fractional calculus and attempted to put together a complete theoretical framework for the subject [1]. Perhaps one of the earliest works is that of Diaz and Olser [2]. Successively, several types of discrete operators have been proposed, including some fractional *h-difference* operators, which represent further generalizations of the fractional difference operators [3–5]. Furthermore, numerical formulas and stability conditions corresponding to fractional difference systems can be found in [6, 7]. Most recently, some advances have been made in the applications of discrete fractional calculus [8]. The introduction of different discrete fractional operators has led to the publication of several papers regarding the chaotic behaviors of fractional nonlinear maps [9–17].

* Corresponding author: <mailto:dr.ouannas@gmail.com>

Dynamics and control of fractional-order chaotic systems have received considerable attention over the last few years [18, 19]. So far, nonlinear control laws have been mainly used for controlling at zero the chaotic dynamics of new three-dimensional fractional maps. Some interesting results have been recently published regarding this challenging topic [20–24]. For example, in [20], nonlinear control methods for some three-dimensional fractional chaotic maps (i.e., the Stefanski map, the Rössler map and the Wang map) have been studied. In [21], a novel control law for stabilizing a new three-dimensional fractional Hénon map has been proposed. In [22], the fractional-order Grassi–Miller chaotic map has been stabilized via nonlinear controllers. In [23], a control scheme to control hidden chaotic attractors in a new fractional map has been illustrated. In [24], the chaotic behavior of a new three-dimensional fractional map with no equilibrium has been studied along with a control method that exploits the stability properties of linear fractional discrete systems.

It is worth noting that all the control methods developed so far for fractional chaotic maps have exploited *nonlinear* control laws. This work aims to provide a contribution to the topic by presenting a very simple *linear* control law to control chaotic dynamics of the well-known fractional generalized Hénon map. This map is defined via the Caputo h -difference operator. The asymptotic convergence of the states is established using the Lyapunov method. The paper is organized as follows. In Section 2, some basic notions of the Caputo h -difference operator and discrete fractional calculus are introduced. In Section 3, a novel control result is proved which enables the dynamics of the three dimensional fractional Hénon map to be controlled by a *two-dimensional linear* control. Finally, simulation results are reported through the paper, with the aim to show the effectiveness of the proposed approach.

2 Basic Tools

In this section, some basic concepts related to the Caputo h -difference operator are briefly summarized.

Definition 2.1 [4] Let $X : (h\mathbb{N})_a \rightarrow \mathbb{R}$ and $0 < \nu$ be given. a is a starting point. The ν -th order h -sum is given by

$${}_h\Delta_a^{-\nu} X(t) = \frac{h}{\Gamma(\nu)} \sum_{s=\frac{a}{h}}^{\frac{t}{h}-\nu} (t - \sigma(sh))_h^{(\nu-1)} X(sh), \sigma(sh) = (s + 1)h, a \in \mathbb{R}, t \in (h\mathbb{N})_{a+\nu h}, \tag{1}$$

where the h -falling factorial function is defined as

$$t_h^{(\nu)} = h^\nu \frac{\Gamma\left(\frac{t}{h} + 1\right)}{\Gamma\left(\frac{t}{h} + 1 - \nu\right)}, \quad t, \nu \in \mathbb{R},$$

where $(h\mathbb{N})_{a+(1-\nu)h} = \{a + (1 - \nu)h, a + (2 - \nu)h, \dots\}$.

Definition 2.2 [5] For $X(t)$ defined on $(h\mathbb{N})_a$ and $0 < \nu, \nu \notin \mathbb{N}$, the Caputo-like difference is defined by

$${}_h^C\Delta_a^\nu X(t) = \Delta_a^{-(n-\nu)} \Delta^n X(t), \quad t \in (h\mathbb{N})_{a+(n-\nu)h}, \tag{2}$$

where $\Delta X(t) = \frac{X(t+h) - X(t)}{h}$ and $n = \lceil \nu \rceil + 1$.

Now a theorem reported in [25] is briefly illustrated, with the aim to identify the stability conditions of the zero equilibrium point for the fractional nonlinear difference system written in the form

$${}_h^C \Delta_a^\nu X(t) = f(t + \nu h, X(t + \nu h)), \quad (3)$$

where $X(t) = (x_1(t), x_2(t), \dots, x_n(t))^T$, $t \in (h\mathbb{N})_{a+(1-\nu)h}$ and f is a nonlinear function.

Theorem 2.1 *Let $x = 0$ be an equilibrium point of the nonlinear discrete fractional system (3). If there exists a positive definite and decrescent scalar function $V(t, X(t))$ such that ${}_h^C \Delta_a^\nu V(t, X(t)) \leq 0$, $t \in (h\mathbb{N})_{a+(1-\nu)h}$, then the equilibrium point is asymptotically stable.*

In the following, a useful inequality for Lyapunov functions is introduced.

Lemma 2.1 [25] *For any discrete time $t \in (h\mathbb{N})_{a+(1-\nu)h}$, $0 < \nu \leq 1$, the following inequality holds*

$${}_h^C \Delta_a^\nu (X^T(t) X(t)) \leq 2X^T(t + \nu h) {}_h^C \Delta_a^\nu X(t). \quad (4)$$

3 The Three-Dimensional Fractional Generalized Hénon Map

Recently, a new three-dimensional fractional Hénon map with Lorenz-like attractors has been proposed in [26]. This map is an example of a fractional discrete-time system with the ν Caputo-like operator that can display chaotic behavior. In the following, by adopting the Caputo h -difference operator we described the fractional generalized Hénon map as

$$\begin{cases} {}_h^C \Delta_a^\nu x(t) = M_1 + Bz(t + \nu h) + M_2y(t + \nu h) - x^2(t + \nu h) - x(t + \nu h), \\ {}_h^C \Delta_a^\nu y(t) = x(t + \nu h) - y(t + \nu h), \\ {}_h^C \Delta_a^\nu z(t) = y(t + \nu h) - z(t + \nu h), \end{cases} \quad (5)$$

where x, y, z are the states of the fractional map (5) and M_1, M_2 and B are parameter values, with $t \in (h\mathbb{N})_{a+(1-\nu)h}$.

To study the properties of the fractional generalized Hénon map (5), the following discrete numerical solution is defined based on the h -fractional sum (1) as

$$\begin{cases} x(n+1) = x_0 + \frac{h^\nu}{\Gamma(\nu)} \sum_{j=0}^n \frac{\Gamma(n-j+\nu)}{\Gamma(n-j+1)} (M_1 + Bz(j+1) + M_2y(j+1) - x^2(j+1) - x(j+1)), \\ y(n+1) = y_0 + \frac{h^\nu}{\Gamma(\nu)} \sum_{j=0}^n \frac{\Gamma(n-j+\nu)}{\Gamma(n-j+1)} (x(j+1) - y(j+1)), \\ z(n+1) = z_0 + \frac{h^\nu}{\Gamma(\nu)} \sum_{j=0}^n \frac{\Gamma(n-j+\nu)}{\Gamma(n-j+1)} (y(j+1) - z(j+1)), \end{cases} \quad (6)$$

where x_0, y_0 and z_0 are initial states. According to the discrete equation (6), the fractional generalized Hénon map (5) has memory effects, which means that the implicit solution is determined by all the previous states with the state $x(n+1), y(n+1)$ and $z(n+1)$. Considering parameter values $M_1 = 1.4$, $M_2 = 0.2$ and varying B from 0 to 0.3, the resulting bifurcation diagram and the largest Lyapunov exponents are depicted in Figure 1 with fractional order $\nu = 0.98$. Different dynamic behaviors including chaos periodic windows are observed in the fractional generalized Hénon map (5). From this, it can be seen that the system has the positive largest Lyapunov exponent when B takes the smallest values, indicating that the system has indeed a chaotic attractor, as shown in Figure 1(a) for $B = 0.1$.

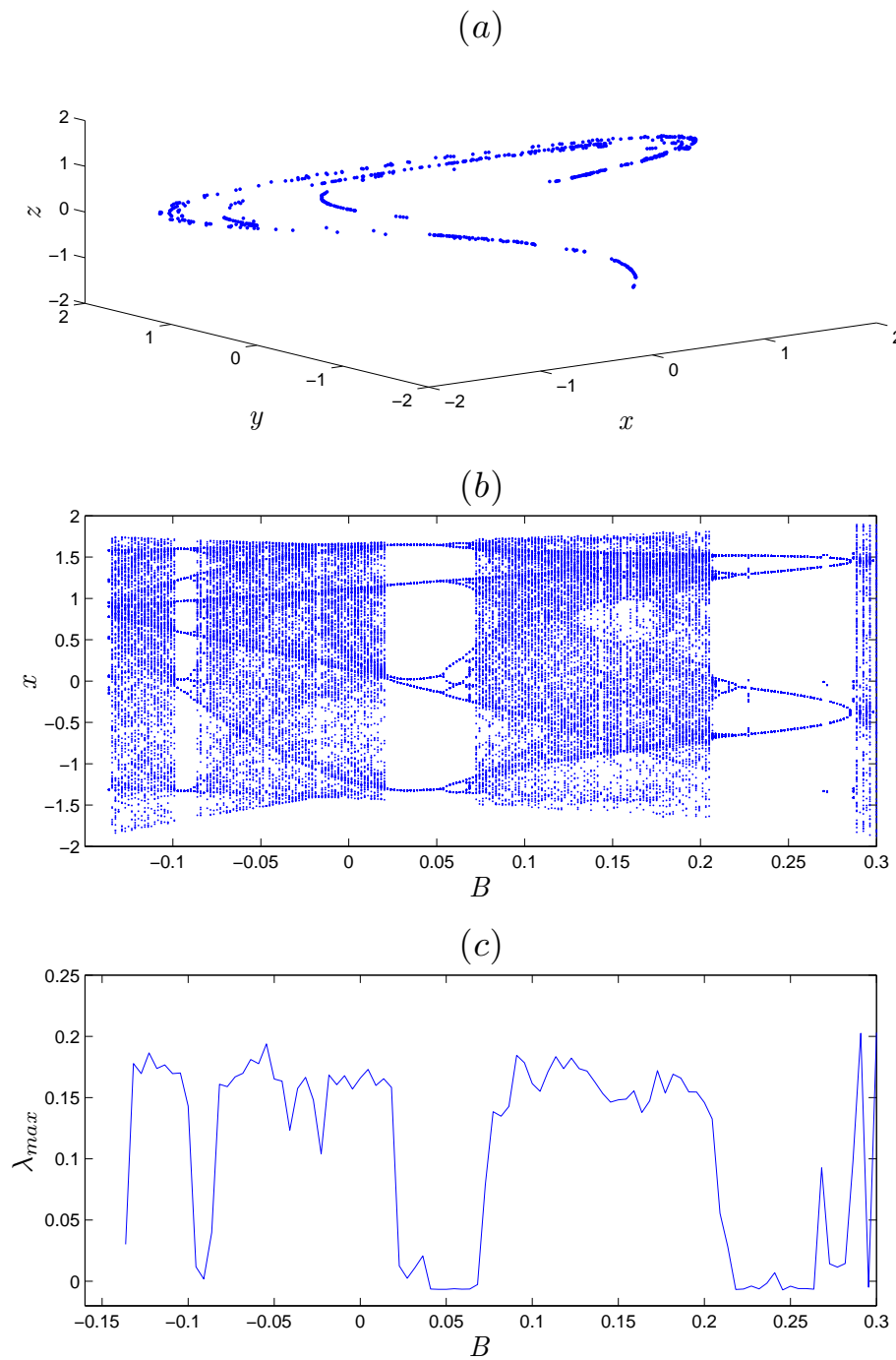


Figure 1: Numerical simulation of the fractional generalized Hénon map for the fractional order value $\nu = 0.98$. (a) The chaotic attractor for $M_1 = 1.4$, $B = 0.1$. (b) The bifurcation diagram versus B . (c) The corresponding largest Lyapunov exponents diagram.

4 Two-Dimensional Chaos Control Law

In this section, by exploiting a novel theorem based on a suitable Lyapunov function, a two-dimensional linear control law is illustrated, with the aim to control the chaotic dynamics of the three-dimensional fractional Hénon map. To obtain our results, the following theorem is presented.

Theorem 4.1 *The three-dimensional fractional Hénon chaotic map is controlled under the following linear two-dimensional control law:*

$$\begin{cases} \mathbf{C}_1 = -lx(t) - (M_2 + 1)y(t) - Bz(t) - M_1, \\ \mathbf{C}_2 = -z(t), \end{cases} \quad (7)$$

where $|x(t)| \leq l$, for $t \in (h\mathbb{N})_{a+(1-\nu)h}$.

Proof. The controlled fractional Hénon chaotic map involves the time-varying control law $(\mathbf{C}_1, \mathbf{C}_2)^T$ and is given by

$$\begin{cases} {}^C_h \Delta_a^\nu x(t) = M_1 + Bz(t + \nu h) + M_2 y(t + \nu h) - x^2(t + \nu h) - x(t + \nu h) + \mathbf{C}_1(t + \nu h), \\ {}^C_h \Delta_a^\nu y(t) = x(t + \nu h) - y(t + \nu h) + \mathbf{C}_2(t + \nu h), \\ {}^C_h \Delta_a^\nu z(t) = y(t + \nu h) - z(t + \nu h). \end{cases} \quad (8)$$

Substituting the proposed control law (7) into (8) yields the simplified dynamics

$$\begin{cases} {}^C_h \Delta_a^\nu x(t) = -y(t + \nu h) - x^2(t + \nu h) - (l + 1)x(t + \nu h), \\ {}^C_h \Delta_a^\nu y(t) = x(t + \nu h) - y(t + \nu h) - z(t + \nu h), \\ {}^C_h \Delta_a^\nu z(t) = y(t + \nu h) - z(t + \nu h). \end{cases} \quad (9)$$

Now, by taking a Lyapunov function in the form

$$V = \frac{1}{2} (x^2(t) + y^2(t) + z^2(t)), \quad (10)$$

it follows that

$${}^C_h \Delta_a^\nu V = \frac{1}{2} {}^C_h \Delta_a^\nu x^2(t) + \frac{1}{2} {}^C_h \Delta_a^\nu y^2(t) + \frac{1}{2} {}^C_h \Delta_a^\nu z^2(t), \quad (11)$$

and by exploiting Lemma 1, we get

$$\begin{aligned} {}^C_h \Delta_a^\nu V &\leq x(t + \nu h) {}^C_h \Delta_a^\nu x(t) + y(t + \nu h) {}^C_h \Delta_a^\nu y(t) + z(t + \nu h) {}^C_h \Delta_a^\nu z(t) \\ &= -x(t + \nu h)y(t + \nu h) - x^3(t + \nu h) - (l + 1)x^2(t + \nu h) \\ &\quad + y(t + \nu h)x(t + \nu h) - y^2(t + \nu h) - y(t + \nu h)z(t + \nu h) \\ &\quad + z(t + \nu h)y(t + \nu h) - z^2(t + \nu h) \\ &= -(l + 1)x^2(t + \nu h) - y^2(t + \nu h) - z^2(t + \nu h) - x^3(t + \nu h) \\ &\leq -(l + 1)x^2(t + \nu h) - y^2(t + \nu h) - z^2(t + \nu h) + |x|x^2(t + \nu h) \\ &\leq -(l + 1)x^2(t + \nu h) - y^2(t + \nu h) - z^2(t + \nu h) + lx^2(t + \nu h) \\ &= -x^2(t + \nu h) - y^2(t + \nu h) - z^2(t + \nu h) < 0. \end{aligned}$$

It can be concluded that the controlled states of the fractional Hénon chaotic map (5) are stabilized at the origin by the two-dimensional linear control law (7).

To verify the theoretical results obtained above, numerical simulations are performed using Matlab. We start by employing h -fractional sum (1) to obtain the numerical formula of the controlled dynamical system (5). The parameter values are taken as $M_1 = 1.4$ and $M_2 = 0.2$, $B = 0.1$ to ensure the existence of chaos. Figures 2 and 3 show the states trajectories and the phase portrait, respectively, of the controlled fractional map (5) when the fractional order value is taken as $\nu = 0.98$. These plots clearly show that the chaotic dynamics of the fractional map (5) are controlled to equilibrium point $(0, 0, 0)$ by control law (7).

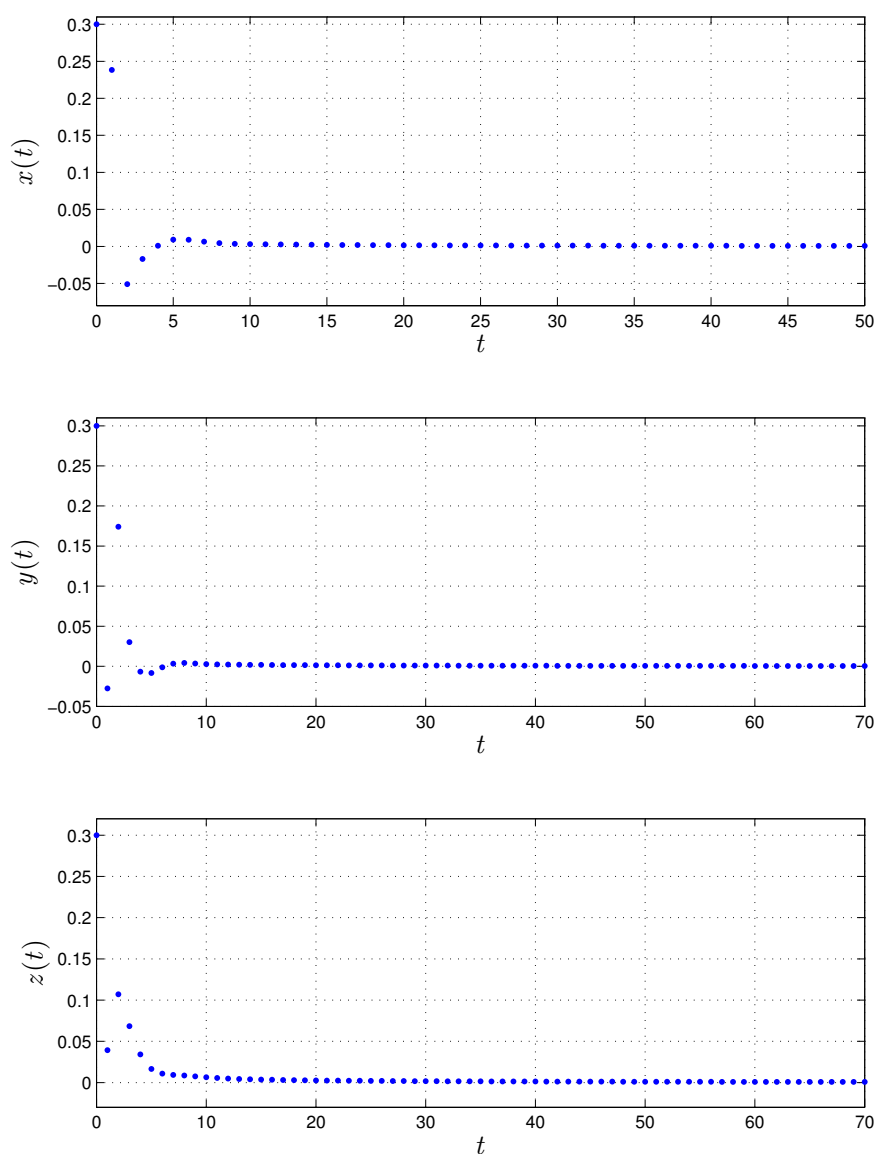


Figure 2: Phase portrait of the controlled fractional generalized Hénon map with $\nu = 0.98$.

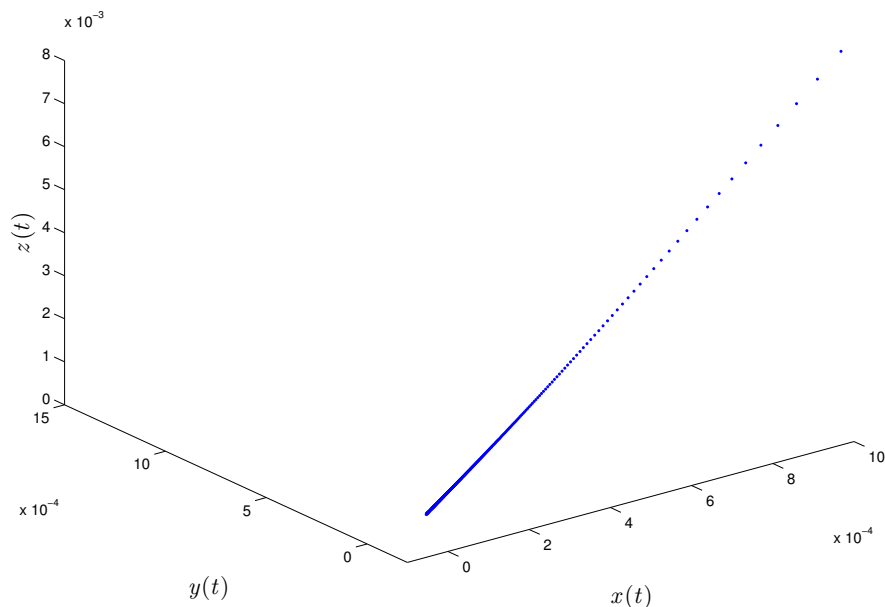


Figure 3: Evolution of the controlled fractional generalized Hénon map with $\nu = 0.98$.

5 Conclusion

Using linear control laws, this paper has studied the control of a new fractional chaotic map. Specifically, the three-dimensional fractional Hénon map has been controlled by a two-dimensional control law. All the results have been achieved by exploiting a new linear control law based on the Lyapunov method as well as on the properties of the Caputo h -difference operator. Note that, by virtue of the linearity of the control law proposed herein, the conceived method for controlling the chaotic dynamics requires less control effort with respect to the nonlinear techniques developed in literature to date. Finally, simulation results have been presented to highlight the effectiveness of the proposed approach.

Acknowledgment

The author Adel Ouannas thanks the Directorate General for Scientific Research and Technological Development in Algeria who supported the research to be at hand.

References

- [1] C. Goodrich and A. C. Peterson. *Discrete Fractional Calculus*. Springer, Berlin, Germany, 2015.
- [2] J. B. Diaz and T. J. Olser. Differences of fractional order. *Math. Comput.* **28** (1974) 185-202.

- [3] F.M. Atici and P.W. Eloe. A transform method in discrete fractional calculus. *Int. J. Differ. Equ.* **2** (2007) 165–176.
- [4] F.M. Atici and P.W. Eloe. Discrete fractional calculus with the nabla operator. *Electron. J. Qual. Theory Differ. Equ. Spec. Ed. I* **3** (2009) 1–12.
- [5] T. Abdeljawad. On Riemann and Caputo fractional differences. *Comput. Math. Appl.* **62** (2011) 1602–1611.
- [6] G.A. Anastassiou. Principles of delta fractional calculus on time scales and inequalities. *Mathematical and Computer Modelling* **52** (2010) 556–566.
- [7] R. Abu-Saris and Q. Al-Mdallal. On the asymptotic stability of linear system of fractional order difference equations. *Fract. Calc. Appl. Anal.* **16** (2013) 613–629.
- [8] L. Huang, D. Baleanu, G. Wu and S. Zeng. A new application of the fractional logistic map. *Rom. J. Phys.* **61** (2016) 1172–1179.
- [9] F. Hadjabi, A. Ouannas, N. Shawagfeh, A.A. Khennaoui and G. Grassi. On Two-Dimensional Fractional Chaotic Maps with Symmetries. *Symmetry* **12** (5) (2020) 756.
- [10] A. Ouannas, A.A. Khennaoui, S. Momani, G. Grassi, V.T. Pham, R. El-Khazali and D.V. Hoang. A Quadratic Fractional Map without Equilibria: Bifurcation, 0–1 Test, Complexity, Entropy and Control. *Electronics* **9** (5) (2020) 748.
- [11] A. Ouannas, A.A. Khennaoui, S. Bendoukha, Z. Wang and V.T. Pham. The Dynamics and Control of the Fractional Forms of Some Rational Chaotic Maps. *Journal of Systems Science and Complexity* (2020) 1–20.
- [12] A.A. Khennaoui, A. Ouannas, S. Bendoukha, G. Grassi, R.P. Lozi and V.T. Pham. On fractional–order discrete–time systems: Chaos, stabilization and synchronization. *Chaos, Solitons & Fractals* **119** (2019) 150–162.
- [13] A. Ouannas, A.A. Khennaoui, Z. Odibat, V.T. Pham and G. Grassi. On the dynamics, control and synchronization of fractional-order Ikeda map. *Chaos, Solitons & Fractals* **123** (2019) 108–115.
- [14] A. Gasri, A. Ouannas, A.A. Khennaoui, S. Bendoukha and V.T. Pham. On the Dynamics and Control of Fractional Chaotic Maps with Sine Terms. *Int. J. of Nonlinear Sciences and Numerical Simulation* **21** (6) (2020) 589–601.
- [15] A. Ouannas, A.A. Khennaoui, S. Momani and V.T. Pham. The Discrete Fractional Duffing System: Chaos, 0–1 Test, Complexity, Entropy and Control. *Chaos* **30** (2020) 083131.
- [16] A. Ouannas, A.A. Khennaoui, S. Bendoukha and G. Grassi. On the Dynamics and Control of a Fractional Form of the Discrete Double Scroll. *International Journal of Bifurcation and Chaos* **29** (06) (2019) 1950078.
- [17] A.A. Khennaoui, A. Ouannas, S. Boulaaras, V.T. Pham and A.T. Azar. A fractional map with hidden attractors: chaos and control. *Eur. Phys. J. Special Topics* **229** (2020) 1083–1093.
- [18] R. Barkat and T. Menacer. Dynamical Analysis, Stabilization and Discretization of a Chaotic Financial Model with Fractional Order. *Nonlinear Dynamics and Systems Theory* **20** (3) (2020) 253–266.
- [19] B. Labed, S. Kaouache and M. S. Abdelouahab. Control of a Novel Class of Uncertain Fractional-Order Hyperchaotic Systems with External Disturbances via Sliding Mode Controller. *Nonlinear Dynamics and Systems Theory* **20** (2) (2020) 203–213.
- [20] A.A. Khennaoui, A. Ouannas, S. Boulaaras, G. Grassi, X. Wang, V.T. Pham and F. Alsaadi. Chaos, control, and synchronization in some fractional-order difference equations. *Advances in Difference Equations* (1) (2019) 1–23.

- [21] L. Jouini, A. Ouannas, A. A. Khennaoui, X. Wang, G. Grassi and V. T. Pham. The fractional form of a new three-dimensional generalized Hénon map. *Advances in Difference Equations* **122** (1) (2019).
- [22] A. Ouannas, A. A. Khennaoui, G. Grassi and S. Bendoukha. On chaos in the fractional-order Grassi–Miller map and its control. *Journal of Computational and Applied Mathematics* **358** (2019) 293–305.
- [23] A. Ouannas, A. A. Khennaoui, S. Momani, V. T. Pham and R. El-Khazali. Hidden attractors in a new fractional-order discrete system: Chaos, complexity, entropy, and control. *Chin. Phys. B* **29** (5) (2020) 050504.
- [24] A. Ouannas, A. A. Khennaoui, S. Momani, G. Grassi and V. T. Pham. Chaos and control of a three-dimensional fractional order discrete-time system with no equilibrium and its synchronization. *AIP Advances* **10** (2020) 045310.
- [25] D. Baleanu, G. C. Wu, Y. R. Bai and F. L. Chen. Stability analysis of Caputo-like discrete fractional systems. *Communications in Nonlinear Science and Numerical Simulation* **48** (2017) 520–530.
- [26] A. A. Khennaoui, A. Ouannas, Z. Odibat, V. T. Pham and G. Grassi. On the Three-Dimensional Fractional-Order Hénon Map with Lorenz-Like Attractors. *International Journal of Bifurcation and Chaos* **30** (11) (2020) 2050217.